The book deals with some problems of the hydraulics of combined hydroelectric power plants (HPPs). Methods for analyzing ejection into the tailrace are described, and recommendations on the design of HPPs are made.

The book is intended for those concerned with the design, construction, and operation of HPPs, and also for students of technical colleges and universities.

IPST Cat. No. 5100

Translated by A. Barouch, M.Sc.
Edited by IPST Staff

Printed in Jerusalem by S. Monson

Binding: Wiener Bindery Ltd., Jerusalem

IV/2/5

S. M. Slisskii

EJECTION INTO TAILRACES OF HYDROPOWER PLANTS

(Ezhektsiya v nizhnii b'ef na sovmeshchennykh gidroelektrostantsiyakh)

GEI
Gosudarstvennoe Energeticheskoe
Izdatel'stvo
Moskva-Leningrad
1953

Translated from Russian

Israel Program for Scientific Translations
Jerusalem 1968

Chapter I

TECHNICAL AND HYDRAULIC PREMISES OF USE AND DESIGN OF EJECTION

1. PRELIMINARY NOTES

A rise in the level of an HPP tailrace during high water causes a drop in the available head. A drop of the head H below the value corresponding to optimum operating conditions leads to a decrease of the discharge Q through the turbine and to a drop in its efficiency η. The power $N = 9.81\,QH\eta$ kw of medium- and low-head HPPs may become zero when the head drops to $^1/_3$ of its rated value (Figure 1).

The head, and hence the power of the HPP, can be restored by lowering the tailrace level: this is done by ejection, in which part of the excess discharge is carried either through the turbine bays or in their immediate vicinity.

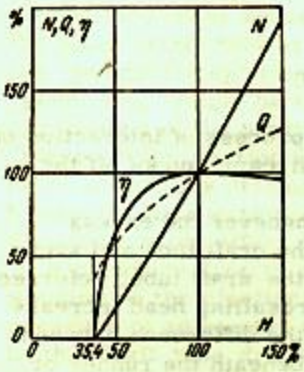

FIGURE 1. Turbine power, discharge, and efficiency as functions of head.

The idea of employing ejection in HPPs is not new. First experiments were made already in 1905. Although employed in several installations,* this method has not been widely used because of the concomitant difficulties in design and its negligible effect on the power and efficiency of existing installations. In fact, with proper design, ejection may considerably affect the power delivered. In some cases, use of ejection has led to an increase in annual output by several percents in a year of average water level. Thus, laboratory tests showed that in a large HPP at high water of 1 % probability, the power was restored from 73 % of the installed capacity to 87 % by ejection; at high water of 0.1 % probability, the corresponding figures were 50 % and 72 %.

Efficient utilization of ejection requires correct design. However, existing possibilities have not yet been fully exploited.

Study of the ejection process and development of methods for computing its effect, accompanied by experiments permit near-optimum solutions to be obtained at the design stage. Protracted and costly laboratory investigations may thus be reduced or even dispensed with altogether.

The advantages of combined HPPs have not so far been fully exploited outside the Soviet Union. The ejection effect was not used in the Kembs HPP

* The historical evolution has been given in detail by Perfil'ev /15/ and Egorov /4/. In this book the present state is discussed briefly in § 4.

(1932), the Rostin HPP (1936), and the HPPs on the Lech and Iller rivers (1938). Where ejection is used, on the other hand, as in the Mitchell HPP (the number of such HPPs is very small, their total power being only slightly above 80,000 kw), the discharge is carried through the turbine bays in order to restore the power, and not to shorten the spillway.

Soviet hydro-power engineers, who had to find means for tapping the energy of large lowland rivers, have found a new solution to this problem. Utilization by ejection of the energy of the spillway discharge in these rivers is not an aim in itself, but a consequence of exploiting the peculiarities of combined HPPs: both a shortening of the spillway front and a restoration of the power during high water are achieved.

A high discharge capacity of the turbine bays is easily obtained in combined HPPs if the water is carried to the tailrace through overflows or spillways, bypassing the draft tubes, whose dimensions and configuration are not affected. We are therefore mainly interested in tailrace ejection, with either overflow or spillway discharge. Nevertheless, carrying the discharge through a draft tube in order to restore the power is also of interest, and may offer so far unexploited possibilities.

The solution of the structural and hydraulic problems of ejection in a draft tube (for restoration of power), and the development of designs for ejection turbines are therefore topical questions.

This is accentuated by the desire to achieve in large HPPs ejection discharges of 100 to 200% or more of the turbine discharges, so as to use the draft tubes as spillways.

2. THE EJECTION PROCESS AND ITS EFFECT

Ejection is understood in engineering to be the process of interaction of two streams of liquid, one of which, the ejecting stream, sucks off the other, ejected stream.

As applicable to HPPs this term can be used whenever the excess discharge creates an additional pressure drop in the draft tube and sucks off the turbine discharges. The pressure drop in the draft tube, referred to the pressure existing without ejection, and the resulting head increase (at constant turbine discharge) are determined by the difference between the piezometric heads, with and without ejection, beneath the runner or at the outlet of the draft tube* (Figure 2). Ejection in HPPs can therefore be considered as additional pressure drop in the draft tube when the excess discharge is carried through the structure or in its vicinity.

This difference between the piezometric heads beneath the runner is sometimes called "ejection-action effect" (Perfil'ev /15/), or "ejection effect" (Kumin /8/).

In other works the same terms denote the difference between the tail-water level at a certain distance from the HPP and the piezometric-head plane (the level of the free surface in a piezometric tube) at the draft-tube outlet (Egorov /4/, Kachanovskii /7/). Such a difference exists even without ejection (or with ejection, but without turbine discharge); this

* At the outlet of the draft tube only in the case of tailrace ejection.

definition of the gain in head through tailrace ejection is therefore erroneous: firstly, with the turbine in operation the "ejection effect," defined as the difference of these two levels, slightly exceeds the actual gain in head; secondly, at zero turbine discharge the magnitude of the ejection effect, considered as useful gain in head, becomes meaningless.

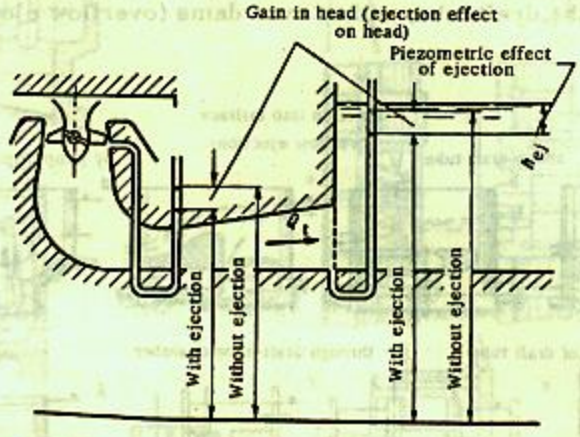

FIGURE 2. Head increase by ejection.

The difference between the tailrace level and the free-surface level in the piezometric tube at the outlet of the draft tube is sometimes called the "geometric ejection effect." This is not suitable, since the term "geometric" might be incorrectly interpreted as an increase in the dimensions of the structure. We shall replace this term by the expression "piezometric ejection effect," which reflects better the physical meaning of the magnitude discussed. In addition, we shall use the following terms: head effect of ejection, discharge effect of ejection, power effect of ejection, output effect of ejection.

A pressure drop is observed in the suction chamber of a jet apparatus working on the ejection principle when flow takes place, irrespective of the presence of an ejected stream. This is also true for HPPs: the pressure in the draft tube drops during spillway discharge, irrespective of the presence of a turbine discharge. The pattern of pressure variation in the draft tube, as function of the spillway discharge and other factors (dimensions of structure, tailrace level and depth, difference between headwater and tailwater levels) remains basically the same as with a turbine discharge. This has been verified by many experiments.

The phenomenon of pressure drop in the draft tube, due to spillway discharge at zero turbine discharge, does not correspond to the above definition of ejection, since in this case no interacting streams exist. The pressure drop in the draft tube becomes meaningless from the viewpoint of power as a gain in head. The magnitude of the pressure drop is, however, in this case practically equal to the piezometric ejection effect* observed at a turbine discharge approximating zero.

* This fact was used by the author in the hydraulic analysis of a mixed HPP. Several variants were compared for zero turbine discharge; only the selected optimum variant was analyzed in detail, assuming a turbine discharge.

3. HYDRAULIC SCHEMES OF HPPs WITH EJECTION

We distinguish two basic schemes (Figure 3): ejection into the tailrace, and ejection in the draft tube.

In the case of ejection into the tailrace, the water from the headrace by-passes the draft tube. The ejection effect on the turbine discharge takes place outside the draft tube, either over dams (overflow ejection) or through conduits.

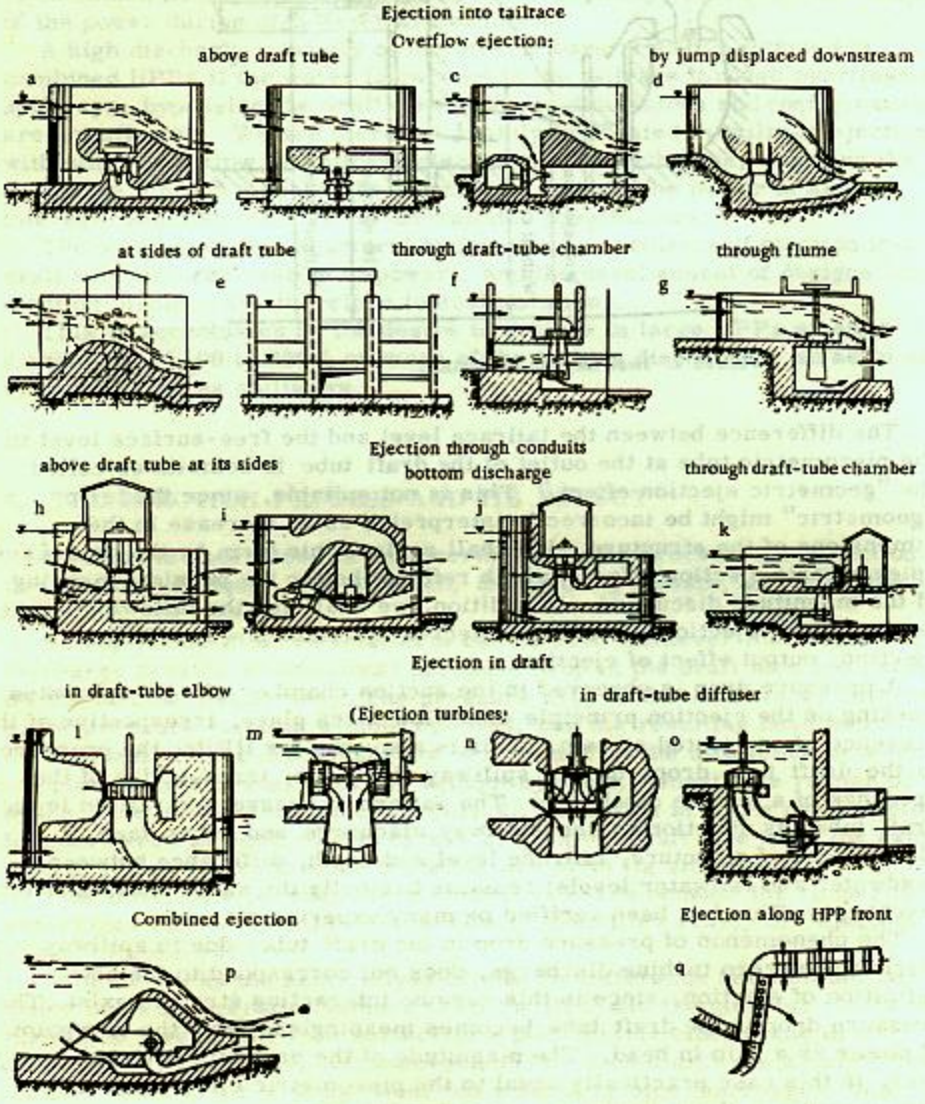

FIGURE 3. Hydraulic schemes of HPPs with ejection.

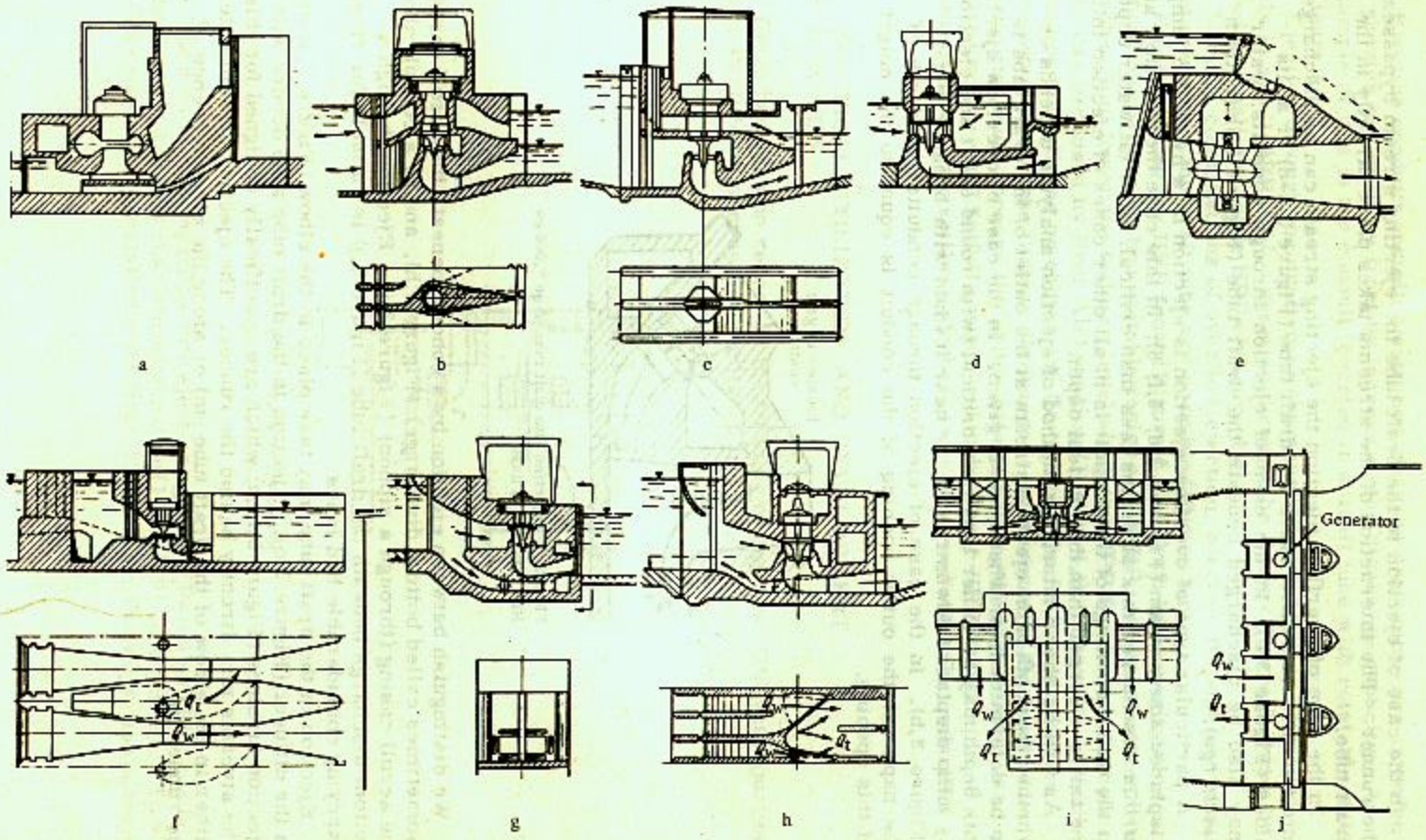

FIGURE 4. Different designs of combined HPPs.

In the case of ejection in the draft tube the ejecting stream bypasses the runner. The interaction of the streams takes place directly in the draft tube.

In the case of overflow ejection the ejecting stream can be discharged into the tailrace either above the draft tube (Figure 3,a-d) or at its sides (Figure 3,e). In the case of ejection through conduits, water may also be discharged beneath the draft tube (Figure 3,j) (bottom discharge).

A particular type of overflow ejection is ejection by a hydraulic jump displaced downstream (Figures 3,d; 4,f; 6); in this case the overflow and turbine discharges mix at depths less than critical. The tailwater depth at the outlet openings of the conduit is in all other cases of ejection into the tailrace larger than the critical depth.

As will be shown later, the method of ejection analysis depends on whether the depth of the ejecting stream at the outlet of the draft tube is to be determined, or whether it is given. In the case of overflow ejection this depth may be either less than critical (with round crest and ejection by jump displaced downstream), or near it (dam with broad crest, (Figure 3,b). In the case of ejection through conduits the depth of the nappe at the outlet opening of the conduit is equal to the height of this opening.

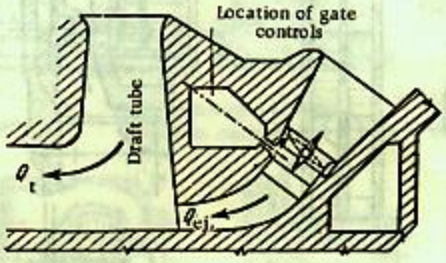

FIGURE 5. Ejection into draft tube in an 8,000 kw HPP with 12.5 m head.

We distinguish between ejection by a conduit beneath the scroll casing (sometimes called bottom discharge) (Figure 3,h), and by a conduit above the scroll casing (through a siphon) (Figure 3,i). Ejection through a bottom discharge beneath the draft tube (Figure 3,j) is suitable for rivers carrying considerable bed loads.

Ejection in the draft tube may take place in the elbow (Figure 3, l) or in the diffuser (Figure 3,o). Ejection in the draft tube also occurs with ejection turbines (Figure 3,m,n) which are specifically designed for this. The streams mix directly behind the runner. The ejecting stream enters either in the elbow of the draft tube (m) or along the circumference of the runner (n).

Ejection conduits installed until now in large draft tubes are intended to shorten the spillway front by increasing the discharge capacity. An example of this is the conduit inserted in a draft tube with rotatable walls (Figure 4,h).

Ejection through the draft-tube chamber (Figure 3,f,k) is employed only in small HPPs /5/. Ejection through the flume (Figure 3,g) can be used in small and large HPPs (Figure 4,d).

Various combinations of overflow ejection, ejection through conduits, and ejection in the draft tube are possible (Figure 3,p).

Ejection along the HPP front (Figure 3,q) (which has a negligible ejection effect) can be possible by a suitable design of the HPP, and causes the spillway discharge to lower the tailrace level along the HPP front. An example of this was proposed by Prof. Aleksandrov (Figure 4,i). The water, which reaches the tailrace by chutes and flows along the HPP front, has an ejection effect on the turbine discharge. An increase in the head, due to the discharge through the sluice gates adjoining the powerhouse, is according to Lecturer D.O.Seifulla, observed in the Dnepr HPP imeni Lenin. A similar effect of the spillway discharge was observed at the Shevrskii HPP /4/.

4. PRACTICAL UTILIZATION AND DEVELOPMENT OF EJECTION

There has been no report on the building of any new HPP with ejection since Perfil'ev's survey was published in 1932.

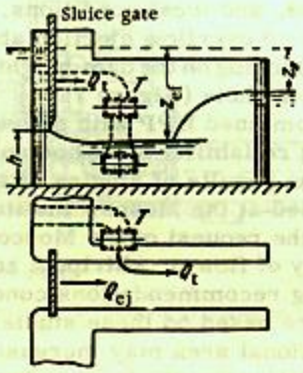

FIGURE 6. HPP with ejection by jump displaced downstream.

The data on existing HPPs with ejection, given by Perfil'ev /15/, can be supplemented only by obsolete information (1927) /19/ on two HPPs. Two 8,000 kw units were installed in the first (Figure 4,a); three ejection conduits

lead into the draft tube of each unit. Two 4,000 kw units were installed in the second HPP; the ejection conduits leading into the draft tubes were closed by gates (Figure 5).

Including these two HPPs, the total capacity of existing HPPs using ejection is only 85,000 kw, that of the largest being 17,700 kw.*

In pre-revolutionary Russia the development of hydropower was in an embryonic stage, and no attempts were made to utilize ejection. However, even then the artificial increase of the head in turbine installations during high water was considered by Russian engineers. An analysis of ejection with jump displaced downstream was published in 1911** (Figure 6). The calculation showed that in one particular case the head can be increased to $z_{ef} = 3{,}68$ m at a difference of levels $z_0 = 2$ m.

Ejection by the scheme shown in Figure 6 is feasible even today for small HPPs installed in the dam piers and supplying local needs.

Ejection has been widely applied in hydroengineering construction only in the USSR, mainly recently. The Kuibyshev HPP, now being built, far exceeds in capacity the sum total of all other existing HPPs with ejection.

Much development in this direction is due to the Soviet hydro-power engineers V. V. Gavrilov, A. M. Morozov, A. Z. Nemchenko, Master of Technical Sciences V. A. Kutsenov, Prof. B. K. Aleksandrov, Doctor of Technical Sciences and Stalin Prize Laureate P. P. Laupman, Master of Technical Sciences S. V. Luzan, N. A. Malyshev, A. I. Baumgol'ts, I. G. Petrov, N. M. Ivantsov, Doctor of Technical Sciences S. A. Egorov (small HPPs), and many others. Thus, all schemes of ejection in the tailrace, shown in Figure 3 (except scheme d) represent designs† of Soviet engineers, mainly those mentioned.

Figures 3 and 4 do not include all possible designs of combined HPPs, which may vary greatly, depending on the capacity and hydraulic parameters, the power equipment used, and local conditions. We shall consider some arrangements of HPPs with overflow ejection above the draft tube. These arrangements differ, depending on the dam height which is determined by the hydraulic scheme as a whole (Figure 7).

Figure 4,b shows a combined HPP with siphon spillway. Previous doubts concerning the operating reliability of siphon spillways in combined HPPs have been removed by the results of studies of spillways of different shapes and dimensions, conducted at the Moscow Institute of Hydraulic Engineering imeni V. R. Williams at the request of the Moscow branch of VNIIG imeni B.E. Vedeneev. No instability of flow or whirlpool zones were observed in siphon spillways. The following recommendations concerning the cross-sectional areas of the spillways are based on these studies. When the head is less than 7 m, the cross-sectional area may increase by up to 30 % from the crown section to the outlet; when the head is between 7 and 10 m, the cross-sectional area should be kept constant; when the head exceeds 10 m, the cross-sectional area should decrease by 15 to 20 %.††

* Perfil'ev includes the 5,000 kw Black River HPP amongst the installations in which ejection is used. Actually, however, ejection is used only in two of its units (8,000 kw each) out of six.

** Izvestiya SPB Politekhnicheskogo Instituta, Vol. 15, No. 1—2, 1911.

† Cf. also Uspenskii, B. S. Gidroelektricheskie stantsii bol'shoi moshchnosti (High-capacity HPPs).—Elektrichestvo, 1952, No. 1.

†† Kovalenko, I. I. Napornye vodosbrosy, sovmeshchennye s turbinnymi blokami gidroelektrostantsii (Spillways Combined with Turbine Bays of HPPs).—Ph. D. thesis, Moskva, 1952.

Designers are, however, cautious in the use of siphon spillways with cross sections constant or increasing toward the outlet, despite the favorable results of model tests. Intricate shapes of spillways may cause zones of negative pressure, not evident from model tests.

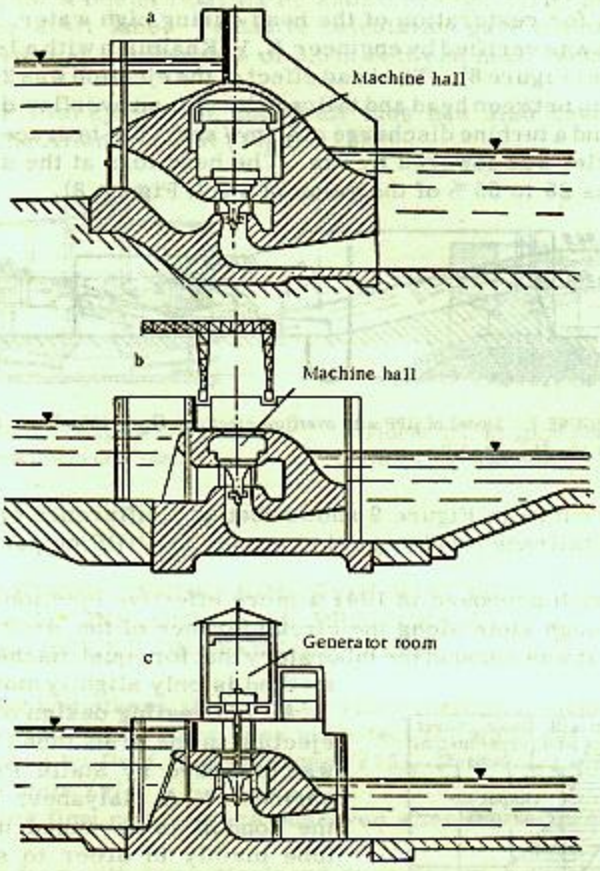

FIGURE 7. Overflow HPPs.

a—built-in machine hall; b—built-in generator room; c—machine hall above weir.

Conduits passing under the scroll casings (Figures 3,h and 73), whose outlets are usually below the tailrace level, are better. Negative pressures are less likely to appear in them, provided their outlines are sufficiently smooth. Many combined HPPs with heads exceeding 10 m have conduits with constant cross section.

Figure 4,c shows an HPP with overflow ejection. Steady flow in the semi-closed spillways is not guaranteed, so that this design will hardly ever be carried out. Figure 4,d shows an ingenious design of a "tower-type" HPP without scroll casing. Overflow ejection is possible here with a suitable configuration of the weir.

Figure 4,e shows an overflow HPP with tubular turbines. The installed capacity of each unit is 1,600 kw, the head is 6.5 m, and the runner diameter is 2 m.

The overflow HPP proposed by Stalin Prize Laureate S. N. Kritskii, Doctor of Technical Sciences, is shown in Figure 4,f. The depth at the draft tube outlet is less than critical (jump displaced downstream). This provides for restoration of the head during high water. The efficacy of this design was verified by engineer N. V. Khalturin with a 1:50 model without turbine (Figure 8). The head effect of the ejection was 2.8 m at a difference of 4.5 m between head and tailrace levels, an overflow discharge of 400 m^3/sec, and a turbine discharge of 40 m^3/sec. The tailrace level at the draft-tube outlet was lowered by 4 m. The head loss at the draft-tube outlet was thus 25 to 35 % of the value of z (cf. Figure 8).

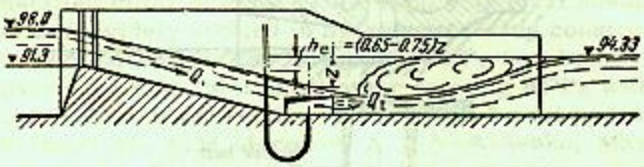

FIGURE 8. Model of HPP with overflow ejection: $Q_w = 400\ m^3$/sec, $Q_t = 40\ m^3$/sec; $z = 4.0$ m.

The output curve in Figure 9 shows that at a difference of 4.5 m between the head- and tailrace levels ejection causes the HPP output to be more than doubled.

Prof. Milovich proposed in 1941 a more effective ejection method by discharge through slots along the circumference of the draft tube (Figure 4,g). It was found in the laboratory that for equal discharges this method is only slightly more effective.

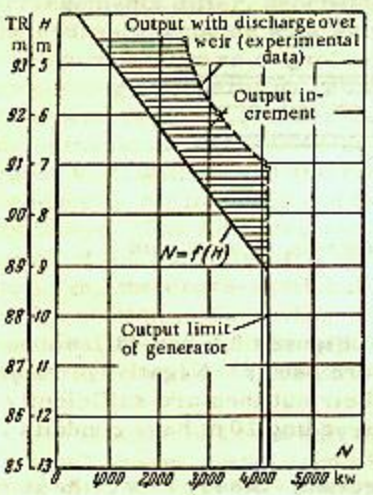

FIGURE 9. Output curve of HPP with weir ejector.

An interesting design of an HPP with ejection in the draft tube (Figure 4,h) was proposed by Stalin Prize Laureate engineer N. A. Malyshev. In this case the conduit is arranged in the draft tube mainly in order to shorten the spillway front and to carry the construction discharges through the HPP. This is achieved through the large discharge capacity of the ejection conduits. The draft tube has its normal shape when the rotating gates of the conduit outlets are closed. It was found in the laboratory that the output effect of ejection is 13 to 14 % with equal excess and turbine discharges.

A very unusual HPP design is shown in Figure 4,i. Discharge of flood water through the spans adjoining the HPP permits ejection along the HPP front.

An 8,000 kw HPP in operation /18/ is shown in plan in Figure 4,j. Three turbine bays forming piers are located along the dam. This makes possible ejection by flood water at the sides of the draft tubes.

Output restoration by ejection* forms part of existing designs of tidal HPPs.

One design for a Soviet tidal HPP, shown in Figure 10, provides for ejection in the draft tube. Tentative calculation gave the head effect of ejection as 0.18 m at a difference of 0.5 m between head- and tailrace levels.

A tidal HPP with ejection in the draft tube has also been designed for a bay on the Atlantic coast (Figure 11).

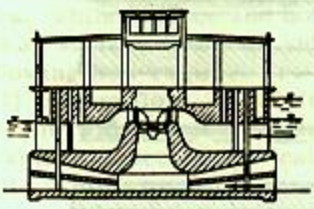

FIGURE 10. Design of Soviet tidal HPP with ejection in draft tube.

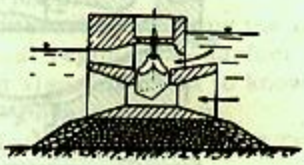

FIGURE 11. Design of tidal HPP with ejection in draft tube.

5. WAVE PATTERN BEHIND HPP WITH EJECTION INTO TAILRACE. INFLUENCE OF PRESSURE AT DRAFT-TUBE OUTLET ON WAVE PATTERN

Prof. Egorov and others showed that with overflow ejection the turbine discharge entering the tailrace does not affect the wave pattern behind the HPP, established by Prof. A. A. Sabaneev /16/, Prof. I. I. Levi /13/, and later by D. I. Kumin /9/.

The following flow regimes are observed when the tailrace level** rises (Figure 12).

A. Bottom flow with jump displaced downstream. This flow can exist whatever the height of the end sill, but is acceptable only with ejection by a jump displaced downstream, as at the Mitchell HPP (Figure 3,d).

B. Bottom flow with submerged jump. This is a possible and at times unavoidable operating condition of an overflow HPP. Thus, if no ordinary spillway dam is provided, or when the spillway-dam apron is located at a high level on the floodplain, this flow regime is sometimes unavoidable at the beginning of flood-water discharge. A characteristic feature of this flow regime is the surface roller, which ordinarily stops floating bodies entering from the headrace. An air pocket may form beneath the nappe if air has free access.

Bottom flow with submerged jump is in this book called simply bottom flow.

* Slisski, S. M. Sovremennoe sostoyanie problemy ispol'zovaniya prilivno-otlivnoi energii okeanov i morei (Present State of Utilization of Tidal Power of Oceans and Seas).— Trudy MEI, No. 5. 1950.

** When the tailrace level drops, the sequence of flow regimes is inverse.

When the end sill is low, bottom flow is maintained until the end sill is submerged. No gradual change of flow regime with rise of tailrace level is observed. Kumin /9/ calls this case an anomaly in the change of flow regimes.

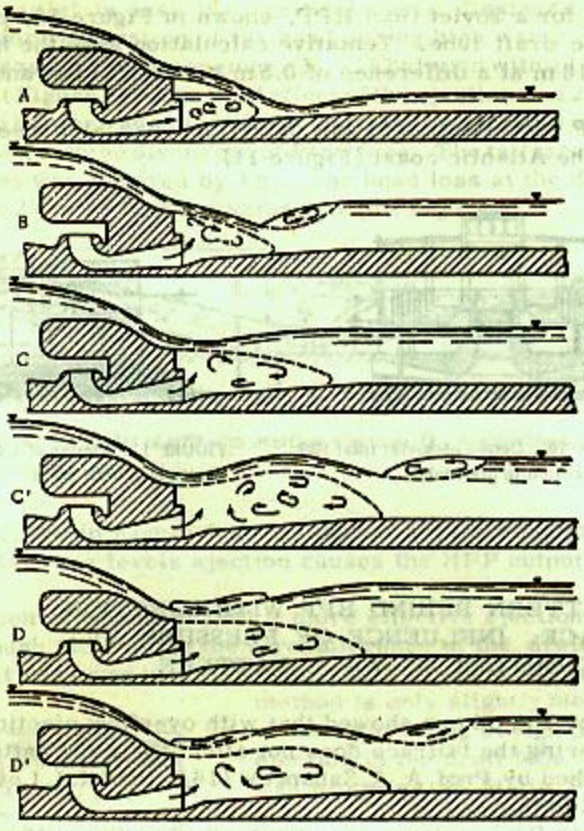

FIGURE 12. Variation with tailrace level of wave patterns behind an overflow HPP.

The first critical regime is generally unstable. A gradual transition from the bottom flow (B) to surface flow (C) and vice versa, accompanied by large fluctuations of the tailrace level, is usually observed.

If the tailrace is much wider than the length of the spillway front, no instability is observed during transition from bottom flow to surface flow and vice versa. The first critical regime does not appear in this case.

C. Flow with surface jump is characterized by the absence of surface rollers: floating bodies entering from the headrace are carried away by the stream without being stopped. This flow regime will be called surface flow.

The second critical regime does not exist by itself, but corresponds to the instant of transition from surface flow (C) to surface flow with submerged jump (D).

D. Surface flow with submerged jump is characterized by the presence of surface and bottom rollers. This flow regime is undesirable when ejection is used, since it reduces its effect.

Kumin /9/ showed that, in addition to the pure "classic" wave patterns (bottom and surface flows), there also exist mixed forms: surface flow with several surface rollers, surface and bottom flow (C') (which appears when the surface flow regime approaches the second critical regime), and finally, surface and bottom flow with submerged jump (D'). Mixed flow regimes have not yet been sufficiently investigated; the conditions under which they appear and change have not been determined. These flow regimes are not characteristic of the ejection process. Surface flow with several rollers as well as surface and bottom flow can be considered as surface flow, while surface and bottom flow with submerged jump can be considered as surface flow with submerged jump.

The following flow regimes are thus of interest in studying the ejection process: 1) bottom flow; 2) the first critical regime; 3) surface flow; 4) surface flow with submerged jump. It is also important to know the instant at which the second critical regime appears.*

We shall examine now the connection between the type of flow regime and the pressure beneath the nappe.

Prof. A. A. Sabaneev /16/ found that for a given discharge the pressure beneath the nappe is a function of the tailrace level.

According to him, the flow regime depends on the sign of the magnitude

$$\gamma(h_0 - h_1),$$

where h_0 is the piezometric head beneath the nappe, measured from the toe level; h_1 is the depth of the nappe at the end sill.

When $h_0 - h_1 > 0$ the nappe is deflected upward and surface flow occurs; when $h_0 - h_1 < 0$ the nappe is deflected downward, and bottom flow ensues.

D. I. Kumin observed the curvature of the free nappe surface and discovered a certain discrepancy between A. A. Sabaneev's hypothesis and reality /9/.

Thus, according to A. A. Sabaneev, the first critical regime corresponds to flow of the nappe from the end sill along the tangent to its surface ($\eta = 0$),** while, according to Kumin "the position of the boundary considered (i.e., of the first critical regime – S.S.) in the region $\eta < 0$ is an unquestionable experimental fact" (Kumin, D. I., /9/, p. 37).

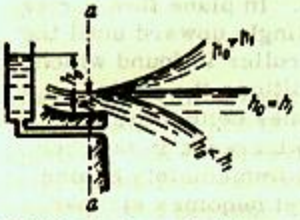

FIGURE 13. Connection between nappe curvature and piezometric head beneath nappe (according to A. A. Sabaneev).

The correctness of Kumin's assertion has been verified experimentally by the author who found that at the transition from surface flow to bottom flow the piezometric head h_0 beneath the nappe is always less than the nappe depth at the toe, i.e., $h_0 < h_1$ or $\eta < 0$. Furthermore, when the discharge over the dam is small a negative value † of h_0 may correspond to the first critical regime.

* The flow regimes not mentioned, which appear with further rise of the tailrace level, are discussed in N. N. Belyashevskii's paper "K raschetu sopryazheniya b'efov za nizkonapornymi plotinami" (Analysis of Wave Pattern Behind Low-head Dams). – Izvestiya instituta gidrologii i gidrotekhniki AN Ukr. SSR. Vol. 8. 1951.

** Here η is the nappe curvature; for $\eta < 0$ the nappe is convex upward.

† Experimental data by the author, verifying this assertion, are given in § 19.

The piezometric height h_0, which determines the pressure below the jet, is thus always less than the jet depth at the toe during bottom flow, the first critical regime, and surface flow approximating bottom flow. The jet is convex upward when it descends from the batter. The pressure below the jet rises with the tailrace level; the piezometric head becomes larger than the jet depth; the jet assumes a direction tangential to the toe, and then becomes concave upward.

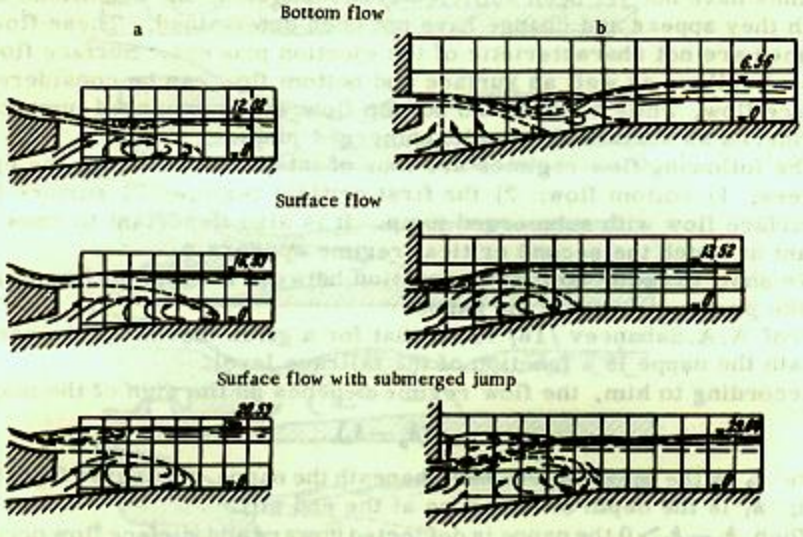

FIGURE 14. Sequence of flow regimes in three-dimensional models of combined HPPs.

a — spillway HPP; b — HPP with pressure conduits.

The sequence of flow regimes behind a combined HPP with pressure conduits is the same as that behind an overflow.

This sequence of flow regimes is altered under three-dimensional conditions, i.e., when the total width of the spillway bays (excluding the piers) is considerably less than the tailrace width. In plane flow a rise of the tailrace level causes the jet to bend increasingly upward until the surface jets turn back toward the toe. A surface roller is found which submerges the jet. Under three-dimensional conditions the jet is submerged by water coming from the whirlpool zones behind the piers or from adjacent bays which carry no discharge. An increase in tailrace depth is accompanied by a rise of the free surface immediately behind the HPP. An inverse slope is formed which at first becomes steeper rapidly. When the toe or spillway openings are flooded, the slope decreases until the free surface of the tailrace becomes almost horizontal. Figure 14 shows the flow regimes observed in the hydraulic laboratory of MEI imeni V. M. Molotov with models of combined HPPs under three-dimensional conditions. No second critical regime appeared: the surface jump was submerged by water coming from the whirlpool zones behind the piers.

The ratio of the width of the dam openings to the tailrace width was 0.40 in the model of an overflow HPP (Figure 14,a), while the [corresponding] ratio was 0.57 in the model of an HPP with conduits (Figure 14,b).

Transition from surface flow to bottom flow under three-dimensional conditions (Figures 14,a) is peculiar. The surface roller characteristic of bottom flow is, in contrast to plane flow, formed near the end sill. This is also due to the influx of water from the whirlpool zones behind the piers.

The direction of the turbine discharge leaving the draft tube should be noted in Figure 14; this flow is deflected sharply upward in all cases.

6. PIEZOMETRIC EFFECT OF EJECTION, HEAD EFFECT OF EJECTION, AND ACTUAL HEAD WITH EJECTION INTO TAILRACE

The hydraulic aspect of computing the ejection effect consists in determining the piezometric effect h_{ej} and the head effect ΔH of ejection.

The piezometric effect of ejection is determined by the distance between the tailrace level ∇TR (at a distance from the HPP) and the plane of the piezometric head ∇h_0 at the draft-tube outlet (Figure 15,b).

In the case of overflow ejection the plane of the piezometric head at the draft-tube outlet does not coincide with the free surface of the tailrace in section I-I, since the head h_0 beneath the nappe may be either larger or smaller than the nappe depth h_1 at the toe. In this case the piezometric effect of ejection is

$$h_{ej} = \nabla TR - \nabla h_0, \qquad (1)$$

where

$$\nabla h_0 = \nabla \text{ (toe)} + h_0.$$

With spillway ejection, h_{ej} is also determined by the distance between ∇TR and ∇h_0 when the spillway openings are not flooded.

When the spillway openings are flooded (Figure 35), the pressure at the draft-tube outlet corresponds to the level ∇h_{tr} in section I-I. In this case

$$h_{ej} = \nabla TR - \nabla h_{tr} \qquad (1')$$

where h_{tr} is the tailrace depth in section I-I.

The gain in head is not solely determined by the piezometric effect of ejection, since a pressure drop at the draft-tube outlet (a drop Δh in the level of the free surface of the tailrace in section I-I) occurs also without ejection, and because additional losses ΔH_w are caused by the spillway discharge passing through the receiver ahead of the turbine.

The head effect ΔH of ejection, which determines the gain in head,* is therefore

$$\Delta H = h_{ej} - \Delta h - \Delta H_w \qquad (2)$$

* The change in the velocity head in the headrace can be neglected.

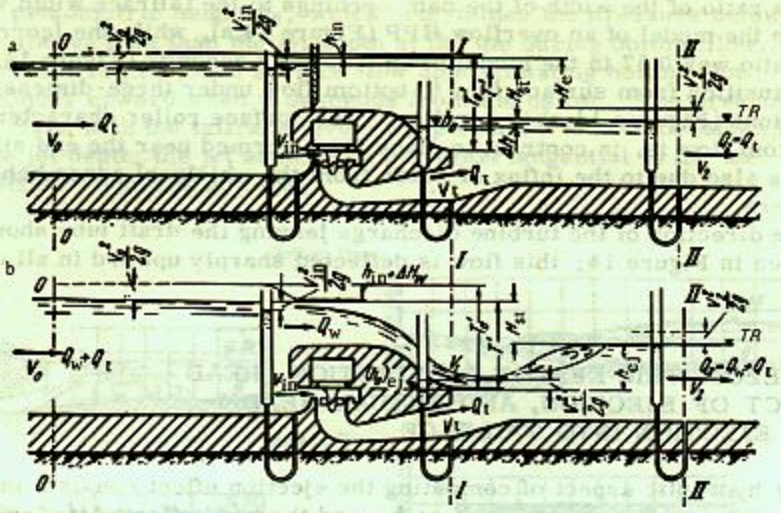

FIGURE 15. Hydraulic schemes of overflow HPP.

a—sluice gate of dam lowered — no overflow discharge; b—overflow discharge exists.

The additional losses ΔH_w depend on the flow conditions in the receiver ahead of the turbine and in the scroll casing.

The great variety of possible designs of combined HPPs, the differences in the ratios of the areas of conduit outlets and scroll casings and in their relative positions, the variations in receiver length and in the ratio between excess and turbine discharges, cause considerable complications. In a detailed analysis it is necessary to distinguish: 1) with overflow ejection, between designs in which the directions of the turbine and overflow discharges in the headrace essentially coincide (Figure 3,a, b) and designs in which they are mutually perpendicular (Figure 3,f); 2) with ejection through conduits, between designs with bottom intake and with surface intake (Figure 3,h, i), i.e., with intake below or above the scroll casing.

Experimental data show that the additional energy losses ΔH_w depend on the effects of the excess discharge on the magnitude and direction of the turbine discharge inside the receiver.

When a large contraction of the excess and turbine discharges takes place in the receiver, as shown in Figure 18, the additional energy losses ΔH_w are considerable, and their neglection may lead to exaggerated values of the ejection effect.

If additional energy losses are small, the head effect of ejection can be assumed to be

$$\Delta H = h_{ej} - \Delta h. \tag{3}$$

The head effect of ejection can be expressed through the levels of the piezometric-head plane in section I-I without ejection (∇h_0) and with ejection ($(\nabla h_0)_{ej}$:

$$\Delta H = \nabla h_0 - (\nabla h_0)_{ej}, \tag{4}$$

where

$$\nabla h_0 = \nabla TR - \Delta h,$$
$$(\nabla h_0)_{ej} = \nabla TR - h_{ej}.$$

The drop Δh is caused by the difference between the velocities in sections I-I and II-II. The value of Δh in (3) and (4) is determined as for submerged broad-crested dams,* using either the momentum equation or Bernoulli's equation. For instance, we obtain from the difference between the velocity heads in sections I-I and II-II:

$$\Delta h = \eta \frac{(V_m^2 - V_3^2)}{2g}, \tag{5}$$

where η is a correction coefficient, found by the author to vary between 0.5 and 0.9. It can be taken as 0.7 on the average.

In a combined HPP with ejection into the tailrace the effective head corresponds at zero ejection to the head in an ordinary river HPP (Figure 15,a):

$$H_e = (H_{st} + \frac{V_0^2}{2g} - h_{in}) - \frac{V_3^2}{2g}, \tag{6}$$

where H_{st} is the geometric difference between the headrace and tailrace levels, or the so-called static head; $\frac{V_0^2}{2g}$ and $\frac{V_3^2}{2g}$ are the velocity heads in sections 0-0 and II-II, respectively; h_{in} is the inlet loss.

When ejection takes place, the effective head can no longer be determined from (6). Taking into account the head gain due to ejection, i.e., the head effect ΔH of ejection, we obtain

$$(H_e)_{ej} = H_e + \Delta H. \tag{7}$$

7. POWER EFFECT OF EJECTION. ADDITIONAL ENERGY LOSSES DURING EJECTION

The final aim of the analysis of a combined HPP is to determine the power effect of the ejection. The question arises whether the head increment, obtained by (2), (3), and (4), corresponds to the true power increment (i.e., to the power effect of the ejection).

We shall first examine the experimental data which permit the accuracy of (3) and (4) to be verified.

As already noted, (3) and (4) are applicable when no large contraction of the excess and turbine discharge takes place in the receiver, as, for example, in Figure 3,a.

A model of an overflow HPP (with turbine), corresponding to Figure 3,a, was studied by Kh. Sh. Mustafin /14/. The curves obtained by him are shown in Figure 16,a. The abscissae represent the head effect $\Delta H_{p/\gamma}$ of the ejection,** determined from the readings of piezometric tubes (hence the subscript p/γ), while the ordinates represent the head effect ΔH_N

* Cf., for instance, Berezinskii, A. R. Propusknaya sposobnost' vodosliva s shirokim porogom (Carrying Capacity of a Broad-crested Dam). — Stroiizdat. 1950.

** Neglecting the additional losses ΔH_w

of the ejection, referred to the power increment ΔN caused by ejection* (hence the subscript N). The experimental points lie on a line making angles of 45° with the axes when ΔH_{pi_T} and ΔH_N coincide. This agreement is best for a horizontal apron and small values of ΔH_{pi_T}.

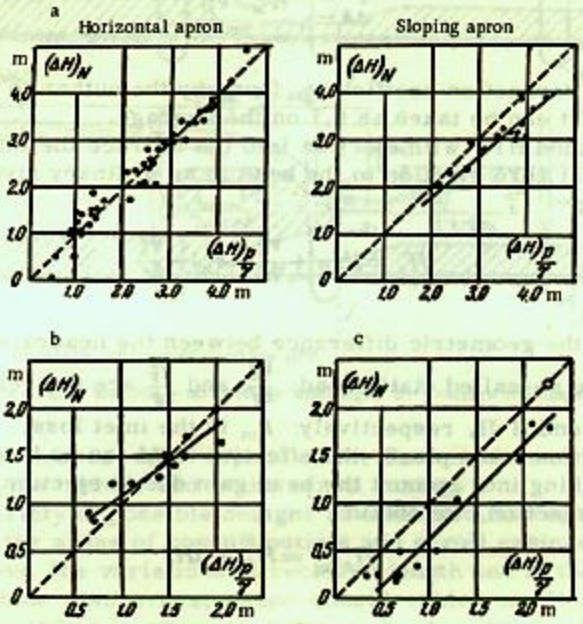

FIGURE 16. Comparison of head effect ΔH_{pi_T} of ejection, found from readings of piezometric tubes, with head effect ΔH_N, referred to power increment due to ejection.

a—Mustafin's experiments with 1:20 model of overflow HPP; b—Kumin's and Preobrazhenskii's experiments with 1:50 model with ejection through conduits; c—author's experiments with 1:50 model with ejection through conduits.

Kh. Sh. Mustafin, who studied this problem thoroughly, concluded that piezometric tubes placed at the draft-tube outlet indicate the ejection effect correctly only when the bottom of the draft tube goes over smoothly into the apron; when the transition is steep, the ejection effect indicated by piezometric tubes (including Δh) will be incorrect.

No additional losses were observed by Mustafin during ejection.

According to Prof. S. A. Egorov, who studied overflow ejection /4/ on a model with a turbine, corresponding to Figure 3,c, full agreement exists between the turbine power and the head measured by piezometric tubes placed at the draft-tube outlet and in the scroll casing. The experimental points $N = f(H_t)$ for experiments with and without ejection lie on the same curve (Figure 17); this is convincing proof that the actual head corresponds in this case to the head H_t determined from the difference between

* ΔH_w is obtained from ΔN by means of the model-turbine characteristic.

the pressures in the scroll casing and at the draft-tube outlet. However, the losses at the entrance to, and inside the scroll casing are not included in this calculation; thus, such losses, if present, were not detected.

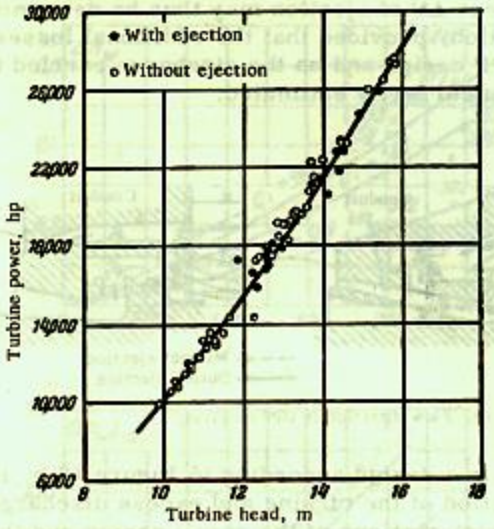

FIGURE 17. Power as function of head with and without ejection, according to S.A Egorov.

P.M. Slisskii studied a model without turbine, similar to that tested by S.A. Egorov. He found that when the sluice-gate opening is small, the pressure in the inlet section of the scroll casing is practically determined by the headrace level. At large openings of the sluice gate the pressure drop in the inlet section of the scroll casing (at the same turbine discharge) becomes considerable. The decrease in energy, determined by this pressure drop, is probably due both to the lowering of the free stream surface above the scroll casing and to losses during deflection in the scroll casing. In the case studied by P.M. Slisskii these additional losses ΔH_w (referred to full scale) were 10 cm, or about 1 % of the actual head.

The ratio between the excess and turbine discharges in the experiments of S.A. Egorov and P.M. Slisskii did not exceed 5:1. At these discharge ratios the additional losses in such designs are apparently small and may be neglected.

The magnitudes $\Delta H_{p/t}$ and ΔH_N (Figure 16,b) were also compared by D.I. Kumin and N.A. Preobrazhenskii, who used an HPP model with conduits above the scroll casing. The results are basically similar to those of Kh.Sh. Mustafin.

This same problem was studied in detail by the author at the MEI laboratory imeni V.M. Molotov on a model corresponding to Figure 18,b. The magnitude $\Delta H_{p/t}$ was always larger than ΔH_N when the additional losses ΔH_w were neglected (Figure 16,c); the difference between $\Delta H_{p/t}$ and

ΔH_N increased with the discharge through the receiver. This indicates that the difference between $\Delta H_{p/T}$ and ΔH_N is mainly due to the additional losses ΔH_w which are equivalent to the lost power,* i.e.,

$$\Delta H_w = \Delta H_{p/T} - \Delta H_N$$

The power effect ΔN of ejection may thus be determined from the head effect ΔH of ejection, provided that the additional losses ΔH_w, which depend on the HPP design and on the discharge carried through the receiver, have been correctly estimated.

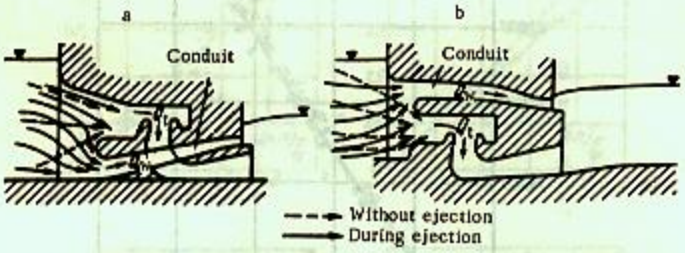

FIGURE 18. Flow direction in HPP receiver.

The loss ΔH_w in a design according to Figure 18,b, is represented in Figure 19 as function of the turbine and excess discharges for a ratio of 3:1 between the inlet sections of the scroll casing and the conduit; the curves have been plotted from experimental results obtained with a model. The abscissae represent the excess discharge Q_w, while the ordinates represent the additional losses ΔH_w; the curves are plotted for different values of the turbine discharge Q_t. The data of Figure 19,a correponds to a scroll-casing inlet section area of 290 m^2.

Thus, ΔH_w is 0.55 m at an excess discharge of 900 m^3/sec and a turbine discharge of 580 m^3/sec. These losses are due to the contraction of the turbine stream in the receiver during ejection. They may also be due to flow perturbations at the scroll-casing inlet, and should be reduced to a minimum by experimental determination of the optimum shape and dimensions of the receiver.

In any particular case ΔH_w can be determined only in the laboratory, as was done for the design shown in Figure 18,b. For similar designs, in which the ratio between the areas of the inlet sections of scroll casing and conduits is approximately 3:1, ΔH_w can be estimated from Figure 19,b. The curves have been referred to a model having a scroll-casing inlet section area $(\omega_v)_M$ of 1 m^2. When the inlet section area of the scroll casing is ω_v m^2, the scale factor is $\lambda = \sqrt{\frac{\omega_v}{1.0}} = \sqrt{\omega_v}$.

The condition of equality of Froude numbers yields

$$(Q_w)_M = \frac{Q_w}{\lambda^{5/2}}, \quad (Q_t)_M = \frac{Q_t}{\lambda^{5/2}};$$

* Nevertheless, the reasons for the difference between $\Delta H_{p/T}$ and ΔH_N in Kh. Sh. Mustafin's experiments with a sloping apron remain unclear. Mustafin himself suggested that this was due to the effect of the steep slope of the apron on the readings of the piezometric tubes. The difference $\Delta H_{p/T} - \Delta H_N$ might therefore not be entirely due to the additional losses, especially in the case of flow perturbations at the draft-tube outlet.

the additional losses are $\Delta H_w = \lambda \cdot (\Delta H_w)_M$, where $(\Delta H_w)_M$ is found from Figure 19,b.

An example of the use of this diagram is given in § 29.

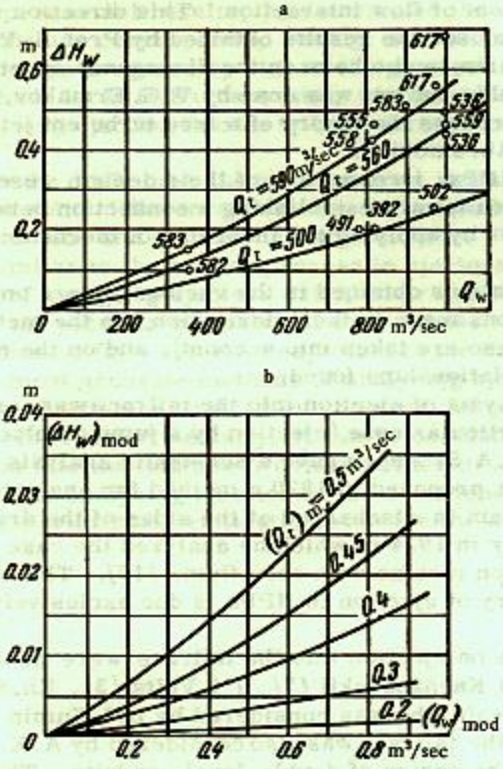

FIGURE 19. Additional losses during ejection as function of excess and turbine discharges (HPP design according to Figure 18,b).

a—referred to full scale; area of scroll-casing inlet section = = 290 m²; b—model; area of scroll-casing inlet section = = 1 m².

8. CONTEMPORARY STATE OF THE THEORY OF EJECTION IN HPPs

The impulse effect of the mixing of two streams, utilized for the first time in 1852 in the water-jet pump, is today exploited in jet devices of different functions and designs.

The many theoretical studies of the mixing of streams in jet devices, the first of which appeared in 1863, can be divided into two groups.

The first and larger group deals with the mechanical and energetical aspects of the process. Their purpose is to determine the connection

between the pressures and velocities on surfaces and in sections forming the flow boundaries, by solving simultaneously the equations of momentum, kinetic energy, and continuity. The equation of the kinetic-energy theorem is generally used in the form given by D. Bernoulli.

The second group deals with the internal structure of the mixing zone, and the mechanism of flow interaction. This direction was taken by N.A. Rzhanitsin,* who used the results obtained by Prof. A. Ya. Milovich, Prof. V. G. Zamarin, and others on the divergence of jets. The most recent work on this subject was done by V. G. Ermakov,** who applied to the ejection process the theory of a free turbulent jet, developed in TsAGI by G. N. Abramovich.

As regards HPPs, irrespective of their design, research has until now only been directed toward establishing a connection between the pressures and the velocities by applying the theorems of mechanics to an isolated mass of water.

The final equations obtained in the various papers on ejection depend on the assumptions made in their derivation, on the methods of estimating the losses (if these are taken into account), and on the mathematical development of the relationships found.

The first analysis of ejection into the tailrace was carried out in Russia in 1911 for a particular case (ejection by a jump displaced downstream). In 1917, Prof. A. A. Sabaneev gave a schematic analysis of ejection in the draft tube. Krei proposed in 1920 a method for analyzing ejection when the ejecting stream is discharged at the sides of the draft tube. Alfors published a paper in 1924 in which he analyzed the case of a double-runner horizontal ejection turbine with open flume /15/. The subsequent development of the theory of ejection in HPPs is due exclusively to Soviet scientists.

Recent papers on ejection into the tailrace were published by S. A. Egorov /4/, B. D. Kachanovskii /7/, I. I. Veits /3/, Kh. Sh. Mustafin /14/. Ejection in the draft tube was considered by D. I. Kumin /10/.

Ejection into the tailrace was also considered by A. K. Ananyan /2/ in connection with the design of double-level conduits. This paper is, however, not directly concerned with ejection in HPPs. Ananyan considered the increase in carrying capacity of bottom culverts of scours, due to ejection above the culverts; his analysis is based on the premises made by others in earlier papers, and on the same basic equations of mechanics.

We mention the schematic analysis of ejection in the draft tube, made by Prof. P. N. Kamenev in 1939 during his work on a Soviet tidal power plant in the Barents Sea. The paper of Prof. I. I. Levi on overflow ejection will be discussed below.

Ejection into the tailrace takes place when a free surface exists in the mixing zone. Its analysis, in particular in the case of overflow ejection, is based on papers by A. A. Sabaneev /16/ and I. I. Levi /13/ on the wave pattern behid a dam during the surface flow. The method by which the pressure beneath the nappe is determined in these papers makes it possible to apply the theorem of momentum to the analysis of overflow ejection and of most cases of ejection through conduits.

* Rzhanitsin, N. A. Vodostruinye nasosy (Water-jet Pumps).— Moskva-Leningrad. 1938.

** Ermakov, V. G. Primenenie teorii strui k raschetu protsessa ezhektsii (Application of the Jet Theory to the Analysis of the Ejection Process).— Trudy TsKTI. Vol. 12, Moskva-Leningrad. 1949.

Since the analysis of ejection into the tailrace is based on the same premises as that of the wave pattern behind a weir during surface flow, the same formulas may be used when the turbine discharge is negligibly small.

S.A. Egorov's study, devoted mainly to overflow ejection, was accompanied by experiments with a large-scale model with a turbine. Comparing the theoretical and experimental results, he determined the extent to which the theoretical relationships correspond to reality; it thus became possible to use the relationships proposed by him in design practice. A similar comparison was made by B.D. Kachanovskii, who proposed his own formulas for analyzing ejection into the tailrace through a conduit beneath the draft tube.

With ejection in the draft tube there is no free surface in the mixing zone. This causes some differences between the methods of analyzing ejection in the draft tube and ejection into the tailrace. The former process is very similar to the mixing process in ejectors. Although very accurate methods of analyzing ejectors exist, their application to HPPs is complicated by the peculiar geometry of draft tubes. This is why the ejector theory cannot be fully applied to ejection in the draft tube.

Comparing the most accurate methods of analyzing ejection into the tailrace and in the draft tube, taking into account the extent to which they have been verified experimentally, it can be concluded that while the analysis of ejection into the tailrace provides sufficient accuracy in many cases, the methods of analyzing ejection in the draft tube require further development and experimental verification even for the simplest cases.

Chapter II

ANALYSIS OF OVERFLOW EJECTION

9. ASSUMPTIONS MADE AND THEIR EXPERIMENTAL VERIFICATION

The analysis of ejection is always based on the equations of momentum and energy.

The momentum equation, established for sections I-I and II-II of the tailrace of a combined HPP (Figures 15,b and 27), in particular of an overflow HPP, is

$$\frac{1}{g}[\alpha_1(Q_s+Q_t)V_2-\alpha_2 Q_w V_1\cos\alpha-\alpha_3 Q_t V_t\cos\theta]\Delta t=\Sigma P\Delta t, \qquad (8)$$

where Q_w and Q_t are the overflow and turbine discharges respectively; V_1, V_2 and V_t are the flow velocities in sections I, II, and at the outlet of the draft tube; α, θ are the angles between the vectors of the average velocities and the horizontal; α_1, α_2 and α_3 are coefficients by which the nonuniformity of the velocity distributions are taken into account; γ is the specific weight of water; g is the gravitational acceleration; Δt is an element of time.

The left-hand side of (8) represents the change in momentum of the mass of water enclosed between sections I-I and II-II, while the right-hand side represents the total impulse due to the forces acting on this mass.

The energy equation is applied to sections 0-0 in the headrace and I-I in the tailrace in the form given by D. Bernoulli.

In considering overflow ejection, we make the following assumptions:

1. The pressure distribution in the overflowing nappe is linear in the zone of the end sill during surface flow; the gage pressure varies from zero at the surface to γh_0 beneath the nappe (Figure 20,a).

2. During bottom flow, irrespective of the pressure beneath the overflowing nappe, the pressure diagram for section I-I, which [in fact] is parabolic (see below), is assumed to form a triangle with base equal to the nappe depth h_1 and height equal to $\frac{1}{2}h_1$ (Figure 20,b).

3. The pressure in the nappe flowing over a nonflooded broad-crested dam (Figure 20,c) (where the depth is nearly critical) varies according to the hydrostatic law $p\approx\gamma h$ and is independent of the tailrace level.

4. The pressure beneath the nappe in the zone of the end sill (including the draft tube outlet), varies according to the hydrostatic law.

5. The pressure at the pier ends in the whirlpool zones is determined by the piezometric head beneath the nappe in the toe plane of the end sill and varies also according to the hydrostatic law (Figure 21). With ejection at the sides of the draft tube (Figure 28), the free surface level and the pressure in

section I-I of the middle span are determined by the piezometric head beneath the nappes from the adjacent spans.

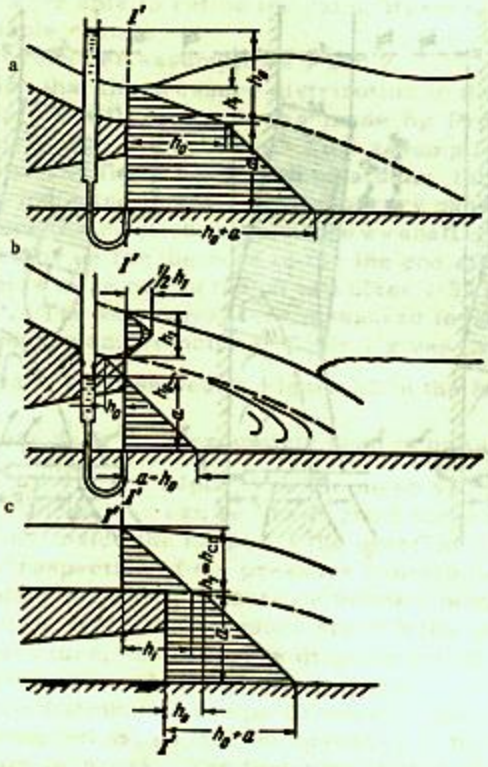

FIGURE 20. Pressure in end-sill zone.

a—surface flow; b—bottom flow; c—broad-crested dam.

6. The pressure distribution over the sloping part of the apron depends on the flow regime in the tailrace and on the point where the nappe impinges on the apron; it is assumed to be as shown in Figure 22.

7. The kinetic energy and the momentum can be calculated with sufficient accuracy from the mean flow velocity, i.e., the correction factors α_i, by which the nonuniformity of the velocity distributions is taken into account, are assumed to equal unity.

8. Friction on the channel bottom of the tailrace is negligibly small.

Assumptions 7 and 8 are generally made when problems similar to the one discussed are being solved. In the case of ejection, the deviation of the averaged local velocities from the mean velocity is negligible both in the nappe on the dam and in the tailrace. These deviations may be considerable at the draft-tube outlet; this is, however, unimportant since the velocities there are small. It can therefore be assumed that $\alpha_I = 1$.

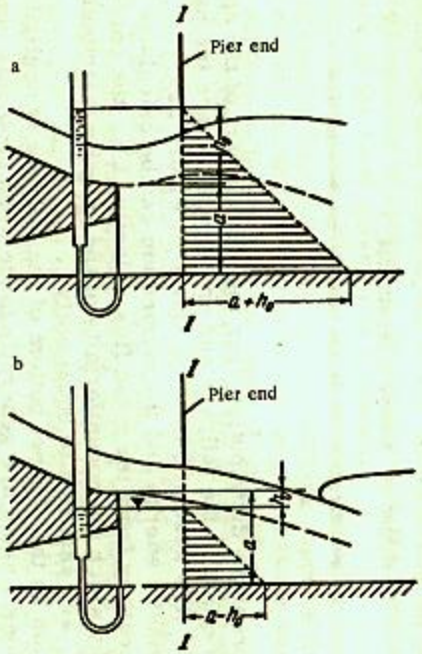

FIGURE 21. Pressures at pier ends.

a—surface flow; b—bottom flow with air pocket beneath nappe.

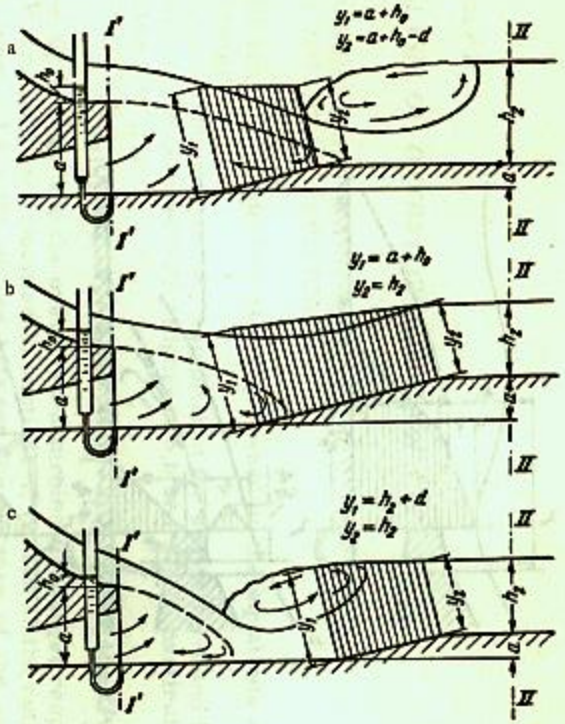

FIGURE 22. Pressures on sloping part of apron.

a—bottom roller on sloping part; b—sloping part in zone of dynamic effect of nappe; c—sloping part far downstream of structure.

Assumptions 1, 3, 4, and, in part, 5 were made earlier by other authors deriving the relationships given in Chapter IV. Nevertheless, they were verified experimentally by us. Assumptions 2, 5, and 6 are new, and are formulated and used for the first time in this book. With the aid of these assumptions we were able to refine the calculations and obtain relationships giving more reliable results.

We shall first consider assumptions 1 and 2.

The assumption that the pressure distribution in the overflowing nappe (in the zone of the end sill) is linear was made by Prof. A. A. Sabaneev /16/, and later by Prof. I. I. Levi /13/. This assumption was then extended by many authors to any flow regime behind a dam; this is arbitrary in the general case, as indicated in some contemporary papers.* To determine the actual pressure distribution in the nappe we shall consider the pressure diagrams obtained by us for the zone of the the end sill.

The experiments were conducted on two plane 1:52 and 1:80 models of an overflow HPP. The velocities were measured in both cases by Pitot tubes. The pressures and velocities (Table 1 gives data on the corresponding flow regimes) are represented in Figure 23 in the form $\frac{p}{\gamma}=f\left(\frac{h}{h_1}\right)$ and $\frac{U}{V_{av}}=f\left(\frac{h}{h_1}\right)$, where $\frac{p}{\gamma}$ is the piezometric head in units of the depth h_1, U is the local velocity in the nappe, V is the mean velocity.

The following conclusions can be drawn from these pressure diagrams:

a) the pressure inside the nappe (at the overflow edge of the toe) is always positive irrespective of the pressure beneath the nappe; only at the lower nappe boundary may the pressure be below atmospheric;

b) in bottom flow, when the pressure beneath the nappe is less than the hydrostatic pressure, the pressure diagram for the nappe is parabolic, its area being assumed equal to that of a triangle;

c) the pressure distribution is approximately linear only in surface flow.

Our third assumption states that the pressure in the water flowing over a broad-crested dam is $p=\gamma h$. The flow may in this case be considered to vary slowly and have a hydrostatic pressure distribution,** as assumed by us. Some authors also assume a hydrostatic pressure distribution in the nappe above the batter of a round-crested dam, considering a section 1.5 to 2 nappe thicknesses † upstream of the end sill. No experimental data verifying a hydrostatic pressure distribution have been published for this case. Our experiments have shown that the pressure distribution upstream of the end sill depends not only on the distance between the section considered and the end sill, but also on the distance of this section from the point where the sloping part of the dam goes over into the straight part forming the end sill. Prof. M. D. Chertousov assumes that when the section considered is located at the end sill far from the batter, the momentum equation cannot be applied.††

The hydrostatic pressure distribution in the end-sill zone (assumption 4) has been repeatedly verified experimentally. A deviation from the hydrostatic distribution can be expected at the draft-tube outlet as a result

* Cf. Kumin, D. I. /19/, p. 13.

** Cf., for instance, Sukhomel, G. I., I. L. Rozovskii, and others. Vodosliv s shirokim porogom (Broad-crested Dams).— Izd. Akademii nauk Ukrainskoi SSR, Kiev, 1949.

† Kumin, D. I. /9/, p. 13

†† Chertousov, M. D. O raschete sopryazheniya b'efov dlya plotin s vertikal'nym ustupom (noskom) (Flow behind Dams with Vertical Batters (Toes)).— Gidrotekhnicheskoe stroitel'stvo, No. 4, 1952.

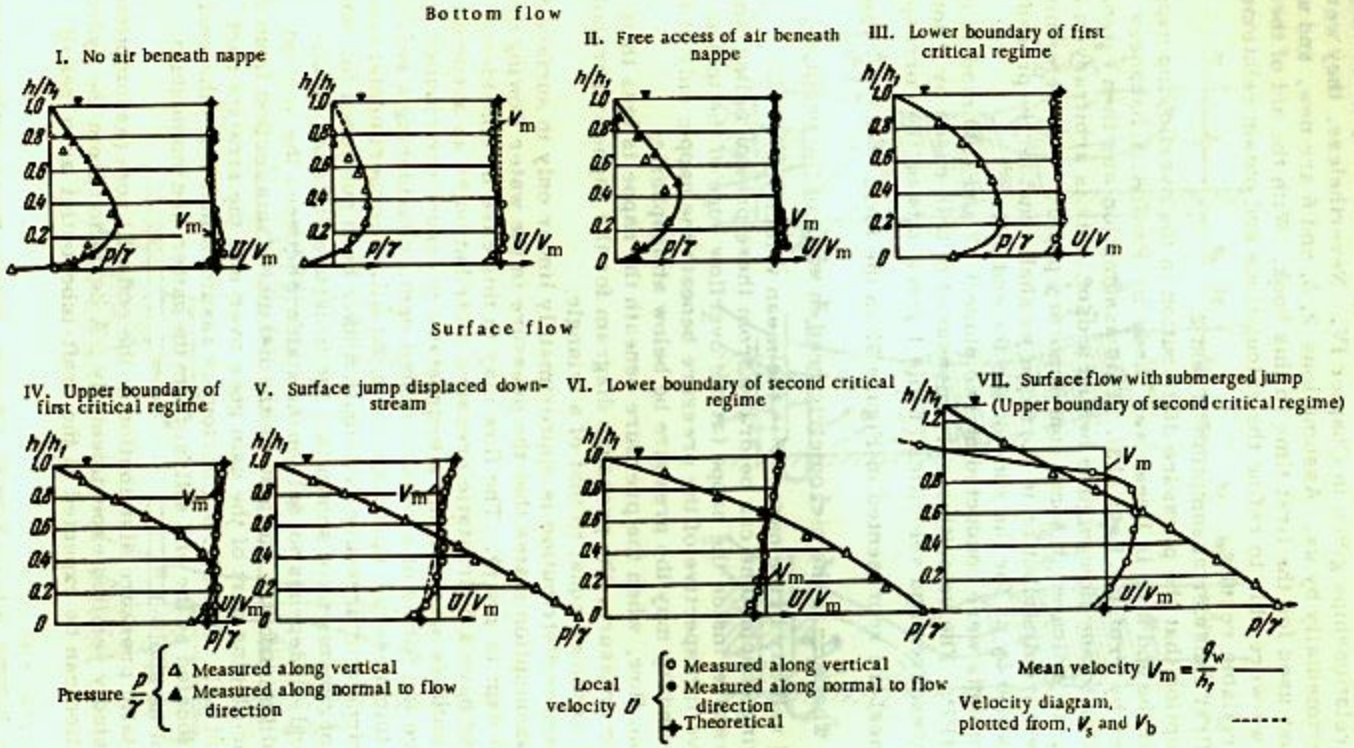

FIGURE 23. Velocity and pressure diagrams in the flow contraction in the end-sill zone.

TABLE 1. Flow regimes at which pressures and velocities were determined in the flow contraction in the end-sill zone

Diagram No.	I		II	III	IV	V	VI**	VII**
Scale* of plane model	1:52	1:52	1:52	1:80	1:80	1:52	1:80	1:80
Head on dam, H, cm	15.80	15.80	15.79	12.28	12.28	15.62	9.14	9.74
Discharge Q_w, l/sec	33.7	33.9	33.7	18.6	18.6	33.3	14.0	14.0
Discharge q_w per unit dam length, l/sec·cm	1.10	1.11	1.10	0.73	0.73	1.09	0.55	0.55
Nappe depth h_1, at toe, cm .	5.22	5.29	5.13	4.20	4.40	5.74	3.8	6.25†
Energy T'_0 per unit mass, above end sill, cm	29.03	29.05	29.03	20.28	20.28	28.86	16.99	17.58
Piezometric head h_0 beneath nappe, measured from end-sill level, cm	−1.33	−1.11	0	1.41	3.71	10.54	7.56	10.10
Flow regime	Bottom, no air beneath nappe		Bottom, with free access of air beneath nappe	Bottom; lower boundary of first critical regime	Surface; upper boundary of first critical regime	Surface jump displaced downstream	Lower boundary of second critical regime	Submerged surface jump

* Dam width b = 30.8 cm in 1:50 model; b = 25.4 cm in 1:80 model.

** Diagrams VI and VII were determined for discharge under sluice gate.

† The value of h_1 in Figure 23 corresponds to that part of the nappe depth in which the velocities are not negative.

of the the nonuniformity of the velocity distribution in the turbine discharge. It has, however, been proved experimentally that even in this case the mean pressure is close to the hydrostatic pressure.

A hydrostatic pressure distribution along the circumference of the draft-tube outlet was observed in a model studied by Kh. Sh. Mustafin. He placed more than 10 piezometric tubes in the draft-tube outlet and found that their readings hardly differed.

We finally reach Prof. I. I. Levi's conclusion that "It can be assumed, in view of the great height of the end sill and the relatively low draft-tube outlet velocity, that the pressure distribution is almost hydrostatic. This assumption has been fully confirmed experimentally... and can therefore be safely made in practice."

The correctness of assumption 5 about the pressure distribution at the downstream pier ends has been confirmed experimentally by the author during a laboratory investigation of a model of an overflow HPP.*

The piezometric head in the bottom-roller zone (at the draft-tube outlet) and the level in the whirlpool zone behind the pier were measured at overflow discharges of about 20 and 40 l/sec and at different tailrace levels. Figure 24 shows that the piezometric-head levels and the whirlpool-zone levels, plotted as functions of the tailrace level, lie on the same straight line. This proves that the variation of the free-surface level behind the piers corresponds to the piezometric head beneath the nappe. The readings of the piezometric tubes arranged along the pier head confirm that the pressure distribution over the depth of the whirlpool zones is hydrostatic.

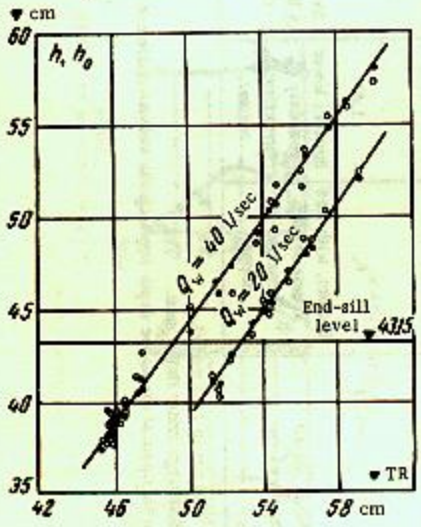

○ Level of free surface of whirlpool zone behind pier

● Readings of piezometric tube placed at draft-tube outlet

FIGURE 24. Level ∇h of free surface of whirlpool zone behind piers, and piezometric-head level ∇h_0 at draft-tube outlet, as functions of level ∇TR of free tailrace surface.

The shape of the pressure diagrams for the sloping part of the apron (assumption 6) is determined from the experimental data given in Figures 25 and 26.**

The piezometric tubes P0, P1, and P2 were placed in the bottom-roller zone behind the end sill. The pressures indicated by them are therefore nearly independent of the flow regime.

The readings of the piezometric tubes P3, P4, and P5 varied with the tailrace flow regime. During bottom flow the pressure curve for each of these piezometric tubes has a "peak" caused by the nappe impinging on the apron at the point where the piezometric tube considered was placed.

* The 1:52 model is shown in Figure 29. The dimensions are given in § 12.

** The experiments were performed at the MEI hydraulic laboratory imeni V. M. Molotov by Eng. P. M. Slisskii.

When the tailrace level rises and the length of the nappe increases (due to the increase of pressure beneath it), the pressure peak is successively shown by the piezometric tubes P3, P4, and P5. During surface flow the pressure shown by all five piezometric tubes becomes equal, being uniform along the entire bottom roller, as indicated already by I. I. Levi /13/.

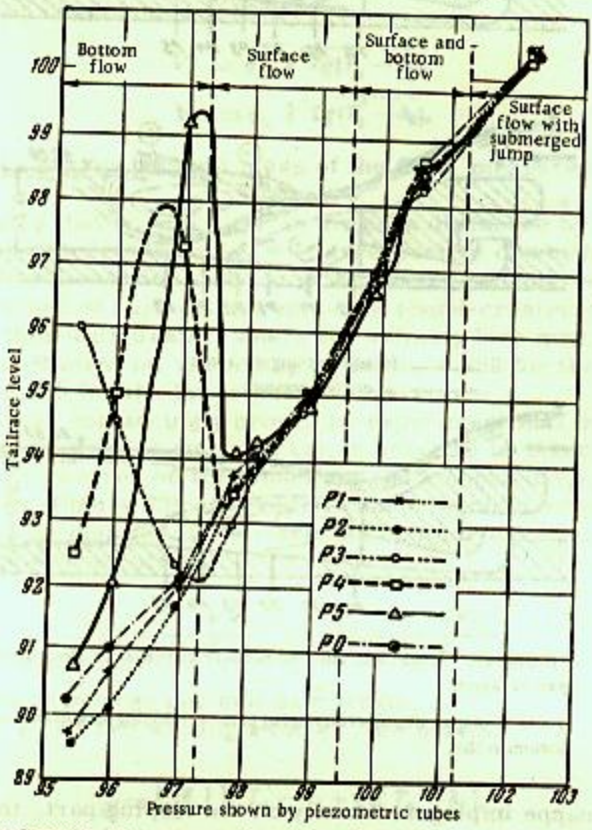

FIGURE 25. Pressures at various points of sloping part of apron (Figure 26) as function of tailrace level (converted to full scale; pressures and levels in m).

Figure 26 shows the pressures along the apron for three cases: a and b for bottom flow, and c for surface flow.

We can therefore conclude that the pressure along the sloping part of the apron depends on the tailrace depth and flow regime, and on the distance between the sloping part of the apron and the end sill.

When the sloping part is located in the bottom-roller zone, the pressure in it is determined, irrespective of the flow regime, by the piezometric head in the roller beneath the nappe (Figure 22,a), in accordance with the laws of hydrostatics.

When the sloping part is located at a sufficient distance from the HPP, outside the bottom-roller zone and the zone of nappe impingement, the pressure depends on the tailrace level (Figure 22,c).

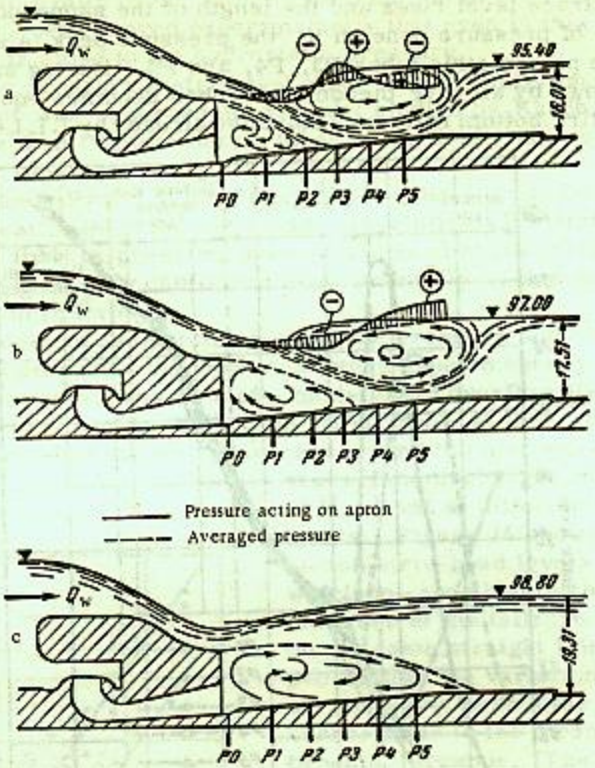

FIGURE 26. Actual and assumed pressure distributions along sloping part of apron.

a and b—nappe impinges on sloping part; c—sloping part in zone of bottom roller.

When the nappe impinges directly on the sloping part, the pressure diagram is trapezoidal, with bases equal to the tailrace depth and to the piezometric head beneath the nappe, measured from the stilling-pool bottom (Figure 22,b).

A pressure peak can occur on the sloping part of the apron during surface flow if a powerful nappe impinges downstream of the bottom roller. However, even if the nappe is weak, the mathematical model represented in Figure 22,b may be used when the bottom roller extends over the sloping part of the apron. The assumed pressure distribution along the sloping part is in this case close to reality, since the diagram shows the averaged pressures ahead of and behind the sloping part.

10. DETERMINATION OF THE DEPTH OF THE OVERFLOWING NAPPE AT THE TOE

Without an accurate analytic expression for the pressures in the overflowing nappe it is impossible to determine exactly its potential energy

per unit mass. Bernoulli's equation, written for the entire stream, does not therefore yield an accurate expression connecting the piezometric head h_0 (measured from the toe level) with the nappe depth h_1 at the end sill.

We shall apply I. I. Levi's conclusion made in his paper "Theory of Surface Jumps and of Analysis of Dams with Surface Flow." Levi applies the energy equation not to the entire stream, but only to the surface and bottom flow and obtains as a result:

$$V_s = \varphi_s \sqrt{2g(T_0' - h_1)},$$

$$V_b = \varphi_b \sqrt{2g(T_0' - h_0)},$$

where T_0' is the energy per unit mass of the flow, measured from the end sill.

Levi assumes that $\varphi_s = \varphi_b < 1$. In the case discussed by us it would have been more correct to set $\varphi_s = 1$, irrespective of whether free flow over the crest or flow under a sluice gate is being considered. In fact, the flow conditions of surface currents on a round-crested dam are similar to those on a thin-walled dam, where the velocity loss may be neglected; the velocity coefficient is, according to Bazin, 0.996 for the upper surface currents and 0.988 for the lower surface currents.*

The author has convincingly proved by experiment that the velocity coefficient for the surface currents can in practice be taken as unity. The velocities measured on the model and the computed surface velocities almost coincide (Figure 23); this result cannot be obtained for $\varphi_s < 1$.

The arithmetic mean of the surface and bottom velocities in section I-I gives the mean flow velocity:

$$V_m = \frac{V_s + V_b}{2} \quad \text{or} \quad \frac{q_w}{h_1} = \frac{V_s + V_b}{2},$$

where q_w is the discharge per unit dam length.

Noting that $\varphi_s = 1$ and writing φ for φ_b, we obtain

$$\frac{q_w}{h_1} = \frac{\sqrt{2g}}{2}\left[\sqrt{T_0' - h_1} + \varphi\sqrt{T_0 - h_0}\right], \tag{9}$$

$$\frac{q_w}{\sqrt{g}} = \frac{h_1\sqrt{2}}{2}\left[\sqrt{T_0' - h_1} + \varphi\sqrt{T_0' - h_0}\right] \tag{9'}$$

and finally

$$h_1 = \frac{q_w\sqrt{2}}{\sqrt{g}} \cdot \frac{1}{\sqrt{T_0' - h_1} + \varphi\sqrt{T_0' - h_0}}. \tag{10}$$

Relationship (10) is in satisfactory agreement with experimental results. A different relationship seems indicated for surface flow with submerged jump (diagram VII, Figure 23); this flow regime is not considered in detail in this book.

In order to plot a nomogram from (10), we first convert it to a dimensionless expression, using the formula for the critical depth.

* For the results of Bazin's experiments cf., for instance, Ofitserov, A. S. Profil' vodoslivnykh plotin (Dam Profiles). — ONTI. 1930.

Taking into account that

$$\frac{q_w}{\sqrt{g}}=\sqrt{\frac{q_w^2}{g}}=\sqrt{h_{cr}^3}=h_{cr}h_{cr}^{1/2},$$

we divide the left-hand side of (9') by $\frac{q_w}{\sqrt{g}}$, and the right-hand side by $h_{cr}h_{cr}^{1/2}$:

$$1=\frac{\xi_1\sqrt{2}}{2}\left[\sqrt{\theta-\xi_1}+\varphi\sqrt{\theta-\xi_0}\right]. \qquad (11)$$

where

$$\xi_1=\frac{h_1}{h_{cr}};\ \xi_0=\frac{h_0}{h_{cr}};\ \theta=\frac{T_0'}{h_{cr}};\ h_{cr}=\sqrt[3]{\frac{q^2}{g}}.$$

A nomogram of (11), which facilitates computation, is given in appendix I.*

11. RELATIONSHIP BETWEEN PRESSURE BENEATH NAPPE AND TAILRACE DEPTH

a. Overflow ejection over round-crested dam

As stated in § 6, it is necessary to know h_0 (the piezometric head at the draft-tube outlet), in order to determine ejection effect, since $h_{ej}=\nabla TR-\nabla h_0$. The value of h_0 depends both on the nappe depth h_1 at the end sill and on the depth h_2 of the tailrace. Hence, in addition to (10), which connects h_1 with h_0, we must also know the relationship between h_0 and the depth h_2 of the tailrace. The required relationship is obtained from the momentum equation (8).

Figure 27 shows a mathematical model of an overflow HPP with bottom flow.

The most general case is that of a nappe impinging on the sloping part of the apron (Figure 22,b), whose superelevation is d in the region of the dynamic effect of the nappe on the apron, with a step of height e at a certain distance downstream.

We introduce the notations

$$q_w=\frac{Q_w}{b};\ q_t=\frac{Q_t}{b_t};\ q_2=\frac{Q_w+Q_t}{B};\ \beta=\frac{b}{B};\ \beta'=\frac{b_t}{B};$$

$$k=\frac{Q_w}{Q_w+Q_t}=\frac{\beta q_w}{q_2};\ \frac{q_2}{q_w}=\frac{1}{k};\ \frac{q_t}{q_w}=\frac{1-k}{k}\cdot\frac{\beta}{\beta'}.$$

The meanings of Q_w, Q_t, b, b_t, B are evident from Figure 27; q_w q_t, q_2 are the discharges per unit width, corresponding to the subscripts w = overflow; t = turbine or draft tube; 2 = tailrace section II-II.

Substituting these notations in (8), we obtain for an end sill whose slope angle is α:

* The nomograms in appendices I and II are due to L. P. Borodulina.

$$\Delta\Sigma mV=\frac{\gamma B}{g}[q_2V_2-\beta q_w V_1\cos\alpha-\beta' q_t V_t]\Delta t=$$

$$=\frac{\gamma B}{g}\left[\frac{q_2^2}{h_2}-\frac{\beta q_w^2\cos\alpha}{h_1}-\frac{\beta' q_t^2}{h_t}\right]\Delta t=$$

$$=\frac{\gamma B\beta q_w^2}{g}\left[\frac{q_2^2}{\beta q_w^2 h_2}-\frac{\cos\alpha}{h_1}-\frac{\beta'}{\beta}\frac{q_t^2}{q_w^2 h_t}\right]\Delta t=$$

$$=\frac{\gamma B\beta q_w^2}{g}\left[\frac{\beta}{k^3h_2}-\frac{\cos\alpha}{h_1}-\frac{(1-k)^3}{k^3h_t}\cdot\frac{\beta}{\beta'}\right]\Delta t=-\frac{\gamma B}{2}A\Delta t, \qquad (12)$$

where

$$A=\beta q_w^2 M; \qquad (13)$$

$$M=\frac{2}{g}\left[\frac{(1-k)^3}{k^3h_t}\cdot\frac{\beta}{\beta'}-\frac{\beta}{k^3h_2}+\frac{\cos\alpha}{h_1}\right]. \qquad (14)$$

From (12) we obtain $\Delta\Sigma mV$:

$$A=-\frac{2\Delta\Sigma mV}{B\gamma\Delta t}, \qquad (13')$$

from which we see that when $\gamma = 1$ t/m^3 and $\Delta t = 1$ sec, A is numerically equal to minus twice the increment of momentum between sections I-I and II-II, per unit width of the tailrace.

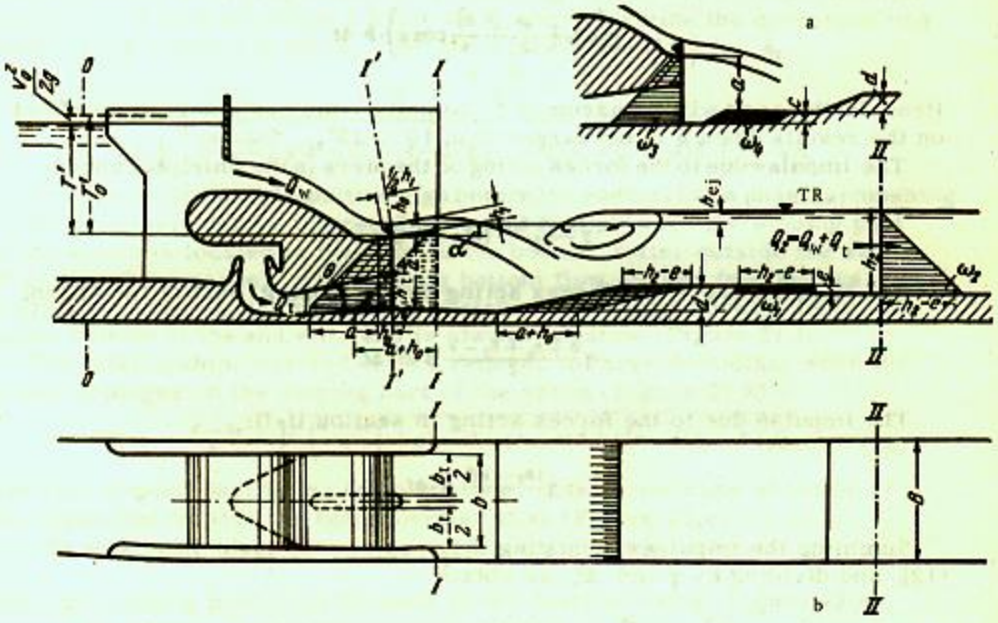

FIGURE 27. Mathematical model of overflow ejection with bottom flow (nappe impinges on sloping part of apron).

When the draft tube has the same width as the dam (at the overflow edge of the end sill), and the slope angle of the end sill is less than 10°, i.e., when

$b_t = b$ and $\cos\alpha$ is almost unity, (14) becomes

$$M = \frac{2}{g}\left[\frac{(1-k)^3}{k^2 h_t} - \frac{\beta}{k^2 h_2} + \frac{1}{h_1}\right]. \qquad (14')$$

When there is a pier in the draft tube, which does not protrude from its outlet, then $b_t = b$, and $\frac{\beta}{\beta'} = 1$.

In forming the expression for the impulse due to the forces acting on the mass of water considered (Figure 27) we omit the forces given by the areas ω_1 and ω_2, since the step e is far from the dam, and the pressure on it depends on the depth h_2.

The apron behind a combined HPP may have two sloping parts: one of superelevation c directly behind the draft tube, and the other of superelevation d at at certain distance from the HPP (Figure 27,a). The first sloping part is always located in the bottom-roller zone, and the pressure on it depends on the pressure beneath the nappe. Hence, the forces given by the areas ω_3 and ω_4 cancel each other out. The end-sill height a in this case is measured from the level of the horizontal part of the apron, which lies behind the first sloping part.

When the areas ω_i are equal, we obtain the following impulse components:

The impulse due to the forces acting in section I-I on the end sill and in the nappe:

$$\gamma\left(ah_0 + \frac{a^2}{2} + \frac{h_1^2}{4}\cos\alpha\right)\cdot b\cdot\Delta t.$$

Henceforth, $\cos\alpha$ will be assumed to be unity; this has a negligible effect on the results when α is not larger than 10 to 15°.

The impulse due to the forces acting on the piers in the whirlpool zones:

$$\gamma\frac{(a+h_0)^2}{2}(B-b)\cdot\Delta t;$$

The impulse due to the forces acting on the sloping part of the apron:

$$\gamma\frac{a+h_0+h_2-e}{2}d\cdot B\cdot\Delta t.$$

The impulse due to the forces acting in section II-II:

$$\gamma\frac{(h_2-e)^2}{2}B\cdot\Delta t.$$

Summing the impulses, equating the result to the right-hand side of (12), and dividing by γ and Δt, we obtain

$$-\frac{B}{2}A = \left(ah_0 + \frac{a^2}{2}\right)b + \frac{h_1^2}{4}b + \frac{(a+h_0)^2}{2}(B-b) - \frac{a+h_0+h_2-e}{2}d\cdot B - \frac{(h_2-e)^2}{2}B. \qquad (15)$$

Here (cf. Figure 27):

a is the height of the end sill above the surface of the lowest part of the apron; b is the width of the dam span; d is the superelevation of the

sloping part of the apron; e is the height of the raised part of the apron above the downstream spillway apron; B is the width of the tailrace; h_0 is the piezometric head beneath the nappe, measured from the overflow edge of the end sill (positive upward, negative downward); h_2 is the tailrace depth.

The second term in the right-hand side of (15) represents the pressure force in the nappe at the end sill, in accordance with Figures 20,b and 27, i.e., when the nappe is convex upward (bottom flow or surface flow near transition to bottom flow). When the nappe is convex downward (Figure 20,a, surface flow) the second term becomes $\frac{h_1 h_0}{2} b$, corresponding to a linear pressure distribution in the nappe.

The fourth term in the right-hand side of (15) represents the horizontal component of the pressure force acting on the sloping part of the apron, in accordance with Figures 22,b and 27.

Multiplying both sides of (15) by $\frac{2}{B}$, we obtain

$$-A=2\left(ah_0+\frac{a^2}{2}\right)\beta+\frac{h_1^2}{2}\beta+(a+h_0)^2(1-\beta)-$$
$$-(a+h_0+h_2-e)d-(h_2-e)^2. \qquad (15')$$

Equation (15') and similar expressions for other cases of nappe impingement on the apron can be solved for h_0 or h_2. Experience shows that frequently (cf. § 28) (especially for comparing theoretical and experimental results) it is best to assign a value to h_0 and determine the corresponding value of the tailrace depth h_2. We therefore solve (15') for h_2:

$$h_2=-\frac{d-2e}{2}\pm$$
$$\pm\sqrt{\left(\frac{d-2e}{2}\right)^2+a^2-e^2+(e-a)d+(1-\beta)h_0^2+(2a-d)h_0+\frac{\beta h_1^2}{2}+A}.$$

Only the solution with positive sign before the radical has a physical meaning.

We similarly derive the required relationships when the sloping part of the apron is located in the zone of the bottom roller outside the zone of action of the nappe. When during bottom flow air has free access underneath the nappe, h_0 is the vertical distance of the free surface from the nappe bottom at the end sill, and is always negative (Figure 21,b).

The relationships derived can be reduced to three formulas: when the nappe impinges on the sloping part of the apron (Figure 22,b) *

$$h_2=-\frac{d-2e}{2}+\sqrt{\left(\frac{d-2e}{2}\right)^2+a^2-e^2+(e-a)d+(2a-d)h_0+A+R}, \qquad (16)$$

when the sloping part is far from the dam, outside the zone of action of the nappe and outside the bottom-roller zone (Figure 22,c)

$$h_2=-(d-e)+\sqrt{a^2+2ah_0+A+R}, \qquad (17)$$

when the sloping part is in the zone of the bottom roller (Figure 22,a)

$$h_2=e+\sqrt{(a-d)^2+2(a-d)h_0+A+R}. \qquad (18)$$

The value R in (16), (17), and (18), which depends on the tailrace flow regime and on whether air has access underneath the nappe, is given in Table 2.

* The downstream end of the ground roller during surface flow is assumed to be the point of nappe impingement on the apron (cf. § 9).

When the sloping part is in the zone of the bottom roller

$$h_0=\frac{(h_2-e)^2-(a-d)^2-A}{2a-2d+h_1}. \tag{18a}$$

At bottom flow the pressure distribution at the pier ends in the whirlpool zones cannot be assumed to equal that in the span in the end-sill zone, since this would lead to a considerable difference between theoretical and experimental results. In the case of bottom flow we therefore proceed from (15') and the analogous equations derived by assuming the pressure distribution behind the piers in the whirlpool zones to be hydrostatic, the pressure being determined by the piezometric head beneath the nappe.

Solving these equations for h_0 we obtain formulas for bottom flow without access of air underneath the nappe.

When the nappe impinges on the sloping part,

$$h_0=\frac{-(2a-d)+\sqrt{(2a-d)^2-4(1-\beta)\left[a^2-(a-e)d-dh_2+\frac{\beta h_1^2}{2}-(h_2-e)^2+A\right]}}{2(1-\beta)}. \tag{16b}$$

When the nappe impinges upstream of the sloping part of the apron,

$$h_0=\frac{-a+\sqrt{a^2-(1-\beta)\left[a^2+\frac{\beta h_1^2}{2}-(h_2-e+d)^2+A\right]}}{1-\beta}. \tag{17b}$$

When the sloping part is in the bottom-roller zone,

$$h_0=\frac{-(a-d)+\sqrt{(a-d)^2-(1-\beta)\left[(a-d)^2+\frac{\beta h_1^2}{2}-(h_2-e)^2+A\right]}}{1-\beta}. \tag{18b}$$

Relationships for bottom flow with free access of air underneath the nappe are obtained similarly.

When the nappe impinges on the sloping part of the apron,

$$h_0=-\frac{2a-d}{2}+\sqrt{\left(\frac{2a-d}{2}\right)^2-a^2+(a-e)d+dh_2-\frac{\beta h_1^2}{2}+(h_2-e)^2-A}. \tag{16c}$$

When the nappe impinges upstream of the sloping part,

$$h_0=-a+\sqrt{(h_2+d-e)^2-\frac{\beta h_1^2}{2}-A}. \tag{17c}$$

When the sloping part is in the bottom-roller zone,

$$h_0=-(a-d)+\sqrt{(h_2-e)^2-\frac{\beta h_1^2}{2}-A}. \tag{18c}$$

The derivation of formulas for the piezometric effect of ejection in the case of a submerged jump, when the roller is located near the end sill is complicated since the additional unknown h_n, being the roller depth at the end sill, enters, and since it is difficult to estimate the flow velocity in the nappe in section I-I.

However, our experiments showed that the plane of the piezometric head, which determines the pressure beneath the nappe, is higher than the level in section I-I * when the submerged depth of the jump is small.

* The pressure beneath the nappe is determined by the level of the stream surface in section I-I when the end sill is flooded to a considerable height.

TABLE 2

Flow regime	Air access underneath nappe	R
Bottom	No	$(1-\beta)h_0^2+\frac{\beta h_1^2}{2}$
	Yes	$h_0^2+\frac{\beta h_1^2}{2}$
Surface	No	$(1-\beta)h_0^2+\beta h_1 h_0$

Equations (16), (17), and (18) remain unaltered when an additional pier, containing the turbine, is located on the dam since b is the width of the dam at the overflow edge of the end sill.

When the apron is horizontal and the downstream spillway apron has no step ($d = 0$ and $e = 0$), we obtain from (17) or (18):

$$h_2=\sqrt{a^2+2ah_0+A+R}. \tag{18'}$$

where R is given in Table 2.

Having by one of these formulas obtained the depth h_2, and therefore the tailrace level corresponding to some piezometric head h_0 at the draft-tube outlet, we determine the piezometric effect of ejection as the difference between the level of the free tailrace surface and the plane of the piezometric head (cf. § 6).

We shall now determine the piezometric head h_0 for a given depth h_2 of the tailrace.

Experimental data show that during surface flow the pressure distribution at the pier ends in the whirlpool zones is very near to that in the plane of the end sill. In the case of surface flow we can thus obtain simpler relationships without significant loss of accuracy (for $\beta=\frac{b}{B}$ above 0.6).

Assuming that during surface flow the pressure distributions at the pier ends and in the plane of the end sill are identical, we obtain instead of (15):

$$-\frac{B}{2}A=\left(ah_0+\frac{a^2}{2}\right)B+\frac{h_1h_0}{2}B-\frac{a+h_0+h_2-e}{2}d\cdot B-\frac{(h_2-e)^2}{2}B.$$

Solving this equation for h_0, we obtain a formula for the piezometric head beneath the nappe in surface flow when the nappe impinges on the sloping part of the apron:

$$h_0=\frac{(a-e)\,d-a^2+dh_2+(h_2-e)^2-A}{2a-d+h_1}. \tag{16a}$$

Similarly, in surface flow with the nappe impinging upstream of the sloping part,

$$h_0=\frac{(h_2+d-e)^2-a^2-A}{2a+h_1}. \tag{17a}$$

despite the presence of a surface roller, even at the end sill. Furthermore, the velocity diagram for this section remains basically similar in pattern and area to that corresponding to a surface jump displaced downstream. This is confirmed by diagram V in Figure 23, which shows that beneath the nappe $\frac{p}{\gamma} > \frac{h}{h_1}$, while V_{av} is near to the theoretical velocity.

We can therefore use in this case the same relationships as for a surface jump, i.e., (10), (16), (17), and (18), with R given in Table 2.

The limits of applicability of the formulas proposed above for computing the ejection effect when the submerged depth of the jump is small, can be determined only by further laboratory tests and experimental results. The theoretical value of the ejection effect, obtained from (10), (16), (17), and (18) for this case is sufficiently near to the experimental value (cf. § 12)

$$\Delta h_2 \leqslant 0.8 \sqrt[3]{q_w^2} \ [m], \qquad (19)$$

where Δh_2 is the height above the end-sill level of the free surface of the tailrace in section II-II, m; q_w is the discharge per unit dam length at the overflow edge of the end sill, m^2/sec.

The position of the sloping part of the apron has a negligible influence on the ejection effect when the submerged depth of the jump is small. When this part is short and located immediately behind the dam we may use (18) to (18c). If it is long and begins immediately behind the dam, (16) to (16c) should be preferred. When the sloping part is far downstream from the dam, (17) to 17c) should be used.

b. Overflow ejection at the sides of the draft tube (discharge over dam having spillways)

We shall consider an overflow HPP with ejection at the sides of the draft tube. Two out of three, or every other sluice are open (Figure 28).

We assume, in accordance with § 9, that, where the sluices are closed, the free surface level in the end-sill zone (draft-tube outlet) and in the whirlpool zones behind the piers corresponds to the piezometric head beneath the nappe.

The author tested a model of an overflow HPP having three bays. When only the lateral sluices were open, the piezometric head at the outlet of the central draft tube was approximately the same as beneath the nappes. At bottom flow this is true only when the nappes do not extend beyond the piers protruding into the tailrace, so that equalization of the pressure beneath the nappes and in the draft-tube outlet is not hindered by them.

We assume the discharges through the different sluices to be equal, and the draft-tube width b_t to differ from the width b of each span.

Let (Figure 28) $\beta' = \frac{b_t}{B}$ and $\beta = \frac{\Sigma b}{B}$. Here, $\Sigma b = 2b$ in Figure 28,a and $\Sigma b = b$ in Figure 28,b. Furthermore

$$q_w = \frac{Q_w}{b}, \quad q_t = \frac{Q_t}{b_t}, \quad q_2 = \frac{\Sigma Q_w + Q_t}{B}, \quad k = \frac{\Sigma Q_w}{\Sigma Q_w + Q_t},$$

where ΣQ_w is the total discharge through the sluices at the sides of the draft tube.

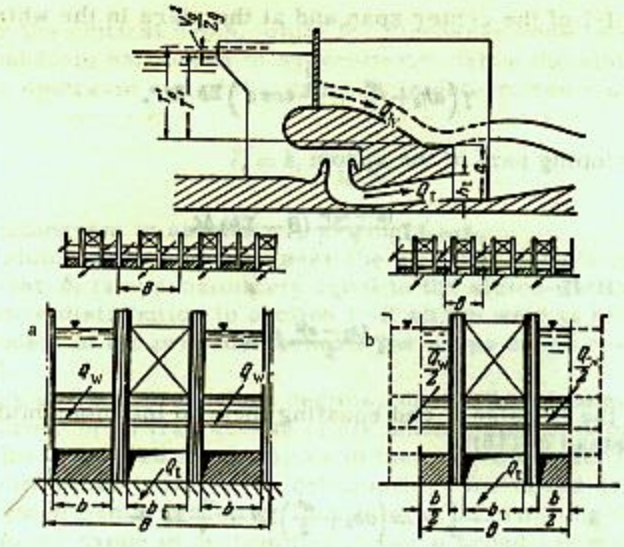

FIGURE 28. Ejection at the sides of the draft tube.

a—two out of three sluices open; b—every other sluice open.

The coefficients α_i, by which allowance is made in the expression for the momentum increment for the nonuniformity of the velocity distribution over the sections, are again assumed to equal unity.

We then obtain as in (12),

$$\Delta\Sigma mV=\frac{\gamma B}{g}\left[\frac{q_2^2}{h_2}-\frac{\beta q_w^2\cos\alpha}{h_1}-\frac{\beta' q_t^2}{h_t}\right]\Delta t=$$

$$=\frac{\gamma B\beta q_w^2}{g}\left[\frac{\beta}{k^2h_2}-\frac{\cos\alpha}{h_1}-\frac{(1-k)^2}{k^2h_t}\frac{\beta}{\beta'}\right]\Delta t=-\frac{\gamma B}{2}A\Delta t,$$

where $A=\beta q_w^2 M$;

$$M=\frac{2}{g}\left[\frac{(1-k)^2}{k^2h_t}\frac{\beta}{\beta'}-\frac{\beta}{k^2h_2}+\frac{\cos\alpha}{h_1}\right],$$

i.e., as for overflow ejection above the draft tube.

In forming the expression for the sum of the impulses we assume that the pressure on the sloping part of the apron is determined over the entire width B by the same laws as for overflow ejection above the draft tube. The actual pressure diagram for the part of the apron over which the turbine discharge flows will differ from that behind the sluices.*

We obtain for bottom flow, when the nappe impinges on the sloping part of the apron, the following expressions for the impulses due to forces acting on the mass of water considered:

In section I-I at the end sill and in the nappes:

$$\gamma\left(ah_0+\frac{a^2}{2}+\frac{h_1^2}{4}\cos\alpha\right)\Sigma b\cdot\Delta t\ **.$$

* Nevertheless, the assumption of a uniform pressure distribution over the entire apron width B yields relationships giving acceptable results.

** We shall henceforth assume, as before, that $\cos\alpha\approx 1$, since this has a negligible effect on the results.

In section I-I of the center span and at the piers in the whirlpool zones:

$$\gamma\left(ah_0+\frac{a^2}{2}+\frac{h_1^2}{4}\cos\alpha\right)\Sigma b\cdot\Delta t^*.$$

Over the sloping part of the apron:

$$\gamma\frac{(a+h_0)^2}{2}(B-\Sigma b)\,\Delta t.$$

In section II-II:

$$\gamma\frac{(h_2-e)^2}{2}B\cdot\Delta t.$$

Summing the impulses, and equating them to the momentum increment, we obtain instead of (15):

$$-\frac{B}{2}A=\left(ah_0+\frac{a^2}{2}\right)\Sigma b+\frac{h_1^2}{4}\Sigma b+$$
$$+\frac{(a+h_0)^2}{2}(B-\Sigma b)-\left(\frac{a+h_0+h_2-e}{2}\right)d\cdot B-\frac{(h_2-e)^2}{2}B$$

or

$$-A=2\left(ah_0+\frac{a^2}{2}\right)\beta+\frac{h_1^2}{4}\beta+$$
$$+(a+h_0)^2(1-\beta)-(a+h_0+h_2-e)\cdot d-(h_2-e)^2.$$

This expression coincides with (15'), which was derived for overflow ejection above the draft tube. The relationships obtained for ejection above the draft tube and at its sides are also identical for other wave patterns in the tailrace and for other cases of nappe impingement on the apron.

Thus, in the case of a round-crested dam, the formulas for overflow ejection at the sides of the draft tube coincide fully with (16), (17), and (18).

The depth h_1 at the toe is also determined by the same formulas as above.

Relationships like (16), (17), and (18) are also applicable when the turbine discharge is uniform over the HPP front, and every other, or two out of three sluices are open. In fact, the expression for the impulses is the same, whether the discharge is uniform along the front or whether every other, or two out of three sluices are open. The expression for the momentum increment is reduced to (14) by writing $\beta'=\frac{\Sigma b_1}{B}$ and $\beta=\frac{\Sigma b}{\omega}$.

These formulas are applicable to bottom flow only if the nappe extends beyond the piers protruding into the tailrace.

c. Ejection over broad-crested dam*

When considering a broad-crested dam we move section I'-I' upstream, as done by I. I. Veits (cf. below). In the case of free flow over the weir h_1

* The assumptions made and relationships obtained have not been tested experimentally for this case.

approximates the critical depth, while for discharge under a sluice gate it can be found from handbooks of hydraulics.* When the sluice gate is located at the upstream end of the dam, h_1 is determined from the equation

$$T_0' = h_1 + \frac{q_w^2}{2g_w^2 h_1^2}$$

or from the nomogram in appendix I, setting $\xi_0 = \xi_1$.

When the sluice gate is located near the overflow edge (Figure 65) we can assume that h_1 is approximately equal to the sluice-gate opening h_s.

The pressure distribution in section I'-I' on the weir is hydrostatic, being independent of the pressure beneath the nappe at the overflow edge (Figure 20,b).

Differences in the tailrace flow regime, due to the presence of a sloping part of the apron, or to free access of air underneath the nappe, will affect the relationships obtained similarly as in the preceding cases.

The only difference between the relationships for broad-crested and for round-crested dams consists** in the term determining the pressure distribution in the nappe in section I'-I'. For a broad-crested dam the pressure force in the nappe in this section is independent of the flow regime and is $\frac{\gamma h_1^2}{2}$, while for a round-crested dam it is $\frac{\gamma h_1^2}{4}$ with bottom flow and $\frac{\gamma h_1 h_0}{2}$ with surface flow. Using again (16), (17), and (18),† the differences in flow regime are taken into account through the term R, which is given in Table 3 for ejection over a broad-crested dam.

TABLE 3

Flow regime	Access of air underneath nappe	R
Bottom or surface	No	$(1-\beta)h_0^2 + \beta h_1^2$
Bottom	Yes	$h_0^2 + \beta h_1^2$

With free access of air underneath the nappe, the value of h_0 is equal to the height of the free surface above the end sill, and is negative as shown in Figure 21,b.

12. COMPARISON OF THEORETICAL AND EXPERIMENTAL RESULTS

The author compared the results of calculations by these formulas with experimental data obtained with HPP models differing in scale and design.

* Pavlovskii, N.N. Gidravlicheskii spravochnik (Handbook of Hydraulics), p. 731. 1937.

** Cf. also § 14,a.

† We can also use (16,b,c) to (18b,c), replacing $\frac{\beta h_1^2}{2}$ by βh_1^2.

Satisfactory agreement between theoretical and experimental results was obtained in all cases. Some results are given in this section in the form of ejection characteristics, i.e., curves of the piezometric effect h_{ej} of ejection (or the head effect ΔH of ejection) as function of the level of the free tailrace surface. Each curve is plotted for a constant ejection discharge.

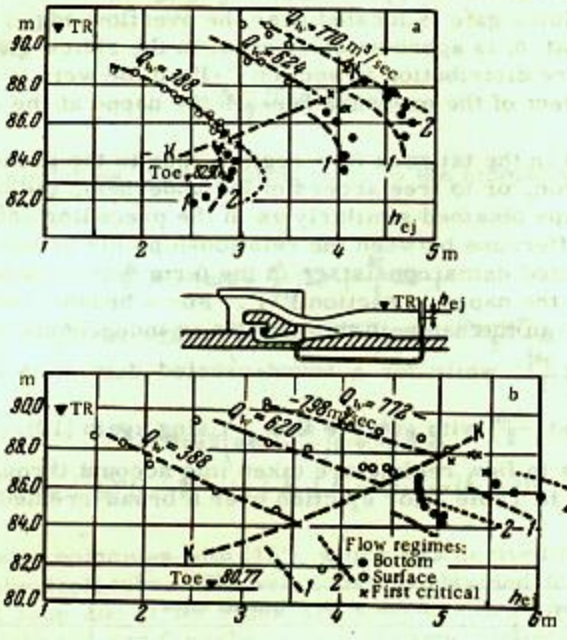

FIGURE 29. Comparison of theoretical and experimental ejection characteristics of an overflow HPP.

1—calculation by formulas valid when sloping part of apron is located in bottom-roller zone (bottom flow); 2—calculation by formulas valid when sloping part of apron is located in zone of dynamic action of nappe; K-K —first critical regime.

The experimental and theoretical ejection characteristics given in Figure 29 refer to a 1:52 model without turbine. The model is shown schematically in the same figure. The full-scale dimensions were: b = 12.35 m, B = 16.0 m, h = 6.40 m, c = 0.45 m, d = 2.77 m, e = 1.07 m. The height of the end sill was $a \approx$ 12.90 m in Figure 24 (level 82.90 m), and 10.77 m in Figure 25 (level 80.77 m). The level of the crest was 89.35 m, and of the apron in section II-II, 73.22 m. The headrace level was in all cases close to 100.0 m. At a discharge of 770 m³/sec the sluice gate was fully opened, while at 620 and 388 m³/sec discharge took place under the sluice gate. The turbine gate had a constant opening, so that the discharge Q_t varied with the head H_t in accordance with curve 1 of Figure 30. The head H_t represents the difference between the levels of the

free headrace surface and the free surface in the piezometric tube located at the draft-tube outlet. The ejection characteristic in Figure 29,a shows that, at $a = 12.90$ m and constant ejection discharge, a lowering of the free tailrace surface causes at first an increase in the piezometric effect of the ejection, which then decreases at bottom flow. At $a = 10.77$ m (Figure 29,b) the piezometric effect of ejection does not decrease at bottom flow. Better agreement between theoretical and experimental results is obtained at surface flow near the first critical regime; this is because the mathematical model used by us in this case was more accurate. The theoretical value of the ejection effect at bottom flow was either larger or smaller than the experimental value, depending on whether the formulas used were those for a nappe impinging on the sloping part of the apron (curves 2), or for the latter being located in the bottom-roller zone (curves 1). The true pressure distribution over the sloping part of the apron apparently differs from that assumed.

Curves *K-K* in Figure 29,a and b, which separate the surface and bottom flow regimes, define the first critical regime. The methods of analyzing the latter are described in §19.

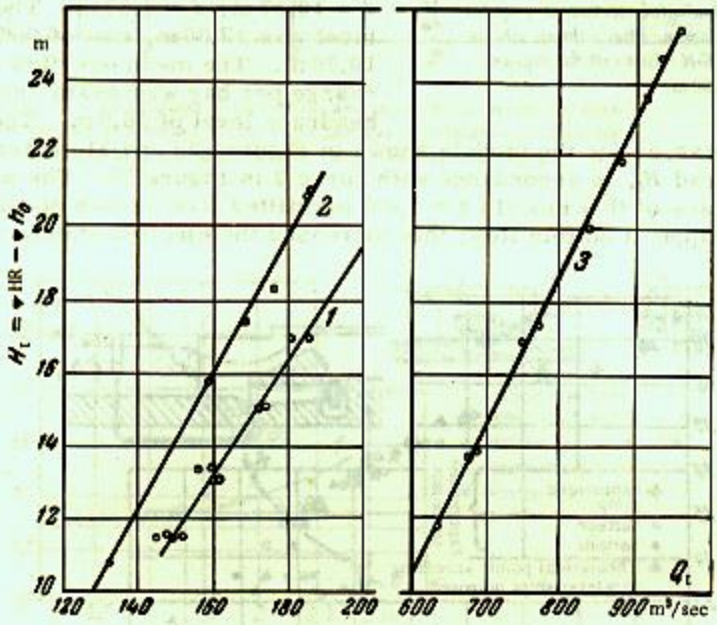

FIGURE 30. Turbine discharge (full scale) as function of head.

1—with reference to Figure 29; 2—with reference to Figure 33; 3—with reference to Figure 34. The head H_t represents the difference between the levels of the free headrace surface and the free surface in the piezometric tube located in the draft-tube outlet.

Figure 31 gives the experimental results obtained with the same model, but with a horizontal apron (at level 74.29 m) and one central pier instead of two half-piers at the sides. The pier had vertical channels, permitting access of air underneath the nappe at bottom flow; the ejection effect thus increased with the drop in tailrace level.* The overflow discharge was 388 m³/sec.

* The influence of the toe level and of free access of air underneath the nappe on the ejection effect is discussed in Chapter V.

The simplicity of the mathematical model for a horizontal apron ensures high accuracy in the calculations.

Results of calculations by the relationships proposed are compared in Figure 32 with the experimental results obtained by Egorov (/4/, p. 93, Table 8). The agreement is satisfactory.

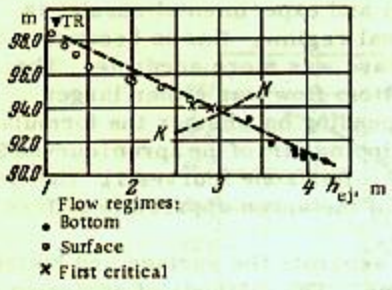

FIGURE 31. Comparison of theoretical and experimental results for ejection in a model with horizontal apron. Pier with an air-intake channel; *K-K* – first critical regime. Toe level = 82.90 m.

The accuracy is less when the water passages are of intricate configuration. A comparison of theoretical and experimental results for such a model having two bays is given in Figure 33. The dimensions of the 1:100 model (without turbine) are: width of one bay at the overflow edge of the end sill, $b = 11.6$ m, width of the draft-tube outlet, $b_t = 17.40$ m, width of tailrace corresponding to one bay, $B = 29.00$, $h_t = 8.43$ m, $a = 19.37$ m, $d = 4.37$ m. The end-sill level was 25.00 m, that of the apron, 10.20 m. The mean overflow discharge per bay was 465 m^3/sec at a headrace level of 46.0 m. The turbine discharge was, as for the models shown in Figures 29 and 31, determined from the head H_t, in accordance with curve 2 in Figure 30. The wide piers in the tailrace of this model ($\beta = 0.40$) permitted free access of air underneath the nappe at bottom flow; this increased the ejection effect.

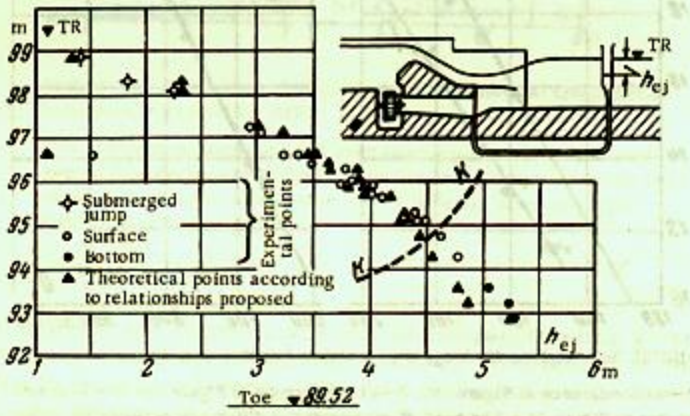

FIGURE 32. Comparison of theoretical results for overflow ejection with Egorov's experimental results (1:17.3 model with turbine).

Theoretical and experimental values of the piezometric effect of overflow ejection above the draft tube are also compared in § 21, Figure 54.

Ejection at the sides of the draft tube was investigated on a 1:156 model having three bays (Figure 34).

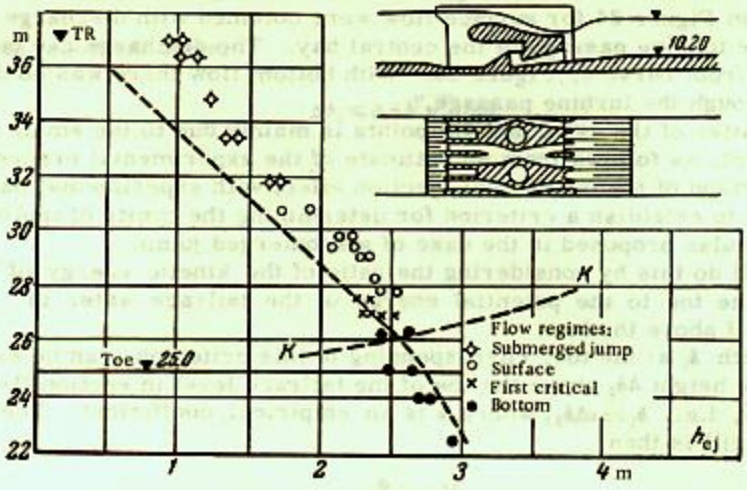

FIGURE 33. Comparison of theoretical and experimental results for overflow ejection in a model having water passages of intricate configuration in plan (1:100 model without turbine): K-K—first critical regime.

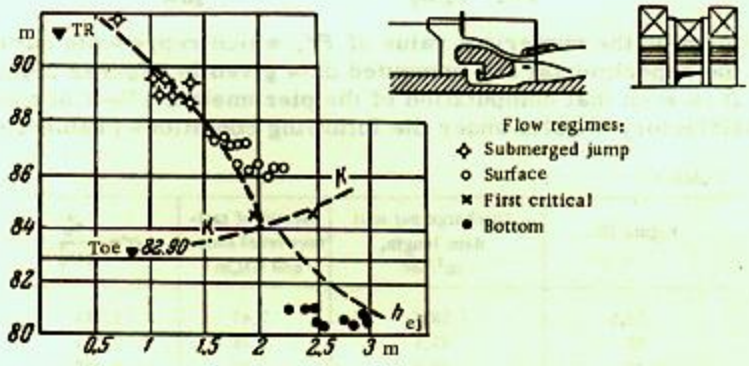

FIGURE 34. Comparison of theoretical and experimental results for overflow ejection at the sides of the draft tube (156 model without turbine): K-K—first critical regime.

The dimensions of each bay of the model were the same as for the model on which Figure 29 is based, but the dam width was 12.00 m. When the headrace level was about 100.0 m the discharge through the outermost spans was 390 to 400 m^3/sec (flow under the sluice gates). The experimental points in Figure 34 for surface flow were obtained with discharge through the turbine passage of the central bay. The discharge can be estimated from curve 3, Figure 30. With bottom flow there was no discharge through the turbine passage.

The scatter of the experimental points is mainly due to the small scale of the model, as follows from an estimate of the experimental errors.

Comparison of the theoretical ejection effect with experimental data enables us to establish a criterion for determining the limits of applicability of the formulas proposed in the case of a submerged jump.

We shall do this by considering the ratio of the kinetic energy of the nappe at the toe to the potential energy of the tailrace water in section II-II above the toe.

The depth h_1 at the toe, corresponding to this criterion, can be expressed through the height Δh_2 above the toe of the tailrace level in section II-II (Figure 45), i.e., $h_1 = \varepsilon \Delta h_2$, where ε is an empirical coefficient. The velocity at the end sill is then

$$V_1 = \frac{q_w}{\varepsilon \Delta h_2},$$

and the ratio of double the kinetic energy at the end sill to the potential energy considered gives the (dimensionless) Froude number Fr

$$Fr = \frac{V_1^2}{g \Delta h_2} = \frac{q_w^2}{\varepsilon^2 g \Delta h_2^3} \quad \text{or} \quad Fr' = \varepsilon^2 Fr = \frac{q_w^2}{g \Delta h_2^3}.$$

We determine the numerical value of Fr', which represents our criterion, by using the experimental and computed data given in Figures 29,b, 32, 33, and 34. It is seen that computation of the piezometric effect of ejection yields satisfactory results under the following conditions (Table 4):

TABLE 4

Figure No.	Discharge per unit dam length, m^2/sec	Height of tailrace level above end sill, m	$Fr' = \frac{q_w^2}{g \Delta h_2^3}$
29,b	29.6	7.47	0.215
32	47.4	9.28	0.287
33	40.0	9.00	0.225
34	33.0	8.93	0.156

When Fr' is larger than, or equal to the values given in the table, the computed value of the piezometric effect of ejection is always close to the experimental value. Thus, in order to obtain sufficiently reliable results by the formulas proposed for the case of a submerged jump, it must be shown that Fr' exceeds the average value 0.220 obtained by us in the cases considered:

$$\frac{q_w^2}{g \Delta h_2^3} \geq 0.22.$$

or

$$\Delta h_2 \leq 1.7 \sqrt[3]{\frac{q_w^2}{g}},$$

or, in technical units,

$$\Delta h_2 \leq 0.8 \sqrt[3]{q_w^2} \text{ [m]}. \tag{19}$$

Chapter III

EJECTION THROUGH CONDUITS

13. INITIAL ASSUMPTIONS

In the case of ejection through conduits we have, instead of the depth h_t at the end sill with overflow ejection, the height of the conduit outlet which will also be denoted by h_t. Its magnitude is determined by the HPP and conduit design, and is here assumed to be known; this is the principal difference between overflow ejection and ejection through conduits.

The assumptions made for the mathematical models of the two types of ejection differ only as regards the pressure distribution in the nappe. All other assumptions remain valid (cf. § 9, assumptions 4 to 8).

The pressure distribution on the sloping part of the apron in the case of a submerged nappe and with ejection through a bottom conduit will be considered separately.

A conduit usually has a platform at the level of the outlet bottom, intended for supporting the shield and stoplogs (Figure 35). This is therefore the interesting case in determining the effect of ejection above the draft tube. When the conduit is located below the draft tube, the conduit apron fulfills the function of this platform. The presence of such a platform simplifies the mathematical model, since in this case the pressure distribution in the plane of the outlets can be considered to be hydrostatic for any tailrace level.

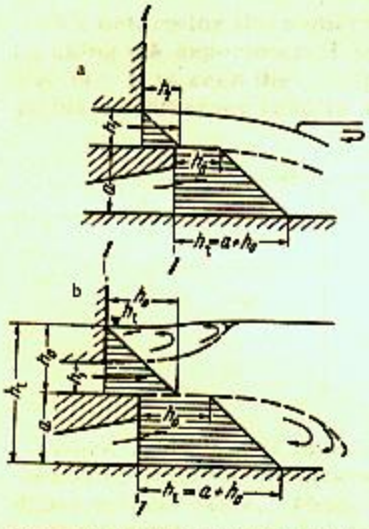

FIGURE 35. Assumed pressure distribution at conduit and draft-tube outlets.

a—conduit outlets not flooded; b—conduit outlets flooded.

Thus, the following assumptions are made in the case of ejection through conduits for determining the pressures at the conduit and draft-tube outlets, and on the sloping part of the apron:

1. When the conduit outlets are not flooded, the pressure distribution in section I-I is hydrostatic (Figure 35,a), and is independent of the tailrace level (i.e., of the pressure beneath the nappe).

2. When the conduit outlets are flooded, the pressure distribution in section I-I is hydrostatic (Figure 35,b).

3. The pressure at the pier ends in the whirlpool zones depends on the piezometric head beneath the nappe, in accordance with § 9, assumption 5, when the outlets are not flooded.

4. When the outlets are flooded, the pressure on the sloping part of an apron located sufficiently near to the HPP is determined either by the levels of the free tailrace surface in sections I-I and II-II, or (when the tailrace is very deep) by the level in section II-II (Figure 36).

5. When the conduit outlets are not flooded, the pressure on the sloping part of the apron depends on its location, in accordance with the mathematical model established for overflow ejection (§ 9).

6. When the sloping part of the apron is located far downstream of the HPP, or when the conduits are located below the draft tube, the pressure on the sloping part of the apron is determined by the tailrace depth in section II-II.

7. Flooding of the conduit outlets (i.e., when the tailrace level rises above their upper edges) begins when the piezometric head h_0 (measured from the overflow edge of the outlets) becomes larger than the outlet height h_1:

$$h_0 > h_1 \quad \text{or} \quad \nabla h_t > \nabla (a + h_1),$$

where ∇h_t is the tailrace level at the conduit outlets; $\nabla (a+h_1)$ is the level of the upper outlet edge (or of the lower edge of the gate under which the water flows).

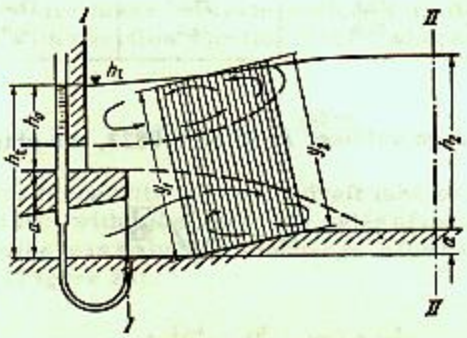

FIGURE 36. Assumed pressure distribution along sloping part of apron behind HPP with conduits having flooded outlets.

The first two assumptions listed above were tested by us on a model of a combined HPP with conduits. We found the pressure distribution to be hydrostatic in section I-I. Assumptions 5 and 6 were tested during studies of overflow ejection. When

$$h_2 < 1.18\sqrt[3]{\frac{q_w^2}{g}} \quad y_1 = h_t = a + h_0, \quad y_2 = h_2.$$

$$h_2 > 1.18\sqrt[3]{\frac{q_w^2}{g}} \quad y_1 = h_2 + d, \quad y_2 = h_2.$$

The fact that the pressure on the sloping part of an apron located near the HPP must be determined from the tailrace level either in sections I-I and II-II or in section II-II, was established by comparing theoretical

results (obtained by the formulas derived below) with the experimental data. When the tailrace was deep, the agreement was better when the pressure on the sloping part of the apron was determined from the tailrace depth in section II-II. On the other hand, when the tailrace was shallow better agreement was obtained when the pressure was determined from the depths in sections I-I and II-II. We shall now derive a criterion determining by which of these two methods the pressure on the sloping part is to be found. Consider the ratio of the kinetic energy of the excess discharge in section II-II (Figure 37) to its potential energy in the same section. The tailrace depth is assumed to be that at which transition from one method to the other gives the best agreement between theoretical and experimental results. This ratio, $Fr=\frac{q_w^2}{gh_2^3}$ is given in Table 5 for two models; its value was obtained from the initial data (Figure 38) corresponding to transition from one method of computing the pressure on the sloping part of the apron to the other.

TABLE 5

Figure 38	Excess discharge q_w m³/sec per running meter of dam	Tailrace level corresponding to change in computing method, m	Tailrace depth h_2, m	$Fr=\frac{q_w^2}{gh_2^3}$
a	59.8	27.0	17.0	0.0742
b	63.0	30.0	20.0	0.0505

Taking the average value of Fr to be 0.0623, we obtain

$$h_2=2.53\sqrt[3]{\frac{q_w^2}{g}}$$

or

$$h_2=1.18\sqrt[3]{q_w^2}\ [m]. \qquad (20)$$

Thus, when $h_2<1.18\sqrt[3]{q_w^2}$, the pressure on the sloping part of an apron beginning immediately behind the HPP is determined by the tailrace depths in sections I-I and II-II. When $h_2>1.18\sqrt[3]{q_w^2}$ the pressure is determined from the depth in section II-II.

It remains to establish the criterion which determines whether the conduit outlets are flooded or not (assumption 7). This criterion ($h_0 \leq h_1$) was adopted on the basis of observations of the changes in flow regime in the tailraces of models of combined HPPs with conduits. It was found (cf. §§ 5 and 19 for more details) that under three-dimensional conditions intense flow from the whirlpool zones behind the piers begins when $h_0 > h_1$,

submerging the nappe and then the outlets * (Figure 49). We can, therefore, establish the pattern of outflow from the conduits by determining h_0.

With overflow ejection the derivation of the formulas for surface flow with submerged jump and flooded end sill is complicated by the difficulty of determining the flow velocity and depth at the end sill. This is not so with ejection from conduits when the outlets of the latter are flooded, since their height h_1 is given. We found that in this case the pressure beneath the nappe depends on the level of the free surface in section I-I, which has to be determined.

14. RELATIONSHIPS BETWEEN PIEZOMETRIC HEAD AT DRAFT-TUBE OUTLET (BENEATH NAPPE) AND TAILRACE DEPTH

a. Ejection from conduits above the draft tube or at its sides, conduit outlets not flooded ($h_0 < h_1$)

The piezometric effect of ejection is $h_{ej} = \nabla TR - \nabla h_0$. We therefore require a relationship determining h_0.

With ejection from conduits the expressions for the increment in momentum of the water mass between sections I-I, II-II (Figure 37), has the same form as with overflow ejection ((12)), where as before, according to (13) and (13'),

$$A = \beta q_w^2 M = -\frac{2\Delta\Sigma mV}{B_1 \Delta t}.$$

With ejection from conduits above the draft tube or at its sides, M is given by (14) or (14'); with ejection at the sides of the draft tube, M is also given by (14), when there is no turbine discharge in the bays carrying the excess discharge (Figure 28).

$$A = \frac{2}{Bg}\left[\frac{Q_w^2}{\omega_w} + \frac{Q_t^2}{\omega_t} - \frac{(Q_w + Q_t)^2}{\omega_2}\right], \qquad (21)$$

where ω is the free area of the section corresponding to the subscript.

When the conduit outlets are not flooded the mathematical model is similar to that for a broad-crested dam. In both cases h_1 is independent of the tailrace level, so that the relationships for a broad-crested dam are applicable here without change.

When the conduit outlets are not flooded we obtain (as in the case of a broad-crested dam) the following expression instead of (15), when the nappe impinges on the sloping part of the apron (Figure 37) (except for

* The amount by which h_0 exceeds h_1 at the instant when the outlets are flooded depends mainly on the ratio $\beta = \frac{b}{B}$ and on the length of the piers protruding into the tailrace.

large tailrace depths, cf. below):

$$-\frac{B}{2}A=\left(ah_0+\frac{a^2}{2}\right)b+\frac{h_1^2}{2}b+\frac{(a+h_0)^2}{2}(B-b)-\frac{a+h_0+h_2-e}{2}d\cdot B-\frac{(h_2-e)^2}{2}B. \tag{22}$$

Since h_1 is given, we need not solve a system of two equations, as for overflow ejection. A more convenient relationship is obtained by solving the general equation for h_0, the piezometric head beneath the nappe, measured from the bottom of the conduit outlet:

$$h_0=\frac{-(2a-d)+\sqrt{(2a-d)^2-4(1-\beta)[a^2-(a-e)d-dh_2+\beta h_1^2-(h_2-e)^2+A}}{2(1-\beta)}, \tag{23}$$

where $\beta=\frac{b}{B}$ (Figure 37); A is given by (13) or (21).

The other magnitudes entering in (23) are shown in Figure 37.

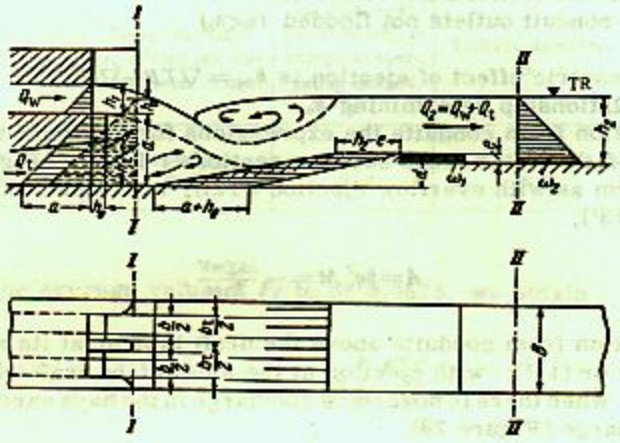

FIGURE 37. Mathematical model for ejection in combined HPP with conduits (bottom flow). Nappe impinges on sloping part of apron.

The relationships for other ways of nappe impingement on the apron are derived in the same way:

when the sloping part of the apron is located far downstream, outside the zone of action of the nappe and the bottom roller, or when the sloping part begins immediately behind the HPP but the tailrace depth exceeds $h_2=1.18\times\sqrt[3]{q_w^2}$, where q_w is the excess discharge per unit dam length:

$$h_0=\frac{-a+\sqrt{a^2-(1-\beta)[a^2+\beta h_1^2-(h_2-e+d)^2+A]}}{1-\beta}. \tag{24}$$

when the sloping part is beneath the bottom roller,

$$h_0=\frac{-(a-d)+\sqrt{(a-d)^2-(1-\beta)[(a-d)^2+\beta h_1^2-(h_2-e)^2+A]}}{1-\beta}. \qquad (25)$$

With bottom flow and access of air beneath the nappe only the expression for the impulse due to the forces acting in section I-I is altered in the momentum equation. The first three terms of the right-hand side of (22) are then replaced by

$$\frac{(a+h_0)^2}{2}B+\frac{h_1^2}{2}b.$$

Here h_0 is the height, above the free surface of the water beneath the nappe, of the overflow edge of the conduit platform; h_0 is in this case always negative.

We then obtain, when the nappe impinges on the sloping part of the apron:

$$h_0=-\frac{(2a-d)}{2}+\sqrt{\left(\frac{2a-d}{2}\right)^2-a^2+(a-e)d+dh_2-\beta h_1^2+(h_2-e)^2-A}. \qquad (26)$$

Equation (26) differs from (23) in that the factor $(1-\beta)$ has disappeared from both numerator and denominator.

When the sloping part is located far downstream or in the zone of the bottom roller, the equations for the case of free access of air beneath the nappe are obtained from (24) and (25) by omitting the factor $(1-\beta)$ in them.

When the apron has a sloping part immediately downstream of the draft tube (similar to the overflow HPP shown in Figure 27,a), the height a of the end sill is measured from the top of the horizontal part of the apron, which lies behind the sloping part.

Equations (23), (24), and (25) may be simplified by assuming the pressure distributions at the pier ends and in the plane of the end sill to be identical. Since, however, β is usually small for bays with conduits this simplification reduces the accuracy.

b. Flooded conduit outlets $[\nabla h_t > \nabla(a+h_1)]$

When the conduit outlets are flooded, the pressure distribution in section I-I is hydrostatic (§ 13, assumption 2) and is assumed to correspond to the level of the free tailrace surface at the conduit outlets.

The piezometric effect of ejection is, in accordance with § 6 and the assumption made, $h_{ej}=\nabla TR-\nabla h_t$, where ∇h_t is the level of the free tailrace surface in section I-I: $h_t=a+h_0$.

Consider the case when the pressure on the sloping part of the apron is determined by the tailrace level in section I-I and II-II (Figure 36),*

* This mathematical model is valid both when the nappe impinges on the sloping part of the apron, and when the latter is sufficiently long, in which case the pressure at any point of the apron is determined by its depth beneath the surface.

i.e., when the tailrace depth is $h_2 < 1.18\sqrt[3]{q_w^2}$. After dividing by γ and Δt the momentum equation then becomes:

$$-\frac{B}{2}A = B\frac{h_1^2}{2} - \frac{h_1+h_2-e}{2}\cdot d\cdot B - \frac{(h_2-e)^2}{2}B. \qquad (27)$$

The pressure force on the step (e) between the apron and the downstream spillway apron is represented by the area ω_1, and is equilibrated by the pressure force corresponding to the area ω_2 (Figure 37).

Dividing (27) by $\frac{B}{2}$ and solving for h_1, the depth in section I-I, we obtain

$$h_1 = \frac{d}{2} + \sqrt{\left(\frac{d}{2}\right)^2 + (d-2e)h_2 + h_2^2 - (d-e)e - A}. \qquad (28)$$

In (26) and (27), $A = \beta q_w^2 M$, where M is given by (14) or (14'). The value of A can be found, as before, from (21).

When the sloping part of the apron is far downstream from the HPP, and also when the tailrace depth $h_2 > 1.18\sqrt[3]{q_w^2}$, irrespective of the position of the sloping part (i.e., when the pressure on it is determined by the tailrace level) we have instead of (27):

$$-\frac{B}{2}A = B\frac{h_1^2}{2} - \frac{(h_2-e+d)^2}{2}B$$

and finally

$$h_1 = \sqrt{(h_2+d-e)^2 - A}. \qquad (29)$$

When the sloping part is very short and is located immediately behind the HPP, the pressure on it can be determined from the depth in section I-I:

$$h_1 = d + \sqrt{(h_2-e)^2 - A}. \qquad (30)$$

c. Ejection through a bottom conduit beneath the draft tube

For the sake of uniformity we represent the relationships for ejection beneath the draft tube in the same form and with the same notations as before.*

In the case of ejection through conduits with flooded outlets the form of the momentum equation is independent of the height of the outlets above the apron.

The most suitable mathematical model is that in which the pressure on the sloping part of the apron is determined by the tailrace level, although the surface level above the sloping part is actually slightly lower. The error thus introduced is compensated to a certain extent by neglecting the dynamic effect of the bottom nappe on the apron. The expression obtained

* Prof. Kachanovskii was the first to use the momentum equation in computing ejection through a bottom conduit beneath the draft tube (Chapter IV).

for the impulses is the same as in the case of conduits above the draft tube. Thus, (29) may be used in the case now considered, h_t being again the tailrace depth in section I-I, since the conduit outlet is flooded.

15. EXPERIMENTAL VERIFICATION OF RELATIONSHIPS FOR EJECTION THROUGH CONDUITS

Theoretical and experimental results for ejection through conduits are compared in Figure 38. Figure 38,a refers to a 1:60 model without turbine. Two conduits of different configuration are arranged beneath the scroll casing. The position of the conduit outlets and their dimensions are shown in Figure 39.*

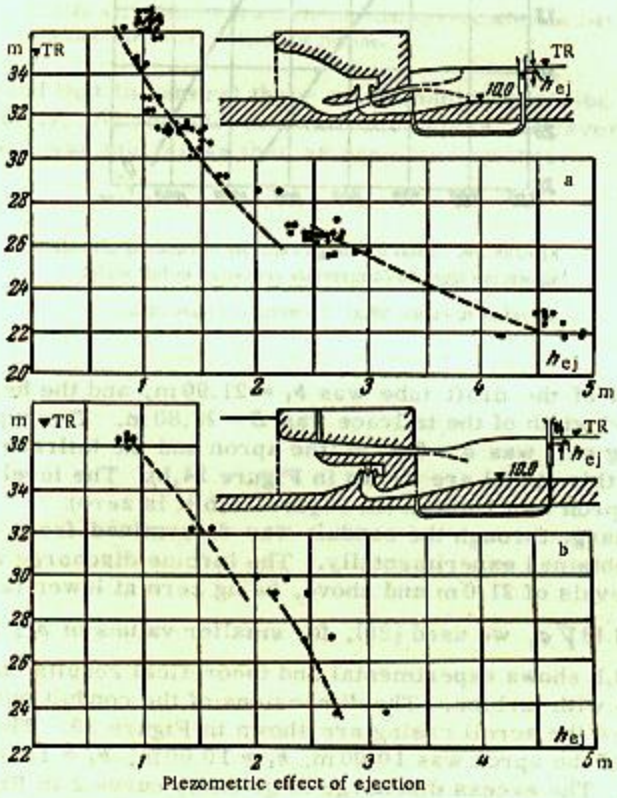

FIGURE 38. Theoretical (broken line) and experimental effect of ejection through conduits.

a—conduits beneath scroll casing; b—conduits above scroll casing.

* The arithmetic mean of the heights of both conduit outlets (3.30 m) was used in the calculations.

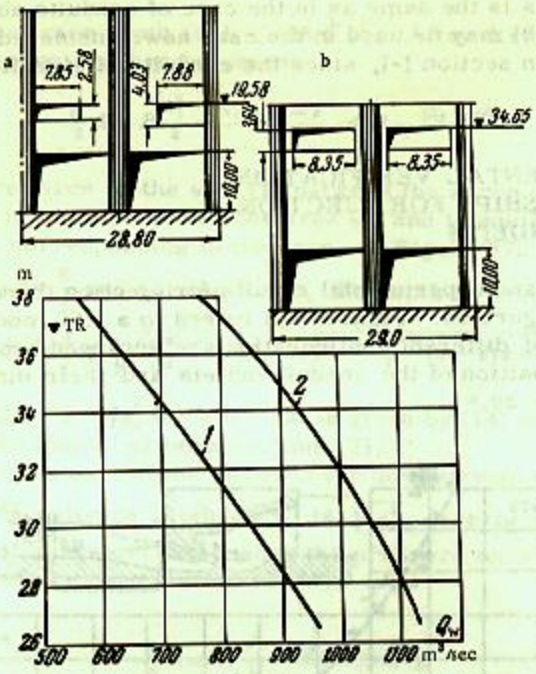

FIGURE 39. Total discharge capacity of conduits of models shown in Figure 38 (dimensions converted to full scale).

1—refers to Figure 38,a; 2—refers to Figure 38,b.

The width of the draft tube was $b_t = 21.90$ m, and the height $h_t = 10.00$ m The computed width of the tailrace was $B = 28.80$ m. The superelevation of the sloping part was $d = 8.47$ m (the apron and the tailrace flow regimes observed on this model are shown in Figure 14,b). The level of the raised part of the apron was 10.00 m (in Figure 14,b it is zero).

The discharge through the conduit was determined from curve 1 in Figure 39, obtained experimentally. The turbine discharge was 600 m^3/sec at tailrace levels of 21.0 m and above, being zero at lower tailrace levels.

For $h_2 > 1.18\sqrt[3]{q_w^2}$ we used (29), for smaller values of h_2, (28).

Figure 38,b shows experimental and theoretical results obtained with a 1:50 model with turbine. The dimensions of the conduit outlets and their location above the scroll casing are shown in Figure 39. The level of the raised part of the apron was 10.00 m; $h_t = 10.00$ m, $b_t = 19.00$ m, $B = 29.00$ m, $d = 12.90$ m. The excess discharge is given by curve 2 in Figure 39 as a function of the tailrace level. The turbine discharge was 462 m^3/sec at a tailrace level of 36.1 m, and increased to 618 m^3/sec with decreasing tailrace level. We used (28) and (29) for the calculations.

In conclusion, Figure 40 gives a comparison of the theoretical results with A. M. Chistyakov's experimental data, obtained at the VNIIG laboratory imeni B. E. Vedeneev with a 1:44 model with turbine.

The reliability of the theoretical relationships for ejection through a conduit beneath the draft tube was tested at the laboratory for dams

and HPPs of VNIIG imeni B. E. Vedeneev /7/. The calculations were performed by relationships proposed by B. D. Kachanovskii, which differ only superficially from ours.

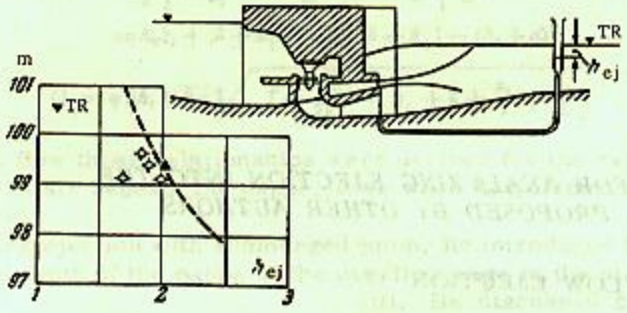

FIGURE 40. Theoretical and experimental ejection effect for 1:44 model of combined HPP with conduits and turbine.

It was found that in general these relationships describe the phenomena quite accurately. At considerable tailrace depths, however, the observed ejection effect was much less than as predicted by theory.

Chapter IV

METHODS FOR ANALYZING EJECTION INTO THE TAILRACE, PROPOSED BY OTHER AUTHORS

16. OVERFLOW EJECTION

a. Ejection by a jump displaced downstream

Ejection by a jump displaced downstream was the first type of ejection in HPPs to be studied theoretically.

In the case represented in Figure 6 the turbine discharge was negligible as compared with the overflow discharge. The drop in the tailrace level at the draft-tube outlet, given by the usual equation for the jump is apparently close to its real value. Laboratory tests of one design of ejection by a jump displaced downstream showed, however (Figure 8), that the drop in the tailrace level at the draft-tube outlet does not by itself determine the gain in head, since part of the head is needed by the turbine discharge to overcome the resistance at the draft-tube outlet. This loss may represent about 1/3 of the tailrace-level drop achieved by ejection.

If the turbine discharge is of the same order of magnitude as the overflow discharge, the usual equations of nonuniform flow become inapplicable.

In this case (e.g., for dimensioning the ejection outlets (Figures 8 and 9)), we may proceed by establishing the energy balance for the different sections. This method was in fact used for the dam shown in Figure 8. Subsequent tests by N. V. Khalturin at the Gidroproekt laboratory confirmed the accuracy of the calculations.

No other methods for analyzing ejection by a jump displaced downstream have been developed so far. Some relevant suggestions have been made by I. I. Veits /3/.

b. Ejection analysis according to S. A. Egorov

S. A. Egorov /4/ was the first to investigate contemporary methods of ejection into the tailrace experimentally and theoretically.* All subsequent works, including this book, are either based on S. A. Egorov's work or duplicate it to a certain extent.

Most of his theoretical and experimental investigations deal with overflow ejection above the draft tube. The relationships proposed by him

* Egorov, S. A. Vosstanovlenie napora gidrostantsii v pavodok otgonom pryzhka (Head Restoration of HPPs during High Water by a Jump Displaced Downstream).— Elektricheskie stantsii. No. 6. 1942.

for the layout shown in Figure 41 in both two-dimensional and three-dimensional cases, and valid for bottom or surface flow, can be reduced to the following:

$$\frac{2}{g}\left[\frac{(Q_x+Q_t)^2}{\omega_2}-\frac{Q_w^2}{\omega_1}\cos\alpha-\frac{Q_t^2}{\omega_t}\right]\frac{1}{B}=$$
$$=h_0h_1+(\delta+h_t)^2+2h_0(\delta+h_t)-(h_2+d)^2, \qquad (I)$$

$$Q_w=\varphi bh_1\sqrt{2g}\sqrt{T+\frac{V_0^2}{2g}-\left(h_t+\delta+\frac{h_1}{2}+\frac{h_0}{2}\right)}. \qquad (II)$$

At bottom flow these relationships were derived for the case when there is no access of air beneath the nappe, even when $h_0 < h_1$ (partial vacuum beneath nappe).

Considering ejection with submerged jump, he introduced the magnitude h_n, being the depth of the nappe at the overflow edge in the plane of the end sill. He discussed separately ejection into a trapezoidal tailrace.

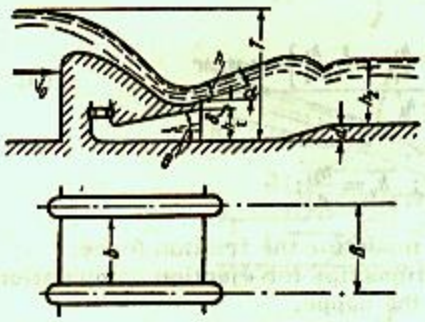

FIGURE 41. Ejection into tailrace, as considered by S. A. Egorov.

We found that with increasing curvature of the nappe, i.e., with increasing difference between h_0 and h_1, the discrepancy between theoretical and experimental values of the ejection effect obtained by him increased, attaining 40 % according to himself. This is due to insufficient correspondence between the mathematical model and the actual conditions. Three of his assumptions are erroneous.

1. Computation of the pressure force in the nappe at any flow regime is based on the assumption of a linear pressure distribution in the nappe. 2. The pressure on the sloping part of the apron is determined in all cases by the hydrostatic law, on the basis of the tailrace level. 3. The pressure at the pier ends in the whirlpool zones is determined by the same law as in the section considered, which lies in the plane of the end sill.

As was shown in § 9 of this book, these assumptions lead to an inaccurate determination of the forces acting on the water mass between sections I-I and II-II. They correspond to reality only in particular cases. S. A. Egorov's first assumption causes an error in determining the potential energy $z+\frac{p}{\gamma}$ in the nappe at the toe, which reduces the accuracy of (II).

The mathematical model used by S. A. Egorov differs considerably from reality at bottom flow, as can be seen by comparing the results of calculations by (I) and (II) with the experimental results.* Better agreement between theoretical and experimental results can be achieved by correctly taking into account all relevant factors.

* Izbash, S. V. Gidravlicheskaya laboratoriya Moskovskogo ordena Lenina energeticheskogo instituta imeni V. M. Molotova (The Hydraulic Laboratory of the Moscow V. M. Molotov Power Institute).— Gidrotekhnicheskoe stroitel'stvo, No. 11. 1950.
Slisskii, S. M. Raschet vodoslivnoi ezhektsii (Computation of Overflow Ejection).— Gidrotekhnicheskoe stroitel'stvo, No. 6. 1951.

c. Analysis of overflow ejection according to I. I. Levi

I. I. Levi introduces /12/ in the momentum equation for the mass of water in the tailrace the friction force F as a function of the momentum:

$$F\left(\frac{\gamma Q_w V_w}{g}\right),$$

and determines the reaction of the piers as a function of the water level in the whirlpool zones, assuming this level to correspond to a depth $a + h_0$.*

Introducing the dimensionless number M', which depends on the discharge per unit length of the dam, the velocity at the end sill, and the end-sill height

$$M' = \frac{q_w V_1}{g a^2},$$

and which characterizes the dynamic flow conditions, I. I. Levi obtains the following expression for the piezometric head at the draft-tube outlet:

$$h_0' = \frac{h_2' - 1 - 2\varphi M'\left[1 + \frac{(1+k)^2}{k^2}\frac{h_1}{h_1} - \frac{\beta}{k^2}\frac{h_1}{h_2}\right] + 2\varphi\xi_F M'}{2 + h_1'}, \qquad \text{(III)}$$

where

$$h_0' = \frac{h_0}{a}; \quad h_1' = \frac{h_1}{a}; \quad h_2' = \frac{h_2}{a};$$

ξ_F is a coefficient by which allowance is made for the friction force.

The same author also proposes relationships for ejection computations in the case of free access of air beneath the nappe.

Levi does not say how the depth at the end sill and the friction coefficient are to be determined. Refraining from issuing recommendations on the use of his formulas in design practice, he gives diagrams which are in fact used in some design organizations for ejection computations. These diagrams relate the piezometric effect of ejection to the tailrace level for different values of M'. This coefficient does not, however, take into account the ratios between the overflow and turbine discharges and between the width of the span and the theoretical width of the tailrace. The diagrams can therefore be used only under conditions corresponding to the experiment, i.e., for

$$\beta = 0.75 - 0.80, \quad k = \frac{q_w}{q_t} = 1 - 3, \quad h_2' = \frac{h_2}{a} = 0.8 - 1.8.$$

d. Solution of the problem, suggested by I. I. Veits

I. I. Veits /3/ gives a solution for the two-dimensional problem, considering turbulent flow, turbulent and smooth flow, and smooth flow, both with and without free access of air beneath the nappe.

Those of the mathematical models considered by him which correspond to HPPs with ejection are shown in Figure 42.

* In developing the initial relationships I. I. Levi makes a simplification equivalent to the assumption that the pressure distribution at the piers is similar to that at the end sill.

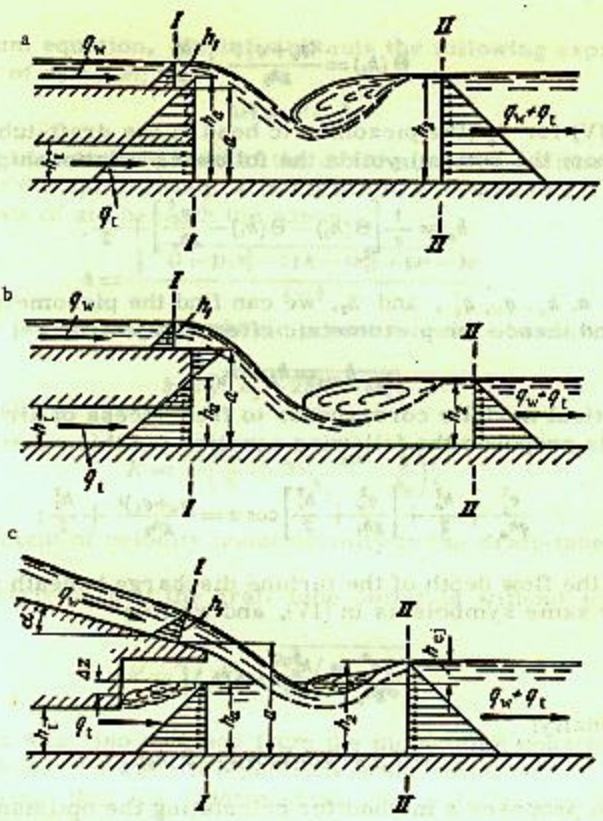

FIGURE 42. Mathematical models for ejection into tailrace, according to I. I. Veits.

Isolating the tailrace, Veits moves section I-I toward the headrace and assumes that the pressure distribution in the nappe is hydrostatic, irrespective of the tailrace level. Thus, the piezometric head h_a beneath the nappe does not affect the nappe depth h_1. This simplifies the relationships.*

The following formula is obtained for mathematical models a and b:

$$\frac{q_t^2}{gh_t}+\left(h_a-\frac{a}{2}\right)a+\Theta(h_1)=\Theta(h_2), \qquad \text{(IV)}$$

where

$$\Theta(h_1)=\frac{q_w^2}{gh_1}+\frac{h_1^2}{2}$$

* The same procedure is also followed by other authors, e.g., D. I. Kumin /9, 10/ and Kh. Sh. Mustafin /14/ as well as by us in discussing a combined HPP with a broad-crested dam.

and

$$\Theta(h_2)=\frac{(q_w+q_t)^2}{gh_2}+\frac{h_2^2}{2}.$$

Solving (IV) for h_a (the piezometric head at the draft-tube outlet, measured from the bottom) yields the following relationship:

$$h_a=\frac{1}{a}\left[\Theta(h_2)-\Theta(h_1)-\frac{q_t^2}{gh_t}\right]+\frac{a}{2}. \qquad (V)$$

Knowing a, h_t, q_w, q_t, and h_2, we can find the piezometric head h_a from (V), and thence the piezometric effect of ejection:

$$h_{ej}=h_2-h_a.$$

Mathematical model c corresponds to free access of air beneath the nappe. Veits proposes the following equation for this case:

$$\frac{q_t^2}{gh_a}+\frac{h_a^2}{2}+\left[\frac{q_w^2}{gh_1}+\frac{h_1^2}{2}\right]\cos\alpha=\frac{(q_w+q_t)^2}{gh_2}+\frac{h_2^2}{2};$$

where h_a is the flow depth of the turbine discharge beneath the nappe.

Using the same symbols as in (IV), and writing

$$\frac{q_t^2}{gh_a}+\frac{h_a^2}{2}=\Theta(h_a),$$

he obtains finally:

$$\Theta(h_a)+\Theta(h_1)\cos\alpha=\Theta(h_2). \qquad (VI)$$

Veits also proposes a method for calculating the optimum height of the end sill. No comparison was made between theoretical and experimental results; there is, however, no reason to doubt the accuracy of his formulas.

The advantage of this method is the absence of involved calculations.* Its application is, however, restricted by the arbitrariness of the assumptions (two-dimensional problem, horizontal apron, end sill of considerable length); this does not, however, prevent use of these relationships for the layout shown in Figure 3,b, and in tentative calculations.

e. Kh. Sh. Mustafin's formulas for overflow ejection

Kh. Sh. Mustafin /14/ considers the simplest mathematical model with horizontal apron at the level of the draft-tube bottom and dam with long horizontal end sill which prevents the tailrace level from affecting the depth in the contracted section at the batter; a hydrostatic pressure distribution in the nappe at the end sill is assumed by the author in all cases; the pressure at the piers in the whirlpool zones is determined by the piezometric head beneath the nappe.

Using the symbols

$$q=q_w+q_t, \quad k=\frac{q_w}{q_w+q_t}, \quad \beta=\frac{b}{B}$$

* The values of $\Theta(h_2)$ are obtained from a nomogram.

in the momentum equation, Mustafin obtains the following expression for the head effect of ejection:

$$\Delta H = h' - h,$$

where h' is the piezometric head at the draft-tube outlet without ejection, measured from the apron level; h is the same with ejection.

In the absence of air beneath the nappe,

$$h = \frac{\sqrt{(1-\beta)(h_2^2 - 2\beta K - \beta h_1^2) + \beta a^2} - \beta a}{1-\beta}. \qquad \text{(VII)}$$

When an air pocket at atmospheric pressure exists beneath the nappe,

$$h = \sqrt{h_2^2 - 2\beta K - \beta h_1^2}. \qquad \text{(VIII)}$$

In (VII) and (VIII),

$$K = \frac{q^2}{g}\left(\frac{h^2}{h_1} + \frac{\alpha_0 (1-h)^2}{h_t} - \frac{\beta}{h_2}\right),$$

α_0 is the coefficient of velocity nonuniformity in the draft-tube outlet section.

The piezometric head at the draft-tube outlet is without ejection

$$h' = \sqrt{h_2^2 - \frac{2q_t^2}{g}\left(\frac{\alpha_0}{h_t} - \frac{\beta}{h_2}\right)}. \qquad \text{(IX)}$$

This formula was also obtained from the momentum equation applied to the mass of water between two sections of the tailrace.

Mustafin claims that his relationships give satisfactory results for engineering purposes.

17. METHODS OF COMPUTING EJECTION THROUGH CONDUITS

a. Computation of ejection at the sides of the draft tube with flooded conduit outlets, according to Krei

Krei also proceeds from the momentum equation established for two sections of the tailrace, assuming a uniform tailrace depth over the entire width in section I-I (Figure 43), and neglecting friction at the bottom between sections I-I and II-II.

He finally obtains:

$$h_{ej} - \frac{h_{ej}^2}{2h_2} = \frac{V_2}{g}\left[V_w\left(1 - \frac{Q_t}{Q_2}\right) - V_2 + \frac{Q_t}{Q_2} V_t\right].$$

Neglection of $\frac{h_{ej}}{2h_2}$ and $\frac{Q_t}{Q_2} V_t$ yields the following expression for the piezometric effect of ejection:

$$h_{ej} = \frac{V_2}{g}\left[V_w\left(1 - \frac{Q_t}{Q_2}\right) - V_2\right].$$

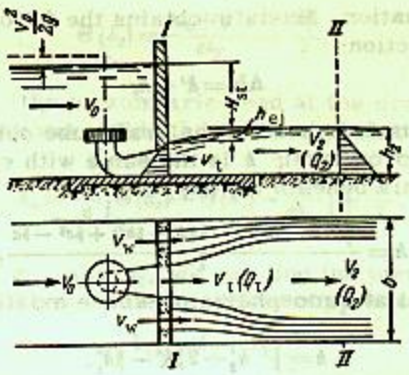

FIGURE 43. Mathematical model for ejection through bottom conduits at the sides of the draft tube, according to Krei.

The velocity V_w in Krei's formula is obtained from Bernoulli's equation:

$$V_w = \varphi \sqrt{2g\left(H_{st} + \frac{V_0^2}{2g} + h_{ej}\right)}.$$

Experimental verification of these formulas /4/, carried out in 1928 and 1929, showed that the theoretical piezometric effect of ejection is 20 to 30 % less than the experimental result (for $\frac{Q_w}{Q_t} = 1.5$ to 4). For $\frac{Q_w}{Q_t} = 7$ to 16 the accuracy is 10 to 1 %. A coefficient $m = 0.70$ to 0.99 should be introduced in the formula

$$h_{ej} = m \frac{V_2}{g}\left[V_1\left(1 - \frac{Q_t}{Q_2}\right) - V_2\right]. \qquad (X)$$

b. Application of S.A. Egorov's relationships to ejection through conduits

S.A. Egorov proposes to use the relationships derived for overflow ejection also for ejection through conduits. The inaccuracies mentioned above are, of course, retained.

Some additional observations on the pressure distribution at the conduit outlets should be made. Considering (/4/, pp. 78, 79) one case with platform at the conduit outlets, and another case without platform, Egorov assumes a hydrostatic pressure distribution at the conduit outlets in both cases, irrespective of the tailrace level. This assumption is, in fact, only true for a conduit outlet with a platform behind it; when no platform exists the pressure distribution in the outlet section is parabolic at tailrace levels corresponding to bottom flow.* Since Egorov ignores this fact, his

* Cf., for instance, Faktorovich, M.E. Gidravlika sopryazheniya s nizhnim b'efom potoka, vykhodyashchego iz napornykh vodovodov (Hydraulics of the Flow into the Tailrace of the Discharge from Conduits).— Izvestiya VNIIG, Vol. 34. 1947.

relationships are correct when there is a platform behind the conduit; when no platform is arranged, the mathematical model corresponds to surface flow.

c. Computation of effect of ejection through bottom conduits (beneath draft tube), according to B. D. Kachanovskii

For HPPs with bottom conduits (Figure 44) B. D. Kachanovskii establishes the momentum equation by assuming a uniform pressure distribution over the width of section I-I, and a hydrostatic pressure distribution (according to the tailrace level) on the sloping part of the apron, located far downstream from the HPP /7/.

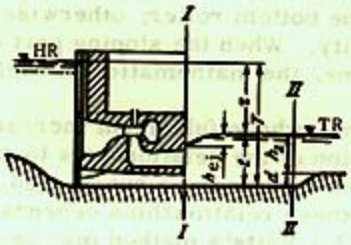

FIGURE 44. Scheme of the combined HPP considered by Kachanovskii.

The discharges through the turbine and the bottom conduits are respectively

$$Q_t = \mu_t \omega_t \sqrt{2g(z+h_{ej})},$$

$$Q_w = \mu_w \omega_w \sqrt{2g(z+h_{ej})},$$

where z is the difference between the headrace and tailrace levels; μ_t and μ_w are the discharge coefficients of turbine passage and bottom conduit, respectively; ω_t and ω_w are the areas of the outlet sections of draft tube and bottom conduit, respectively.

Writing

$$k = \frac{Q_w}{Q_t} = \frac{\mu_w \omega_w}{\mu_t \omega_t},$$

Kachanovskii obtains the following relationship:

$$h_{ej}^2 - 2h_{ej}t + 2c(z+h_{ej}) = 0. \qquad \text{(XI)}$$

Here

$$c = 2\mu_w^2 \frac{\omega_w}{B}\left[1 + \frac{1}{k^3}\frac{\omega_w}{\omega_t} - \left(\frac{1+k}{k}\right)^2 \cdot \frac{\omega_w}{Bt}\right].$$

The mathematical model for ejection through a bottom conduit beneath the draft-tube, used by us in deriving (26), does not differ from that used by Kachanovskii. Calculations by (29) and by (XI) lead to identical results.

18. SOME CONCLUSIONS CONCERNING THE METHODS CONSIDERED FOR COMPUTATION OF EJECTION

The reliability of the calculations by any formula depends on the extent to which the mathematical model, on which this formula is based, corresponds to reality. From this viewpoint, the methods described in this chapter may be used in the following cases:

The relationships considered are most accurate in the case of a horizontal apron. They may be used unconditionally if the apron has a sloping part located in the zone of the bottom roller; otherwise the results will differ considerably from reality. When the sloping part of the apron is located in the bottom-roller zone, the mathematical model is reduced to the case of a horizontal apron.

A second requirement, whose fulfilment increases the accuracy of the results, is the application of the relationships to surface flow with jump. The accuracy is small in the case of a submerged jump and bottom flow.

The applicability of these relationships depends on whether the problem is three-dimensional. I. I. Veits's method may be used in the two-dimensional case only, while the methods of S. A. Egorov and Kh. Sh. Mustafin are applicable in the three-dimensional case. With decreasing $\beta = \frac{b}{B}$ the inaccuracy increases more with Egorov's than with Mustafin's methods.

Computation of ejection through conduits by Egorov's method is subject to all the observations made on the computation of overflow ejection by his method. In the case of ejection through conduits his relationships are, however, applicable also for a submerged surface jump (i.e., when the discharge outlets are flooded).

The methods proposed in this book have the following advantages over earlier ones: 1. They are more accurate in the case of bottom flow.
2. They permit a satisfactory accuracy in the case of an apron with sloping part, as well as when $\beta = \frac{b}{B}$ is small, which is characteristic of ejection at the sides of the draft tube. It is true that the accuracy decreases when the apron has a sloping part and $\beta = \frac{b}{B}$ is small, but this decrease is less than when the relationships of the other authors are used.

The simplest relationships are those of Veits (in the two-dimensional case), particularly because the nomogram proposed by him can be used. Computation by Mustafin's formulas is slightly more complicated and that by Egorov's formulas, far more. Computation by the relationships proposed by us is, of course, more involved, since we consider a mathematical model having an apron with sloping part, and a step between it and the downstream spillway apron. In addition, the form of the relationship

changes with the flow regime behind the dam. Considering the formulas proposed by us for the case of a horizontal apron, the only complication remaining, in comparison with the relationships of Egorov or Mustafin, is that different formulas exist for surface and bottom flow. This increases the accuracy, but cannot complicate the calculations, since the method proposed in this book for determining the type of flow regime is simple.

In conclusion we note that Egorov's formulas for small HPPs /5/ have not been discussed here.

Neither have we considered A.K.Ananyan's work /2/ concerning the carrying capacity of two-level conduits, since it has no direct bearing on the hydraulics of ejection in HPPs.

Chapter V

HYDRAULICS OF THE TAILRACES OF COMBINED HPPs

19. CRITICAL FLOW REGIMES BEHIND THE DAM

Application of the relationships of Chapter II requires in every case knowledge of the flow regime behind the dam, on which the value of the term R entering in these formulas depends. This information is also necessary in order to estimate the forces acting on the structure.

The tailrace depth corresponding to transition from bottom to surface flow differs from the depth at which the inverse transition takes place. These two depths form the limits of the first critical regime, within which there is continuous transition from surface to bottom flow and vice versa. It is called by us zone of instability.

A detailed discussion of instability phenomena will be given in the next section. Here we shall only consider the extent to which the relationships concerning ejection are applicable to critical regimes.

All existing methods of analyzing the first critical regime, proposed by the different authors (except S. A. Egorov's method), are strictly applicable only to a single nappe. Egorov's formulas, which are based on the assumption that in the first critical regime the nappe leaves the end sill along the tangent to its flat, lead to results differing considerably from reality.

The presence of a turbine discharge has no qualitative effect on the variations of the flow regime, but has a quantitative influence. The turbine discharge reduces the instability and causes the first critical regime to correspond to lower tailrace levels.

All the formulas, proposed by the different authors for analyzing the first critical regime, relate the tailrace depth to the discharge. In this book we present, for the first critical regime, empirical relationships between the piezometric effect h_{ej} of ejection (Figure 45) and the height Δh_2 of the free surface of the tailrace above the overflow edge of the end sill.

These relationships were obtained by processing the results of tests of the first critical regime, performed on models of overflow HPPs at MEI, VNIIG, and VIGM. Altogether 181 observations were considered, of which 128 were without, and 53 with turbine discharge; 76 observations corresponded to flow under a sluice gate; in 128 cases the apron had a sloping part immediately behind the HPP, while in the other cases the apron was horizontal along its entire length. The model scales were 1:56 (model with three bays), 1:80 (plane model), 1:52 (plane and semispatial models), 1:20 and 1:17.2 (semispatial models with turbines).

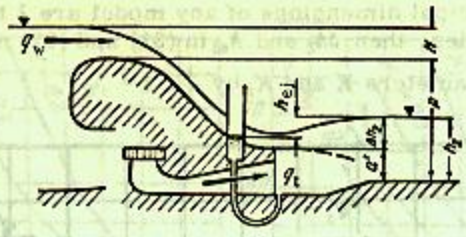

FIGURE 45. Mathematical model of the first critical regime.

The principal [variable] dimensions were the height a' of the overflow edge of the end sill above the raised part of the apron, and the height p of the dam crest above the raised part of the apron.

Converted to full scale, the tests corresponded to

$$6.48\,\text{m} \leqslant a' \leqslant 16.60\,\text{m},\quad 15.10\,\text{m} \leqslant p \leqslant 23.05\,\text{m},$$

with

$$1.33 \leqslant \frac{p}{a'} \leqslant 2.50,\quad 0.13 \leqslant \frac{H}{p} \leqslant 0.75,$$

$$0.74 \leqslant \frac{p}{H+a'} \leqslant 1.40,\quad 0.25 \leqslant \frac{b}{B} \leqslant 1,$$

where H is the head on the dam.

The relationship between h_{ej} and Δh_2 for the models studied is shown in Figure 46. Despite the fairly wide range of variation of the absolute and relative HPP dimensions, the relation between h_{ej} and Δh_2 is relatively close at the first critical regime. The designs studied can therefore be considered as similar. The ratio

$$\frac{p}{H+a'},$$

can be adopted as parameter averaging similar designs, where H is the head on the dam at free overflow.

The curves in Figure 46, which average the experimental points for similar designs, represent the following equations used later in the computations.

Without turbine discharge

$$\Delta h_2 = K h_{ej}^2\,[\text{m}], \tag{31}$$

with turbine discharge

$$\Delta h_2 = K_T h_{ej}^2\,[\text{m}]. \tag{32}$$

In these equations K and K_T are parameters having the dimension $\frac{1}{\text{m}}$:

$$K = 0.40\,\frac{1}{\text{m}},$$

$$K_T = 0.28\,\frac{1}{\text{m}}.$$

We shall now determine how K and K_T vary with the absolute dimensions of the HPP. Consider a series of similar HPP models. If the absolute

values of the principal dimensions of any model are λ times the average values for the series, then Δh_2 and h_{ej} in (31) and (32) must be multiplied by λ, and the parameters K and K_T by $\frac{1}{\lambda}$.

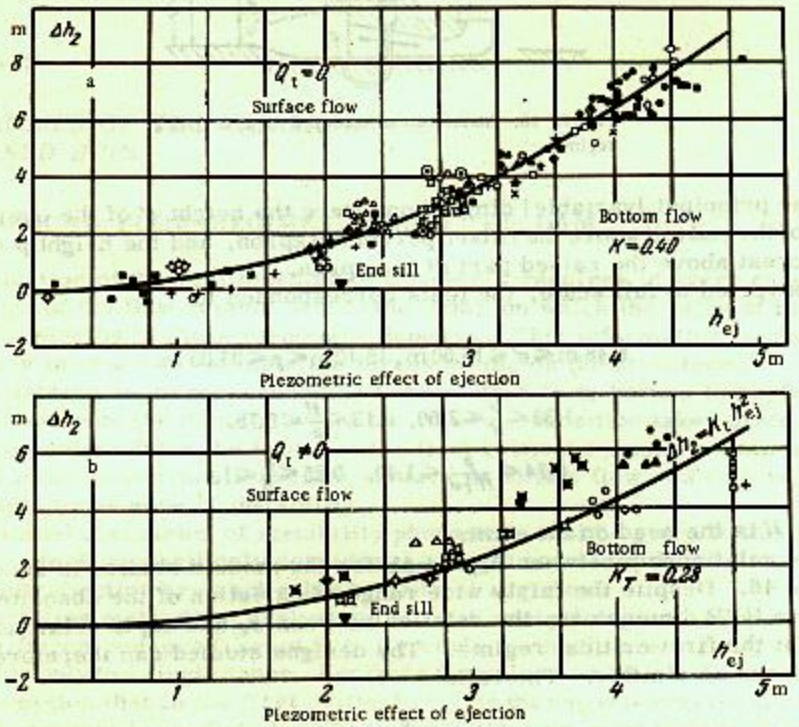

FIGURE 46. Relationship, at first critical regime, between height above toe of free tailrace surface and piezometric effect of ejection.

The average values are $p = 17.20$ m, $a' = 9.98$ m for the the model series considered. The parameter defining the model series is thus

$$\frac{17.20}{H + 9.98},$$

while the discharge over unit length of the dam is

$$q_w = m\sqrt{2g}H^{3/2},$$

where $m = 0.40$ for the selected dam profile.

We now determine the parameter $\frac{17.20}{H + 9.98}$ for different values of H and q_w. The relationship obtained, $q_w = f\left(\frac{17.20}{H + 9.98}\right)$ corresponds to $K = 0.40\frac{1}{m}$ and $K_T = 0.28\frac{1}{m}$.

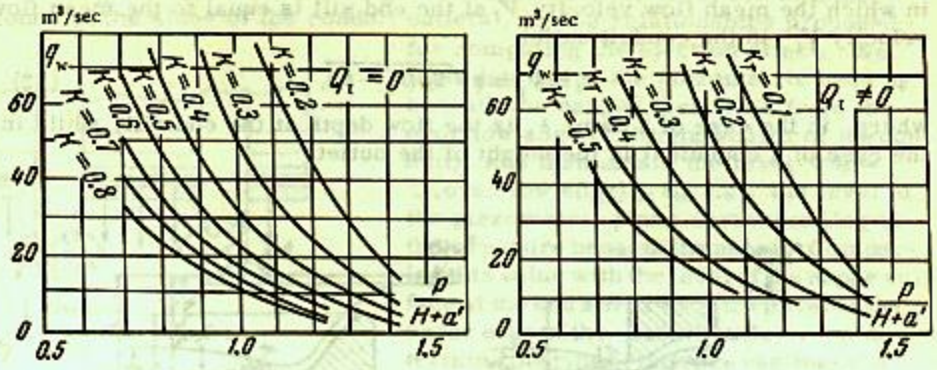

FIGURE 47. Curves of coefficients K and K_T in formulas for analyzing first critical regime.

Multiplying p and a' by λ, and again assuming different values of H, we obtain a new relationship between $\frac{17.20\lambda}{H+9.98}$ and $q_w=m\sqrt{2g}(\lambda H)^{3/2}$, which now corresponds to $K=\frac{0.40}{\lambda}$ and $K_T=\frac{0.28}{\lambda}$. Having thus plotted the family of curves $q_w=f\left(\frac{p}{H+a'}\right)$ (Figure 47), we obtain diagrams for determining the numerical values of K and K_T in (31) and (32). These formulas can now be applied to HPPs having different absolute dimensions, provided that the characteristic parameters lie within the range in which the first critical regime was investigated.

Figure 46 shows that at $Q_t = 0$ the relation between the experimental values of Δh_2 and h_{ej} is fairly close for the model series studied, despite some differences in the absolute and relative dimensions. When $Q_t \neq 0$ (Figure 46) a considerable scatter occurs, due to the influence of the turbine discharge which amounts to between 0.47 and 0.86 of the total discharge. However, the variation of the turbine discharge is not taken into account in (32). This is a shortcoming of the formula, which is accurate for discharge ratios and characteristic design parameters (given at the beginning of this section) near to the average values. This also applies to (31). When the parameters are within the ranges indicated, Δh_2 is obtained at an accuracy of about ±10% from (31) and about ±30% from (32); this has been found by comparing computed and experimental results.

In the analysis we use first (32), since the piezometric effect of ejection interests us only in the presence of a turbine discharge. Of course, this procedure is far from perfect, but it is justified by our purpose, which is to delimit the regions of bottom and surface flow, in order to determine the term R entering in the relationships of Chapter II.

Formula (31) may be used to plot the ejection characteristic for determining the first critical regime when Q_t approaches zero.

This method is also applicable to a discharge through conduits. In this case the conduit (Figure 48,a) must be converted to an "equivalent" dam (Figure 48,b)

in which the mean flow velocity V_1 at the end sill is equal to the mean flow velocity V_1' in the conduit outlet:

$$V_1 = V_1' = \varphi\sqrt{2g(T_0' - h_1)}, \tag{33}$$

where, in the case of a dam, h_1 is the flow depth at the end sill, while in the case of a conduit it is the height of the outlet.

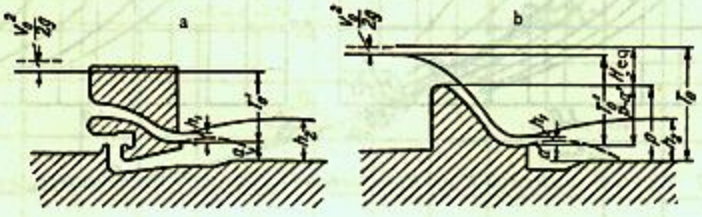

FIGURE 48. Replacing conduit by equivalent dam for computation of surface flow regime behind HPP.

Using this formula, we shall determine the dimensions a' and p, and the head H of the equivalent dam (Figure 48).

Replacing V_1' by $\frac{q_w}{h_1}$, and solving (33) for T_0', we obtain

$$T_0' = \frac{1}{2g\varphi^2}\left[\frac{q_w}{h_1}\right]^2 + h_1. \tag{34}$$

while the condition $\nabla HR + \frac{V_0^2}{2g} = \nabla$ (outlet bottom) + T_0'

$$q_w = m\sqrt{2g}H_{eq}^{3/2}$$

yields the head on, and the height of the equivalent dam:

$$H_{eq} = \left[\frac{q_w}{m\sqrt{2g}}\right]^{2/3},$$

$$p = \nabla HR - H_{eq} - \nabla \text{ (apron)}. \tag{35}$$

We then use (31) and (32), in which K and K_T are determined from the values obtained for a', p, and H.

For the dam profiles for which the empirical relationships were determined, $\varphi = 0.90$ to 0.95, $m = 0.40$.

At the first critical regime the conduit is not flooded. This is important for determining the excess discharge; the computed head is determined from the difference in height between the headrace level and the upper edge of the conduit outlets.

When the characteristic parameters of the HPP lie outside the range investigated, the analysis is carried out without allowing for the turbine discharge, for instance according to A. A. Sabaneev's condition (cf. § 28, point 1). The computed level corresponding to the first critical regime will then be higher than the actual one.

The second critical regime is analyzed under three-dimensional conditions, i.e., when the jump is submerged by the water coming from

the whirlpool zones behind the piers (Figure 49) (or from the whirlpool zones at the sides of the conduit outlets), by the relationships proposed for computing the ejection effect. We first determine the piezometric head h_0 beneath the nappe, measured from the overflow edge of the end sill (or of the conduit), and then obtain the level $\nabla h_0 = \nabla$(overflow edge) $+ h_0$, i.e., the level of the piezometric plane corresponding to the pressure beneath the nappe. Comparing this value with the level of the nappe surface at the end sill or with the level of the upper edge of the conduit outlets, we determine the type of tailrace regime: the jump will be submerged if ∇h_0 exceeds the level of the nappe surface at the end sill or of the upper edge of the conduit outlets.

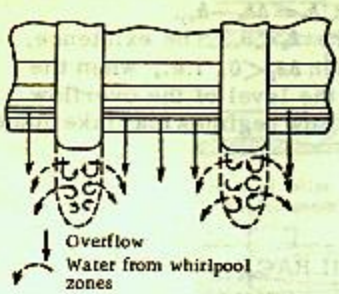

FIGURE 49. Submerging of a jump displaced downstream, by water from whirlpool zones behind piers.

When piers protrude into the tailrace the calculation yields results close to reality only if $\beta = \frac{b}{B}$ is small (submerging of a jump by water from the whirlpool zones was observed by us on a model for which $\beta = 0.58$). When β is of the order of 0.8, sufficiently accurate results are obtained when the piers protrude into the tailrace negligibly beyond the plane of the end sill.

The only method, known to the author, for analyzing the second critical regime with two streams flowing into the tailrace under three-dimensional conditions is that proposed in this book. Under conditions close to plane flow, we must use the relationships derived by I. I. Levi, D. I. Kumin, and M. D. Chertousov for the case when only the overflow discharge enters the tailrace. The computed level corresponding to the second critical regime will differ from the actual one, since the turbine discharge is being neglected. The simplest of these formulas is Chertousov's*:

$$\xi_2 = [1.96\eta + 0.1(1-\beta)(2-\eta)]\cdot(\xi_0 - 0.45\beta - 1.30) + 1.90\beta + 0.40,$$

$$\xi_2 = \frac{h_2 + a'}{h_{cr}}; \quad \xi_0 = \frac{T_0 - a'}{h_{cr}}; \quad \eta = \frac{a'}{p - a'}; \quad \beta = \frac{b}{B};$$

$$h_{cr} = \sqrt[3]{\frac{q^2}{g}}.$$

The magnitudes h_2, a', T_0, and p are shown in Figure 48,b. Chertousov's formulas were derived from experiments with a model with plane apron. They are, however, sufficiently accurate also for an apron with stilling pool provided that a', T_0, h_2, and p are measured from the raised part of the apron, as done in this book.

Chertousov's formula for the second (and also for the first) critical regime is inapplicable to discharge beneath a sluice gate. The dam with sluice gate must in this case be replaced** by an equivalent overflow dam, as was done in the analysis of the first critical regime for a combined HPP with conduit.

* Chertousov, M. D. Spetsial'nyi kurs gidravliki (A Special Course in Hydraulics).— Gosenergizdat, 1949.

** Slisskii, S. M. Raschet sopryazheniya b'efov poverkhnostnym rezhimom pri istechenii iz-pod shchita (Analysis of Surface Flow behind a HPP with Discharge beneath a Sluice Gate).— Gidrotekhnicheskoe stroitel'stvo, No. 4. 1952.

In conclusion, we shall prove that the piezometric head beneath the nappe (measured from the level of the overflow edge of the end sill) may be negative at the first critical regime. In fact, Figure 46 shows that for $h_{ej} < 1.8$ m, $\Delta h_2 < h_{ej}$. But $h_{ej} = \Delta h_2 - h_0$, so that $h_0 = \Delta h_2 - h_{ej}$.

In the case considered $\Delta h_2 < h_{ej}$, and therefore $h_0 < 0$. The existence, in some cases, of the first critical regime, when $\Delta h_2 < 0$, i.e., when the level of the free tailrace surface is lower than the level of the overflow edge of the end sill, also proves that a change of flow regimes may take place when $h_0 < 0$.

20. INSTABLE FLOW REGIMES IN THE TAILRACE

The instable flow regimes observed in the tailraces of models of combined HPPs* are due either to transition from surface to bottom flow (or vice versa), or to periodic breakthroughs of air underneath the nappe (at bottom flow).

The author observed the following three typical cases of instability during the change of flow regimes in models:

1. Periodic horizontal displacements of the roller under conditions of bottom flow at depths close to the lower limit of the first critical regime (Figure 50,a).
2. Similar displacements of the surface roller under conditions of surface flow at depths close to the upper limit of the first critical regime (Figure 50,b).
3. Considerable periodic fluctuations of the tailrace level in the instability zone (Figure 50,c). In this case a surface roller is formed at a certain distance from the structure, and increases in magnitude as it travels upstream. The roller sometimes reaches the end sill and may even flood it if the end sill is low. After the roller submerges the nappe, the latter begins to rise rapidly from the bottom, and the roller becomes spread out over the surface.

When the end sill has an inverse slope, tailrace-level fluctuations of smaller amplitude are observed at a certain distance from the structure. Smaller fluctuations are observed when the turbine is operating.

The instability due to periodic breakthroughs of air underneath the nappe manifests itself in fluctuations of the nappe flowing into the tailrace (Figure 51). This phenomenon is observed only at low levels and a definite ratio between the lengths of the end sill and the piers protruding into the tailrace. If this ratio is such that the piers prevent access of air underneath the nappe, the pressure reduction beneath the latter causes it to be forced toward the batter, but if air penetrates underneath the nappe, the latter is returned to its previous position. A large instability of this type, accompanied by a "snoring" sound of air being sucked underneath the nappe, was observed at an end sill with forward slope.

Converted to full scale, the tailrace level fluctuations observed by the author during flow-regime changes in models of overflow HPPs, had amplitudes reaching 8 to 9 m.

* Cf. Veits, I.I. Kompleksnoe sooruzhenie "GES — vodosbros — sudokhodnyi shlyuz" (The Complex Structure "HPP — Conduit — Navigation Lock"). — Izvestiya VNIIG, Vol. 31. 1946.

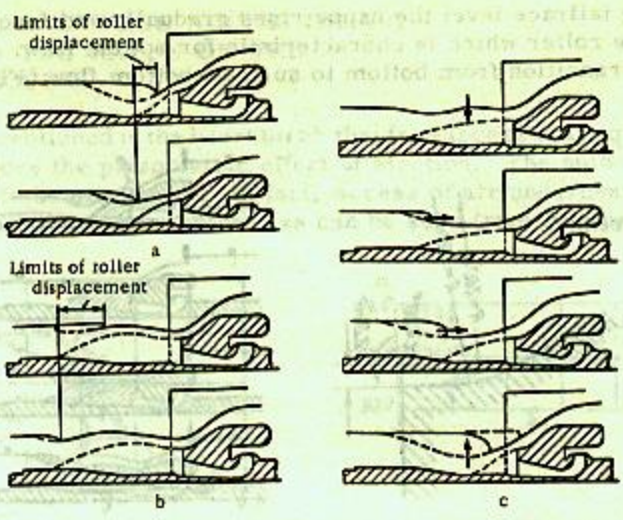

FIGURE 50. Typical cases of instability observed during changes of flow regime.

The question arises whether instable flow regimes exist under field conditions. Since all types of flow regimes and their changes are fully simulated when the Froude number is maintained constant, the instability phenomena are also simulated. If, however, the fluctuation period in a 1:50 model is 8 to 10 sec, it will be $\sqrt{50}$ times larger under field conditions, i.e., of the order of 60 to 70 sec. Since during high water the tailrace level always rises or drops, fluctuations of such a period will, of course, be very rarely observed.

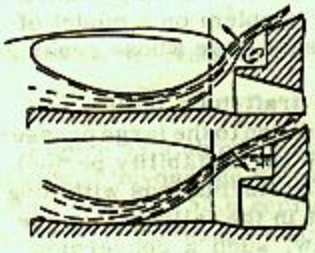

FIGURE 51. Periodic fluctuations of nappe, caused by flow of air from underneath nappe and back.

Practically no instability exists during transition from bottom to surface flow and vice versa under three-dimensional conditions when β is of the order of 0.7 to 0.6 or less. Water coming from the side rollers alters the pattern of flow-regime changes usual under plane conditions.

Attempting to reduce the tailrace-level fluctuations during instable conditions, the author tested end sills having overflow edges at different levels. The end sills were horizontal, or had forward or inverse slopes. It was found that the end-sill height does not significantly affect the instability, but only determines the tailrace depth at which this instability appears. The same is true for sloping end sills.

The author observed a considerable reduction in the fluctuations during instable conditions, up to a complete disappearance of the transitional regime, when teeth were arranged on the end sill. The instability in the tailrace of a plane model with teeth on the end sill is very peculiar. With

increasing tailrace level the nappe rises gradually and forces downstream the surface roller which is characteristic for bottom flow. There is thus a smooth transition from bottom to surface-bottom flow (Figure 52).

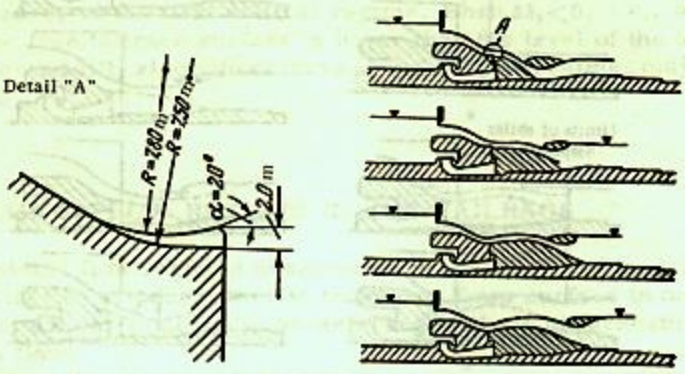

FIGURE 52. Flow regimes behind a dam having teeth on the end sill (plane model).
A—tooth; tooth width = 1.7 m, distance between teeth = 1.7 m (full scale).

Instability caused by breakthroughs of air underneath the nappe can be eliminated by providing for free access of air underneath the nappe.

The question of how tailrace-level fluctuations during instable conditions affect the pressure distribution at the draft-tube outlet is of importance in combined HPPs. The author investigated this problem on a model of an overflow HPP with the aid of an electric pressure gage whose readings were recorded by an oscillograph.

The oscillograms indicated the presence, at the draft-tube outlet, of short-period fluctuations of small amplitude, in addition to the large pressure fluctuations having long periods (corresponding to the instability period). While the amplitude and frequency of the pressure fluctuations with long periods (i.e., those caused by instable conditions in the tailrace) can be converted to full scale by applying Froude's law, such a conversion has not yet been achieved for the high-frequency fluctuations; this problem is being studied at present at several Soviet scientific establishments.

The amplitude of the long-period fluctuations depends on the amplitude of the tailrace-level fluctuations in the same zone. When the turbine is not in operation, the amplitudes of the pressure fluctuations at the draft-tube outlet during instable conditions are about 50 % of those recorded on the apron. When the turbine is in operation, there are almost no pressure fluctuations at the draft-tube outlet, despite the instable conditions in the tailrace.

Teeth on the end sill cause a considerable reduction of the pressure fluctuations at the points considered.

21. INFLUENCE OF FREE ACCESS OF AIR UNDERNEATH THE NAPPE ON THE EJECTION PROCESS

It has been mentioned in the literature* that free access of air underneath the nappe reduces the piezometric effect of ejection. The author found this assertion to be erroneous. In fact, access of air underneath the nappe increases the ejection effect, as can be seen from Figure 53.

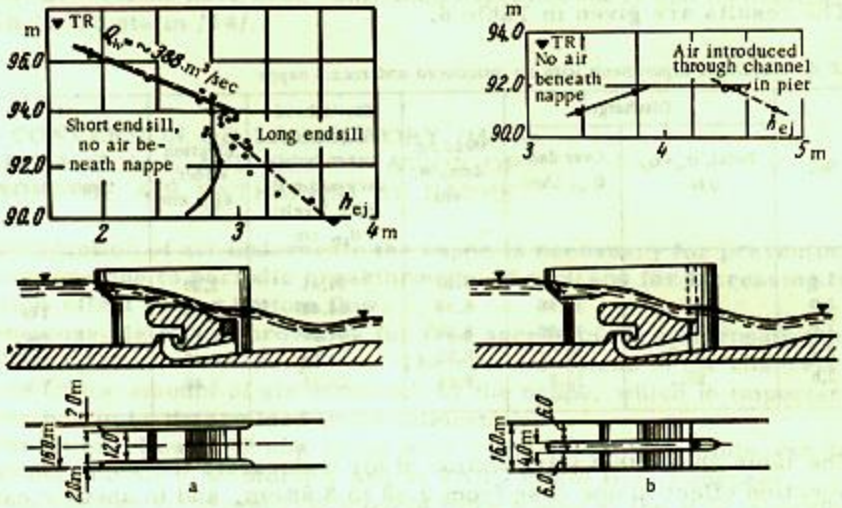

FIGURE 53. Influence of free access of air underneath nappe (converted to full scale from 1:52 model).

Figure 53,a shows a weir with lengthened toe, which caused the nappe to extend beyond the piers; this permitted free access of air underneath the nappe. Figure 53,b represents the case in which air was introduced underneath the nappe through a channel in the pier.

The experiments were performed on a 1:52 plane model without turbine, whose dimensions were:

Width of span (chute width)	30.8 cm
Height of crest above blanket	26.6 cm
Height of overflow edge above apron	29.5 cm
Height of crest above overflow edge .	12.4 cm

Water flowed simultaneously over the weir and through the turbine passage. The total discharge was about 20 l/sec. The sluice gates were fully opened.

The discharge, the levels of headrace and tailrace (at the end of the downstream spillway apron), and the piezometric head at the draft-tube outlet were measured. The ejection effect was determined as the difference between the tailrace level at the end of the downstream spillway apron and the piezometric head at the draft-tube outlet.

* Cf. /4/, p. 52.

The experimental procedure was as follows.

Bottom flow was established; at first, in the absence of air beneath the nappe, the void at this place became filled with water. After the headrace and tailrace levels and the piezometric head at the draft-tube outlet had been measured, a 10 mm-diameter glass tube, intended for the introduction of air, was inserted into the stream at the chute wall. When the air entering through this tube had filled the void beneath the nappe, the free surface beneath the nappe became stabilized at a constant level. The corresponding levels and piezometric head were then measured again.

The results are given in Table 6.

TABLE 6. Results of experiments with air introduced underneath nappe

No.	Discharges		Head on dam, H, cm	Static head (difference between headrace and tailrace levels), H_{st}, cm	Ejection effect, h_{ej}, cm	Introduction of air underneath nappe
	Total, Q_w+Q_t, l/sec	Over dam, Q_w, l/sec				
1,a	19	12.84	8.43	24.41	2.33	No
1,b	19	12.66	8.36	24.40	3.58	Yes
1,c	19	13.00	8.50	24.50	2.64	No
2,a	20.2	14.21	8.95	25.15	2.48	No
2,b	20.1	13.8	8.86	25.35	3.48	Yes

The table shows that introduction of air underneath the nappe increased the ejection effect in one case from 2.33 to 3.58 cm, and in another case from 2.48 to 3.48 cm, i.e., by 53.6 and 40.4 % respectively.

The reason for this is easily explained. In the absence of air beneath the nappe a [partial] vacuum is created there; the nappe is displaced toward the overflow batter, as in the case of discharge over a thin-walled dam without access of air underneath the nappe. The nappe thus forces the turbine discharge upward, reducing the piezometric effect of ejection. This phenomenon does not occur when free access of air underneath the nappe is possible.

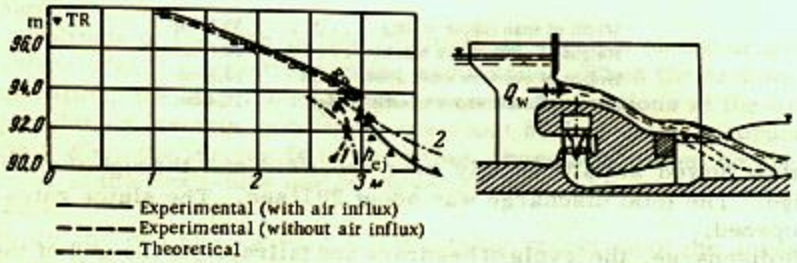

FIGURE 54. Piezometric effect of ejection as function of tailrace level, with and without air underneath nappe (air influx due to lengthening of end sill; surface flow — upper part of curves).

The conclusion that free access of air underneath the nappe has a favorable influence on the ejection effect can also be reached from an examination of the mathematical model. In the presence of a [partial] vacuum, the pressures at the end sill are partly negative. The positive pressure at the draft-tube outlet must therefore be higher to preserve the equilibrium of forces.

The positive influence of free access of air underneath the nappe is expressed in the relationships proposed in Chapter II, as can be seen from Figure 54.

Our deductions have been confirmed experimentally and theoretically by Kh. Sh. Mustafin /14/.

22. CONVERSION OF LABORATORY DATA TO FULL SCALE AND COMPUTATION OF AMOUNT OF AIR ENTRAINED BY NAPPE

Introduction of air underneath the nappe is necessary for preventing fluctuations due to periodic breakthroughs of air, and for increasing the ejection effect during bottom flow.

One possible way of providing for free access of air underneath the nappe is by channels in the piers. The cross sections of the channels depend on the amount of air entrained by the nappe, which in important cases, has to be determined in the laboratory.

For an overflow HPP now being built in the Soviet Union this was done at the MEI imeni V. M. Molotov and at VNIIG imeni B. E. Vedeneev.

Two similar 1:156 and 1:52 models were tested at the MEI laboratory, and a 1:20 model at VNIIG. The experimental procedure was as follows.

TABLE 7.

Model scale λ	$\lambda^{3/2}$	Height of air pocket h, cm	Pocket width (between pier center lines*) b, cm	Volume of air pocket W, cm^3	Time required for pocket to become filled with water t, sec	Air discharge for model Q, l/sec	Full-scale air discharge converted according to Froude's law, m^3/sec
1:20	1,790	16	80	27,300	5	5.46	9.79
1:52	19,470	4.2	30.8	725	5.2	0.139	2.70
1:156	304,000	1.40	10.25	26.9	9.0	0.003	0.91

* The nappe impinged behind the piers, since the latter formed semicircles [in elevation] in the tailrace, the space beneath the nappe was closed and air had no access. Differences in pocket width (inside and outside the piers) were not taken into account in the pocket volume. The distance between the center lines of the piers was taken as width b; this did not affect the final results, since the nappe width was also taken as the distance between the center lines of the piers in computing the air discharge per unit nappe width.

The lowest possible tailrace level, at which no spontaneous breakthrough of air underneath the nappe occurred, was established at a 10.25 m-head

on the dam and a 418 m³/sec discharge over the dam (under the sluice gate). Air was then introduced through a glass tube, so that an air pocket was formed beneath the nappe. After removal of the tube the air in the pocket was gradually entrained by the flow, and the pocket filled with water. The average air discharge was determined by measuring the dimensions of the pocket and the time necessary for it to become filled with water (Table 7).

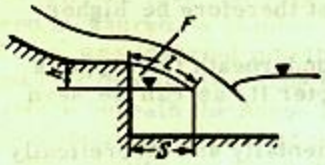

FIGURE 55. Computation of amount of air entrained by nappe.

The [vertical] distance from the free surface of the water beneath the nappe to the overflow edge of the end sill was taken as height h of the air pocket (Figure 55). Although the free surface levels of the headrace and the discharges were in all models in accordance with the similitude conditions, the height h differed when converted to full scale. Thus, in the models it was 16 cm, 4.2 cm, and 1.40 cm, corresponding to 3.2, 2.2, and 2.2 m in full scale. This may be explained both by measurement errors and by some differences between the models: the 1:20 model had grooves in the piers at the tailrace side; the 1:156 model consisted of three bays; the apron of the 1:52 model differed in outline and position from those of the 1:20 and 1:156 models.

The area F of the air-pocket cross section was assumed to equal that of a parabolic segment:

$$F=\frac{2}{3}hS,$$

where S is the pocket base (Figure 55).

The experiments showed that $S\approx 2h$. Thus, the area of the parabolic segment is

$$F=\frac{4}{3}h^2.$$

The air-pocket volume is

$$W=\frac{4}{3}h^2b,$$

where b is the width of the model between the piers.

The last column of Table 7 shows the air discharge, converted to full scale according to Froude's law. It is seen that the phenomenon of air entrainment does not follow this law.

Conversion of the air discharge in the model to full scale necessitates finding a parameter characterizing air entrainment. Such a parameter may be the air-pocket height h, which characterizes the dimensions of air pocket and model, the pressure beneath the nappe, and implicitly, the flow velocity of the nappe.

Applying the dimensional analysis, we shall express the air discharge as a function of h.

Assuming that the air discharge Q is a function of the flow velocity V around the air pocket, and of the area F_0 of the interface between the air and the moving water,* we can write

$$Q=kV^xF_0^y,$$

* The water in the nappe is not saturated with air. Air is entrained only at the lower surface of the nappe, and also along the line of nappe impingement on the tailrace surface (over the apron width), as shown by V. G. Sokolov, in his paper "Ob issledovanii aeratsii potoka na modeli vodoslivnoi GES" (Investigations of Flow Aeration on the Model of an Overflow HPP).— Trudy gidravlicheskoi laboratorii, No. 3. 1952.

where k is a proportionality factor.

We have $V=\frac{l}{t}$ and $F_0=bl$, where l is the length of the nappe, measured from the overflow edge to its point of impingement on the free surface of the tailrace, b is the tailrace width, measured between the piers [and t is the time in sec.]; $l=k_1h$ and $b=k_2h$. We obtain $V=k_1\frac{h}{t}$ and $F_0=k_1k_2h^2$, where k_i is another proportionality factor ($i=1, 2$).

Substituting the expressions obtained for V and F_0 in the formula for the discharge, we obtain

$$Q=k\left(\frac{k_1h}{t}\right)^x(k_1k_2h^2)^y=k_3\left(\frac{h}{t}\right)^xh^{2y}.$$

The exponents x and y are found from the dimensional equation

$$\left[\frac{L^3}{T}\right]=\left[\frac{L}{T}\right]^x[L]^{2y}, \quad \text{i.e.,} \quad T^{-1}=T^{-x},$$

which yields $3=x+2y$; $-1=-x$, and therefore $x=1$; $y=1$.

Thus

$$Q=k_3\frac{h^3}{t},$$

where $t=1$ sec; k_3 is a dimensionless coefficient; writing $\frac{k_3}{t}=k_0$, we obtain finally

$$Q=k_0h^3. \tag{36}$$

The experimental results were

Model 1: λ	1:20*	1:52	1:156
Average air discharge Q, cm³/sec ..	5,460	139	3
Height h, cm	16	4.2	1.40
h^3	4,096	74.09	2.74
$k_0=\frac{Q}{h^3}$	1.33	1.88	1.09

* The experiments were carried out at VNIIG by the author together with Kh. Sh. Mustafin.

The coefficient k_0 is approximately 1.5 on the average.

A similar result is obtained also by a different procedure. Since the air discharge depends on the pressure beneath the nappe, we have

$$Q=k_0h^n,$$

and

$$\lg Q=\lg k_0+n\lg h.$$

Hence for

$1:\lambda=1:20$ $\lg Q=\lg 5{,}460=3.7372$, $\lg h=\lg 16=1.2041$,
$1:\lambda=1:52$ $\lg Q=\lg 139=2.1430$, $\lg h=\lg 4.2=0.6232$,
$1:\lambda=1:156$ $\lg Q=\lg 3=0.4771$, $\lg h=\lg 1.40=0.1461$.

Figure 56 represents $\lg Q$ as a linear function of $\lg h$. At $\lg h=0$ we have $\lg Q=\lg k_0$, where $k_0=1.5$. We determine n from the data obtained

for the largest model (1:20):

$$n = \frac{\lg Q + \lg k_0}{\lg h} = \frac{3.7372 + 0.1761}{1.2041} = 2.96,$$

or about 3.

Thus, $k_0 = 1.5$ indeed satisfies (3b).

Now, to determine the air discharge, we must first find Q_m and h_m experimentally (for the model). From $k_0 = \frac{Q_m}{h_m^3}$ we then obtain the full-scale air discharge

$$Q = k_0 (\lambda h_m)^3 \qquad (36')$$

In the absence of air channels this is the air discharge averaged over the period during which the pocket fills with water. Of course, initially, at a low water level in the pocket, the discharge will be higher than the average, while at the end it will be less. Introduction of air underneath the nappe changes the unsteady process of entrainment into a steady one.

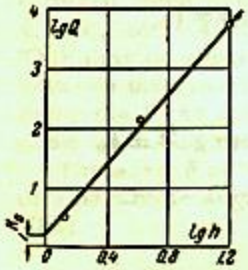

FIGURE 56. Determination of coefficient k_0 in formula for amount of air entrained by nappe.

Additional experimental data indicate that in the general case it would be better to express the air discharge as a function of Sh^2 (Figure 55), which is also correct dimensionally.

We shall now establish a tentative formula for determining in the design stage the air discharge for dams with horizontal end sills and ratios T'/h near to those considered. The following assumptions are made:

1. The coefficient k_0 is independent of the air-pocket height.

2. The coefficient k_0 does not depend on the overflow discharge.

3. When the air-pocket dimensions h, b, and l (Figure 55) are given, the air discharge depends mainly on the flow velocity around the pocket.

4. The flow velocity around the air pocket depends on the [potential] energy T' per unit dam length, referred to the overflow edge of the end sill $T' = \nabla HR - \nabla$ (toe).

The first assumption is arbitrary. Since, however, the relationships are considered as tentative, this is acceptable.

The second assumption is based on observations of nappes, which showed that they are not saturated with air, irrespective of their depth. A negligible influence of the overflow discharge on the entrainment of air by the nappe was observed in V. G. Sokolov's experiments at VODGEO.

We shall proceed from the data obtained with a 1:20 model, which was the largest used: dam width $b_w = 60$ cm, $T' = 83.5$ cm (horizontal end sill),

$$\frac{T'}{h} = \frac{0.835}{0.16} \approx 5.$$

The total and unit (per 1 m dam length) air discharges in the 1:20 model were respectively

$$Q = k_0 S h^2; \quad q = \frac{k_0 S h^2}{b_w},$$

hence $k_0 = \frac{Q}{Sh^2} = \frac{5,460}{2h \cdot h^2} = 0.665$.

The corresponding values for the HPP being designed are

$$Q_{com} = k_0 S_{com} h^2_{com}, \quad q_{com} = \frac{k_0 S_{com} h^2_{com}}{\lambda b_w},$$

where h_{com}, S_{com} are the computed values of the height and length of the air pocket found by the formulas of Chapters I and II; λ is a scale factor, being the ratio of the linear dimensions of the HPP being designed and of the model.

Were the HPP being designed geometrically similar to the model for which k_0 was determined, the formulas obtained would require no further transformations. Usually, however, this is not the case. We must therefore use as scale factor the ratio of those geometric parameters whose magnitudes determine the amount of air entrained by the nappe. One of these is, in accordance with assumptions 3 and 4, the height T' of the headrace level above the overflow edge of the end sill, i.e.,

$$\lambda = \frac{T'_{com}}{T'},$$

where T'_{com} is the [potential] energy per unit dam length, referred to the overflow edge of the end sill in the HPP being designed; T' is the same for the model (scale 1:20).

Substituting the value of λ in the expressions for the unit and total discharges of air in the HPP being designed, we obtain:

$$q_{com} = \frac{k_0 S_{com} h^2_{com}}{b_w} \frac{T'}{T'_{com}}$$

and

$$Q_{com} = \frac{k_0 S_{com} h^2_{com}}{b_w} \frac{T'}{T'_{com}} b_{com} = \frac{0,665 \cdot 0.835 S_{com} h^2_{com}}{0.607 T'_{com}} b_{com},$$

where b_{com} is the width of the dam in the HPP being designed.

Introducing a safety factor of about 2, and omitting the subscripts of h, T', and b, we obtain finally:

$$Q_{com} = 2 \frac{Sh^2}{T} b. \qquad (36'')$$

The average air discharge obtained by this formula corresponds to the case when the pocket height h_{com} varies from its maximum (when a breakthrough of air underneath the nappe is imminent if free access of air is not provided for) to zero (when acess of air is prevented). Having determined h_{com}, we do not know by how much the pocket height differs from its maximum. This does not prevent the use of (36''), since the height of the pocket (into which air must be introduced) cannot exceed this maximum, while with decreasing height the amount of air entrained also decreases.

It could be concluded from an examination of (36'') that it is incorrect, since an increase of $T = T'_{com}$ (which determines the scale factor λ) causes

a reduction of the discharge Q_{com}. However, for a given overflow discharge, tailrace depth, and end-sill height, an increase of T', and thus of the flow velocity of the nappe, leads to an increase of the air-pocket height h, whose square appears in the numerator, and of the length S.

For the design studied by V. G. Sokolov (toe with inverse slope which increases considerably the length of the nappe, $\frac{T'}{h} \approx 8$, $b = 0.26$ m, $T' \approx 0.39$ m, $S = 0.42$ m, $h = 0.05$ m, air discharge $Q = 0.0038$ m^3/sec), we have for the actual (nonaveraged) air discharge: $k_0 = \frac{Q}{Sh^2} \approx 3.5$ and $Q_{com} \approx 5\frac{Sh^2}{T'} b$ (without safety factor).

The cross section of the air channel is determined in accordance with the velocity of the air flowing through it:

$$V = \varphi \sqrt{2g \frac{\Delta p}{\gamma_{air}}},$$

where Δp is the pressure drop; $\gamma_{air} \approx 1.3$ kg/m^3 is the specific weight of air.

The pressure drop was not measured during the experiments described in this section. For a tentative design we determine the pressure drop from the piezometric head h_0 on the overflow edge of the end sill when there is no access of air underneath the nappe: $\Delta p = \gamma h_0$. The pressure drop may also be determined from the height h of the air pocket: $\Delta p = \gamma h$.* This gives a smaller safety margin for the cross-sectional area of the channel. The values of h_0 or h are obtained by the formulas of Chapter II or III.

The magnitude Δp determined from h_0 corresponds to the instant at which the air pocket becomes completely filled with water, which can happen only when there is no access of air underneath the nappe. At this instant the pressure drop exceeds considerably that existing when the pocket begins to fill with water, since, when access of air is cut off, the pressure beneath the nappe is practically atmospheric. When the air channel has a considerable cross-sectional area, the pressure beneath the nappe is thus practically atmospheric. With decreasing cross-sectional area the pressure drop increases, and the level of the free surface in the air pocket rises.

The air velocity determined from the pressure drop γh_0 (and even more, from γh) is too high, since this pressure drop is impossible when there is free access of air underneath the nappe.

Recognizing that (36") is neither rigorously derived nor accurate, it may nevertheless be used (as for the design studied in § 21) until more accurate relationships are obtained by subsequent laboratory investigations.

23. LENGTH OF NAPPE

In order to select the formula relating the tailrace depth to the pressure beneath the nappe, we must know whether the sloping part of the apron lies inside or outside the zone of dynamic action of the nappe.

* Since $|\gamma h| > |\gamma h_0|$ the air velocity corresponding to the pressure drop γh will be larger than that corresponding to γh_0.

When the pressure beneath the nappe is atmospheric, which is possible only during bottom flow, the answer to this question depends on the nappe length

$$X_0 = V_1 \sqrt{\frac{2y}{g}};$$

where V_1 is the average flow velocity at the end sill (or in the outlet section of the conduit); y is the height of the c.g. of the nappe in section I-I above the point at which the nappe impinges on the apron; g is the gravitational acceleration.

We take, for simplicity, the plane 0-0 (Figure 57) as the apron surface. The height, above the plane 0-0, of the c.g. of the nappe in section I-I is $y = a' + \frac{d}{2} + \frac{h_1^*}{2}$, while

$$V_1 = \varphi \sqrt{2gT_0'},$$

where T_0' is the height of the headrace level above the overflow edge of the end sill.

Hence

$$X_0 = \varphi \sqrt{2gT_0'} \cdot \sqrt{\frac{2a' + d + h_1}{g}}. \qquad (37)$$

The depth h_1' at the toe can be determined from the formula for the nappe contraction.

In most cases, however, the pressure beneath the nappe is not atmospheric, being given by the piezometric head h_0 measured from the overflow edge of the end sill or the conduit outlet. When $h_0 \geq 0$ the effect of the excess pressure beneath the nappe (Figure 58) is to increase its length. When $h_0 < 0$, the pressure beneath the nappe is below atmospheric along the first part of its length, which leads to a decrease of the latter. Knowing the effect of h_0 on the nappe length, we can determine approximately whether the nappe will impinge on the sloping part of the apron.

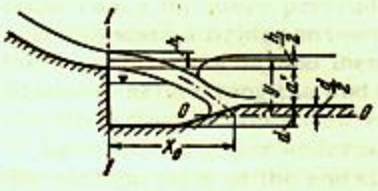

FIGURE 57. Determination of nappe length (atmospheric pressure beneath nappe).

We assume that when the pressure beneath the nappe is atmospheric it impinges on the sloping part of the apron (Figure 59). When $h_0 \geq 0$, the sloping part is in case a located in the bottom-roller zone, while in case b it lies in the zone of dynamic action of the nappe; when $h_0 < 0$, the sloping part is in case a located in the zone of dynamic action of the nappe, and in case b, in the bottom-roller zone.

While the solution thus obtained is approximate, it usually permits a correct selection of the formula.

* h_1 can be determined from the formula for the nappe contraction or from the nomogram in Appendix I for $\xi_0 = \xi_1$.

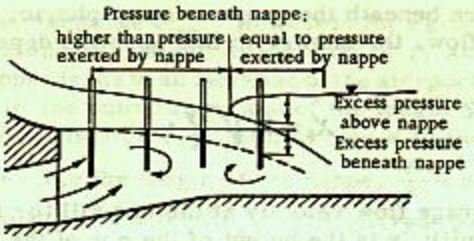

FIGURE 58. Pressure distribution beneath nappe for $h_0 = 0$.

FIGURE 59. Two extreme cases of nappe impingement on apron. Between these limits the pressures on the sloping part of the apron may be assumed to be as shown in Figure 22,b.

Chapter VI

DESIGN OF COMBINED HPPs

24. DESIGN MEASURES PROVIDING FOR FREE ACCESS OF AIR UNDERNEATH THE NAPPE

When bottom flow is possible behind the dam, it is necessary to ensure atmospheric pressure beneath the nappe, i.e., to provide for free access of air underneath it, in order to increase the ejection effect and to prevent instability of the nappe (cf. § 21).

One of the following design measures may be taken for this purpose:

1. Lengthening and heightening the end sill (or giving it an inverse slope), so as to make the lower surface of the nappe extend beyond the piers (Figure 54). The downstream noses of the piers must then be rectangular in plan.*

2. Arranging air channels in the piers, so that the space beneath the nappe is in communication with the atmosphere (Figure 53).

3. Arranging grooves in the piers similar to those for stoplogs and sluice gates, but deeper.

The first measure is the simplest, but is not always possible, since in some cases the piers protrude so far into the tailrace (in order to accommodate a bridge on them) that it becomes impossible to ensure that the nappe extends beyond them by heightening or lengthening the end sill. In addition, heightening the end sill or giving it an inverse slope may reduce the ejection effect at other flow regimes.

Introduction of air underneath the nappe through channels does not alter the configuration of the end sill or piers. The upper edges of the air-channel outlets beneath the nappe must be, as far as possible, at the level of the overflow edge of the end sill. Climatic conditions prevailing during the discharge of flood water may require that measures against the blocking of these outlets by ice be taken.

Introduction of air underneath the nappe through grooves is possible but inconvenient from the point of design. The use of sluice-gate and stoplog grooves is made difficult due to water being sucked in through them from the nappe, as a result of which the supply of the necessary amount of air is not always guaranteed.

If the piers are moved upstream so that their downstream noses are located on the streamlined spillweir face (at a certain distance from the overflow edge of the end sill), the nappes from adjacent bays unite within the

* When the piers form a smooth curve in plan, the nappes from adjacent bays unite behind the piers and close the space beneath the nappe, thus preventing access of air underneath it.

dam limits* and close the space beneath the nappes. Although the latter extend beyond the piers, a free access of air is not ensured when no air channels are in this case provided in the piers. The channel outlets should be located on the end sill.

The width of the conduit outlets in a combined HPP with conduits is very often smaller than the distance between facing surfaces of the piers (cf., for instance, Figure 39). In this case the air flows underneath the nappe through the space between the latter and the sides of the piers. If the width of the conduit outlets is equal to the distance between the piers, air may be introduced underneath the nappe by the same methods as with overflow ejection.

25. SELECTION OF LEVEL OF END SILL OR CONDUIT-OUTLET BOTTOM. LENGTH AND SLOPE OF END SILL

a. General considerations

The following aims may be accomplished by correctly selecting the end-sill level:

1) A tailrace flow regime promoting discharge of ice.
2) Favorable conditions at the apron and downstream spillway apron.
3) A maximum ejection effect.

The most difficult conditions exist for the discharge of ice when a roller is thrust over the end sill; this may occur with a submerged jump and during bottom flow when the end sill is low.** When the depth of the nappe is small compared with that of the roller on the end sill the ice is in either case retained in the roller and strikes the structure.

When the end sill is sufficiently high (cf. below) a roller cannot be thrust onto it during bottom flow. The author found that in model tests of bottom flow with surface roller downstream of the end sill, floating bodies simulating ice struck the apron when the tailrace was shallow, after being ejected from the roller, and even penetrated into the draft tube when there was no turbine discharge.

Thus, if severe ice conditions are to be expected at an overflow HPP (or an overflow dam with end sill), the end-sill height should be such that bottom flow with roller thrust onto the end sill becomes impossible; when the tailrace is shallow, bottom flow with developed surface roller must also be prevented by a sufficiently high end sill.

Favorable conditions for the discharge of ice are created by a surface jump,† which should be aimed at by suitable selection of the end-sill level of dams subjected to severe ice conditions.

When the end-sill level is selected so as to obtain favorable conditions at the apron and downstream spillway apron (at which the flow velocities at the

* Cf., for instance, Sokolov, V.G. Ob issledovanii aeratsii potoka na modeli vodosliynoi GES (Investigations of Flow Aeration on the Model of an Overflow HPP).— Trudy gidravlicheskoi laboratorii, No. 3. 1952.

** When the toe height does not permit transition from bottom to surface flow.

† Cf., for instance, Grishin, M.M. Gidrotekhnicheskie sooruzheniya (Hydraulic Structures).— Part 1, p. 46, Moskva. 1947; or Levi, I.I. Metodika rascheta manevrirovaniya zatvorami na gidrotekhnicheskikh sooruzheniyakh v tselyakh bor'by s razmyvom dna i razrusheniem kreplenii rusla (Computation Methods for Gate Control in Hydraulic Structures in Order to Prevent Scouring and Destruction of Stream-bed Shorings).— Izvestiya VNIIG, Vol. 32, p. 99. 1947.

bottom behind the structure and the direct dynamic effect of the nappe on the apron are reduced to a minimum), a surface-bottom flow regime is frequently the most unfavorable, since it is characterized by a jump having a very high first wave behind which the stream is forced downward; as a result, typical bottom flow with surface roller is established at a certain distance downstream of the structure (Figure 12,C'), with a direct dynamic effect of the nappe on the apron. This was observed on a model of the Molotov HPP, studied at the hydraulic laboratory of MEI imeni V. M. Molotov, and also earlier, during investigations of the structures of the Volgostroi (Yaroslavskii) HPP, the Gor'kovskii HPP, and the Ivan'kovskii HPP (cf., for instance, /6/).

Surface-bottom flow occurs near the second critical regime. Hence, in order to avoid lengthening the tailrace shorings, the end sill should be at a level differing from that at which the second critical regime occurs.

Surface-bottom flow, like the second critical regime with high waves, occurs only under conditions close to the two-dimensional problem, when $\beta = \frac{b}{B} > 0.7$. When β is small, the surface jump is displaced downstream and submerged by water coming from the whirlpool zones behind the piers (Figure 49)* without high waves being formed.

When an end sill is provided, the nappe descends from it during bottom flow almost as in a free fall. Energy is dissipated when the nappe descends from a low dam or buttress. There are examples of a free nappe descending from arch and buttress dams and from unwatering conduits. However, in designing combined HPPs it is usual to aim at preventing a free fall of the nappe (i.e., to avoid an end-sill height at which bottom flow occurs in the tailrace). Unfortunately, it is not always possible to design a HPP so that bottom flow behind it becomes impossible. It may occur at the beginning of high water, when the tailrace level is low. In some of the HPPs being planned this is unavoidable, since no other conduits are provided than those of the HPP.

When the end-sill height and the tailrace depth render bottom flow unavoidable (and also frequently during surface-bottom flow with jump), the flow velocities at the bottom at the beginning of the downstream spillway apron can be reduced by baffles which divert the flow from the bottom to the surface. Baffles should be used in HPPs with circumspection, since they may create a backwater reducing the power.

The conditions at the apron are most favorable when a submerged jump exists; this requirement frequently determines the end-sill height.

The end-sill level ensuring a maximum ejection effect depends also on the end-sill profile (length and slope), the apron profile, and the length and shape of the pier noses protruding into the tailrace.

Lengthening the straight part of the end sill affects the length of the nappe; it was shown above that if the apron has a sloping part, the ejection effect depends on the point at which the nappe impinges on the apron. In addition, at bottom flow the end-sill length determines the possibility of free access of air underneath the nappe, which also affects the ejection effect.

Giving the end sill a forward or inverse slope reduces the ejection effect when the apron is horizontal, as was found both experimentally and from analysis of the formulas. If the inverse slope of the end sill is inclined less than 15°,

* This phenomenon depends also on the amount by which the piers protrude into the tailrace.

this reduction is negligible, but at steep slopes it becomes substantial. An end sill with forward slope is particularly undesirable; its influence on the ejection effect is illustrated in Figure 60.

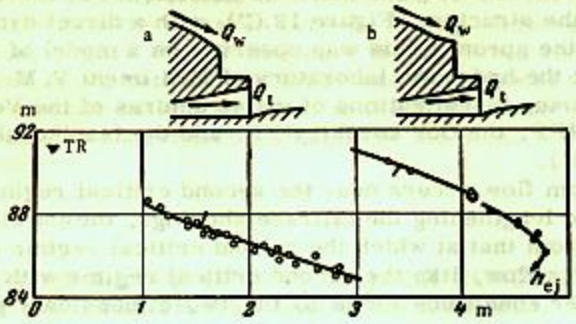

FIGURE 60. Influence of end-sill shape on ejection effect.

a—end sill with considerable forward slope; b—end sill with horizontal part.

If the apron has a sloping part, a 10 to 15° inverse slope of the end-sill may have a favorable effect, since, due to the lengthening of the nappe, the sloping part becomes located in the bottom-roller zone and ceases to have a negative influence on the ejection effect.

Figure 61* illustrates the influence of the end-sill design (height of overflow edge) on the piezometric effect of ejection.

Figure 61,a-d shows how, at given tailrace level, submerging of the jump, due to lower the end-sill level, reduces the ejection effect.

Lowering the end-sill level at low tailrace levels leads to transition from bottom to surface flow. The nappe becomes longer and impinges on the sloping part of the apron at a smaller angle; this increases the ejection effect (Figure 61,a' to c'). When the end-sill level is lowered further (Figure 61, d') the nappe becomes shorter, so that its dynamic effect on the apron increases. This leads to a reduction in the ejection effect.

Only bottom flow was in these cases observed at all tailrace levels and discharges of 50 to 55 m^3/sec per running meter of the dam (end-sill levels of 10.7 and 11.7 m).

Experiments carried out at the Gidroproekt laboratory are no less significant (Figure 62).** End sill (1) and (2) cause a submerged jump, reducing the ejection effect. Bottom flow is observed with end sills (7) and (8), the nappe impinging on the sloping part of the apron; this reduces the ejection effect. End sills (3) to (6) ensure a flow with surface jump, increasing the ejection effect.

With bottom flow and a horizontal apron the end-sill level also influences the ejection effect. The author found that lowering the end sill leads to a considerable increase in the ejection effect (provided a surface roller is not thrust onto the end sill); the reason for this is probably the increase in the flow velocities at the end sill.

* The sketches correspond to a model of an overflow HPP at a discharge over the dam of 30.8 m^3/sec per running meter. There was no turbine discharge; this does not affect the variation of the piezometric effect of ejection. (Author's experiments.)

** The headrace level was 51.00 m, the tailrace level 34.39 m, the discharge about 50 m^3/sec per running meter, and the discharge coefficient of the dam 0.44. The crest level was 45.00 m.

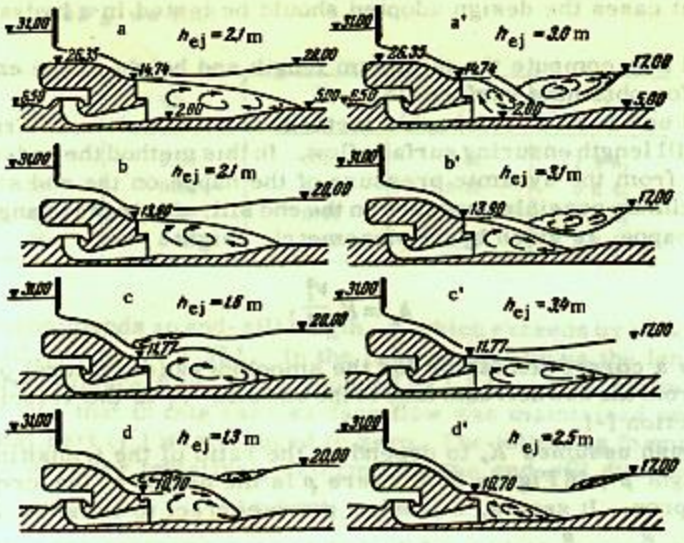

FIGURE 61. Influence of end-sill height on piezometric effect of ejection.

All this refers to overflow HPPs. Ice discharge in HPPs with conduits is usually impossible. The other considerations regarding the location in height of the conduit outlets remain apparently applicable. When the conduit outlets are flooded, the influence of their vertical location on the ejection effect is very small, so that the level of the overflow edge can in this case hardly be determined from power considerations.

FIGURE 62. Influence of configuration and level of end sill on ejection effect.

Piezometric effect of ejection, m	Increase in turbine discharge, m^3/sec	Flow regimes
0.45	65.0	Submerged jump. Roller thrust on end sill
0.50	50.0	
0.97	60.0	Surface jump
1.07	92.0	
0.93	85.0	
0.90	54.0	
0.75	60.0	Bottom flow
0.55	54.0	

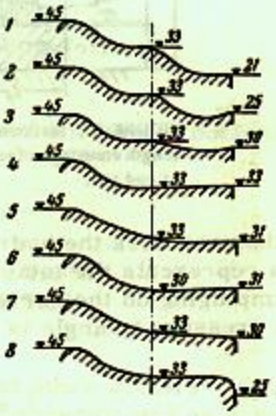

FIGURE 62. Influence of configuration and level of end sill on ejection effect.

It follows that selection of the vertical location of the end sill is difficult, since all requirements cannot be fulfilled simultaneously. It must be

decided in each individual case which requirement should be satisfied. In important cases the design adopted should be tested in a hydraulic laboratory.

We shall now compute the minimum length and height of the end sill, necessary for obtaining surface flow.

We shall use Prof. S. V. Izbash's method* for a tentative determination of the end-sill length ensuring surface flow. In this method the end-sill length is determined from the dynamic pressure of the nappe on the end sill.

The maximum possible pressure on the end sill, due to the change in direction of the nappe, is given by the piezometric height

$$h_p = K_r \frac{V_1^2}{g},$$

where K_r is a correction factor for the smoothness (curvature) of the transition from the downstream face to the end sill; V_1 is the velocity of the nappe in section I-I.

Prof. Izbash assumes K_r to depend on the ratio of the transition radius R to the height $p+H$ (Figure 63), where p is the height of the crest above the apron. It seems, however, more correct to consider K_r as a function of $\frac{R}{(p-a+H)}=\frac{R}{T'}$,** i.e., of the height of the free headrace surface above the end sill.†

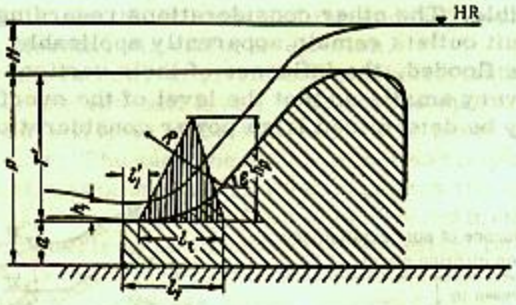

FIGURE 63. Mathematical model for computing end-sill length ensuring surface flow. Triangular pressure diagram at end sill.

Izbash then replaces the hydrodynamic-pressure diagram by a triangle whose area represents the total hydrodynamic-pressure force exerted by the nappe impinging on the curved surface of the end sill at an angle ε. The base of the pressure triangle is according to him

$$l_t = \frac{2(1-\cos\varepsilon)h_1}{K_r}. \qquad (38)$$

The end-sill length l_t, measured from the beginning of the transition from the downstream face to the end sill, must be less than l_m.

* Izbash, S. V. Gidravlika v proizvodstve rabot (Hydraulics in Construction Works).—Stroiizdat, p. 144. 1949.

** [There seems to be a mixup in the symbols. According to Figure 63, $T'=p-a$ and not $p-a+H$.]

† Izbash considered a dam with a very low end sill, i.e., the case when $p=T'+a\approx T'$.

Using A.S. Ofitserov's data* ($\varepsilon = 58°$) and the results of our own experiments ($\varepsilon = 35°$), we find

$\varepsilon°$	$\frac{R}{T}$	$\frac{H}{P}$	K_r	l_t [acc. to (38)]
58	0.35	0.17	0.13	$7.4\,h_1$
58	0.32	0.22	0.17	$5.6\,h_1$
58	0.20	0.20	0.29	$3.3\,h_1$
35	0.40	0.67	0.73	$0.5\,h_1$

Izbash recommends an end-sill length, l_1 which exceeds by 35 % the computed value of l_t, i.e. $l_1 = 1.35\,l_t$. In the case studied by us the length l_1, which ensured surface flow, corresponded to $1.5\,l_t$. Another important observation was that in this case surface flow was maintained even when the horizontal part (l_1') was reduced to zero. The following formulas may therefore be used for tentatively determining the end-sill dimensions:

$$l_1 \geqslant 1.35 l_t, \quad l_1' \geqslant 0. \tag{39}$$

The minimum toe height ensuring transition from bottom to surface flow (with a horizontal apron) is determined from D. I. Kumin's formula (/9/, p. 17):

$$\psi_{min} \geqslant \frac{h_{cr}}{h_1} - 1, \tag{40}$$

where

$$\psi_{min} = \frac{a}{h_1}, \quad h_{cr} = \sqrt[3]{\frac{q_w^2}{g}}.$$

Equation (40) can be represented in the following form:

$$h_1 + a \geqslant h_{cr}, \tag{40'}$$

i.e., for surface flow to occur, the level at the end sill must be not less than the critical depth.

26. SOME OBSERVATIONS ON THE SELECTIONS OF THE EJECTION METHOD AND THE DESIGN OF COMBINED HPPs

Generalizing the results obtained by us and other authors with models of combined HPPs leads to the following recommendations as regards selection of the ejection method and design of the HPP.

The ejection effect increases with the excess discharge and, in the case of ejection into the tailrace, decreases with increasing tailrace depth.

Ejection in the draft tube is the most effective method. However,

* Ofitserov, A.S. Gidravlika vodosliva (Hydraulics of Dams).— ONTI. 1938.

especially in the case of large turbine runners, this necessitates experimental investigation of the influence of the ejection outlets and the ejecting stream on the efficiency and operating conditions of the turbine during ejection. Tests carried out in 1952 at LPI imeni M.I. Kalinin showed that the ejection outlets in the draft-tube bend reduce slightly the turbine efficiency when there is no ejection discharge.

Investigations carried out by the author at the MEI imeni V.M. Molotov on the model of a bay with ejection in the draft tube, showed that there is almost no increase in the pressure pulsations in the turbine discharge at the throat ring (at and above the level of the blades) during ejection. On the other hand, a considerable increase in the pressure pulsations is observed below the blades and the hub extension. It is so far unclear whether this, or the ejection outlet in the draft-tube bend, affect the operating conditions of the turbine.

Overflow ejection and ejection through conduits have practically the same effect at the same flow regimes behind the dam and the same excess discharges.

When the conduit outlets are flooded, their vertical position influences only negligibly the ejection effect if the apron is horizontal. If the apron has a very long sloping part, a certain increase in the ejection effect is observed when the outlets are lowered; this increase is, however, so small that it was hardly detected experimentally on a model with a 180 mm-diameter turbine runner.

Variation within very wide limits of the end-sill height has a negligible influence on the ejection effect. The optimum end-sill height, like the optimum position of the discharge outlets, must nevertheless be determined by calculation. The end-sill level (and the vertical position of the discharge outlets of conduits) must be selected so as to prevent the occurrence of the first and second critical regimes in the tailrace. In the first case instability of the tailrace level is possible, while in the second case the probability exists of surface-bottom flow, which may necessitate lengthening the apron and downstream spillway apron or providing baffles on the former. The observation regarding the second critical regime applies to conditions close to those of the plane problem, i.e. when $\zeta = \frac{b}{B} \geq 0.8$.

Lengthening the horizontal part of the end sill or of the platform at the conduit outlets may in practice influence the ejection effect only when the apron has a sloping part or a step. If lengthening of end sill or platform causes the nappe to impinge behind the sloping part of the apron, the ejection effect is increased. Lengthening the end sill to permit free access of air underneath the nappe has a similar effect.

The minimum end-sill length and height ensuring surface flow can be determined tentatively as explained in §§ 25 and 31.

An inverse slope of the end sill or of the conduit end sections influences the ejection effect in the same way as a variation in vertical position when the apron has a sloping part or step: impingement of the nappe behind the sloping part of the apron and the free access of air underneath the nappe increase the ejection effect. The inverse slope of the end sill has a positive effect at instable tailrace regimes; it contributes to the elimination of large tailrace-level fluctuations near the structure. With increasing steepness of the inverse slope of the end sill or of the conduit end sections it may become necessary to increase the length of the tailrace bottom shorings.

5100

A steepening of the forward slope of the end sill leads to a considerable reduction in the ejection effect.

If the conduit outlets have different heights, their upper edges should be at the same level, since this ensures better flow conditions in the tailrace. If the lower edges are at the same level, but the upper edges at different levels, there is the danger of the flow being diverted toward either bank.

Teeth on the end sill reduce the amplitude of the tailrace-level fluctuations during instable flow regimes and, by breaking up the nappe, improve conditions on the apron.* It has been observed on models that the ejection effect is increased when the tooth profile causes the nappe to become longer and therefore to impinge behind the sloping part of the apron.

Location of the sloping part (or step) of the apron in the bottom-roller zone causes practically no reduction in the ejection effect, but this part (or step) must not induce a high backwater in the absence of an excess discharge. The negative influence, which a sloping part located in the zone of nappe impingement has on the ejection effect, increases with the apron slope, which should therefore be as small as possible in this region. A horizontal apron ensures in all cases a higher ejection effect, and is accordingly to be preferred.

Free access of air underneath the nappe during bottom flow increases the ejection effect and prevents its instability (fluctuations accompanied by breakthrough of air underneath the nappe). When air has no access underneath the nappe, the length of the latter becomes reduced, and it induces a backwater, which reduces the ejection effect. Measures should be taken during bottom flow to ensure free access of air underneath the nappe.

The length of the piers protruding into the tailrace, and the nappe shape of their downstream noses affect the ejection effect during bottom flow. Thus, if the piers prevent free access of air underneath the nappe, the ejection effect decreases slightly with the tailrace level. Such piers must therefore be designed so as to permit free access of air underneath the nappe.

A dam profile and a conduit design for which the discharge coefficients are maximum ensure a high ejection effect.

The following applies to conduits of complex layout: "To ensure smooth continuous flow all critical sections should be larger than the exit section of the water passage; it is recommended that for siphons, $\omega_k \geqslant 1.2\omega_{ex}$, for bottom conduits (passing beneath the scroll casing. — S.) $\omega_k \geqslant 1.1\omega_{ex}$; when the head $H > 15$ m, the ratio $\frac{\omega_k}{\omega_{ex}}$ should be increased in proportion to the head."**

The cross-sectional areas of conduits of smooth configuration, arranged at considerable depths below the tailrace level, may be constant. The inlet sections of the conduits should be as large as possible in order to increase the carrying capacity and to reduce additional head losses (cf. below).

Discharge under sluice gates on a broad-crested dam (or of conduits), located near the overflow edge, induces a higher ejection effect than when the sluice gates are located near the upstream face of the dam (or conduit intakes).

* Teeth have been used behind dams as baffles. Grishin, M. M. Gidrotekhnicheskie sooruzheniya (Hydraulic Structures).— Part 1, p. 52, Moskva, 1947.

** Provisional specifications and design rules for hydraulic structures. HPPs with vertical units, combined with discharge conduits.

Grooves in piers protruding into the tailrace must not cause flow perturbations in the nappe, as is observed in models with conduits forming in plan diffusers, or with curved conduits. In this case the width of the conduit outlets must be smaller than the distance between the lateral surfaces of the piers. The piers may be wider in plan in front of the grooves,* as shown in Figure 64.

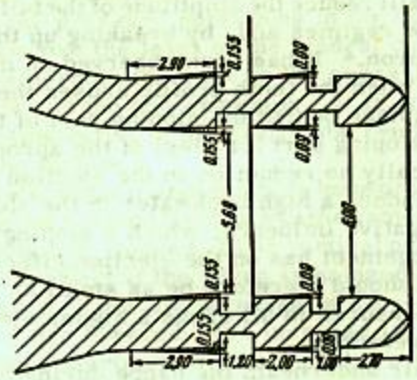

FIGURE 64. Pier design (plan) preventing flow perturbations in nappe, caused by grooves (dimensions in meters).

Additional head losses, depending on the dimensions and shape of the receiver, and the ratio between spilling and turbine discharges in it (HPP with conduits according to Figure 18), lower the ejection effect. These additional losses can be reduced by increasing the inlet sections of conduits and scroll casing.

The interaction (mutual contraction) of the excess and turbine discharges in the receiver may considerably reduce the carrying capacity of the conduits. In the case represented in Figure 18, this reduction amounted to 5 % during turbine operation (this, and the large additional energy losses during ejection, necessitated an increase of the cross sections of the receiver and conduit intakes and the scroll casing).

In selecting the ejection method it should be remembered that ejection does not always ensure a regain in head.

A combined HPP with both overflow ejection and ejection through conduits at the sides of the draft tube, where ejection had a negative effect, is shown in Figure 65. It had been assumed that the discharge over a broad-crested dam, together with that through conduits, would yield a considerable ejection effect. Calculations showed, however, that in the case considered there would not be an increase in power, but, on the contrary, a reduction (Figure 66).

The considerable discharge from the conduit below the nappe induces backwater; this has a negative influence on the ejection effect. Figure 66 also shows the positive effect of free access of air underneath the nappe.

* Pretro, G. A. Opyt proektirovaniya gidroelektrostantsii sovmeshchennogo tipa s donnymi vodosbrosami (Design Experience with Combined HPP with Bottom Conduits).— Gidrotekhnicheskoe stroitel'stvo. 1952.

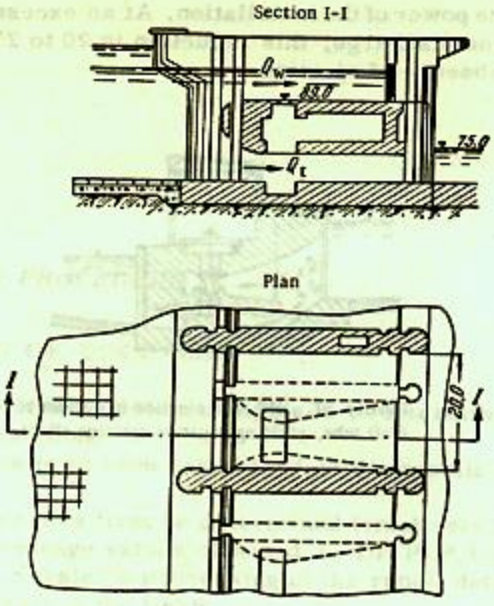

FIGURE 65. HPP with overflow ejection and ejection through conduits, yielding a negative ejection effect.

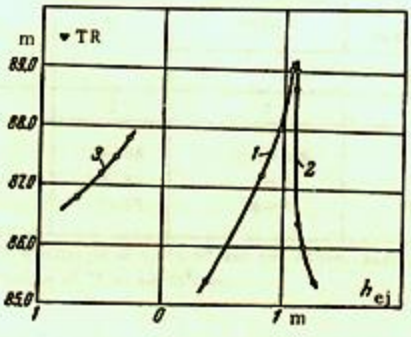

FIGURE 66. Variation of ejection effect in bay shown in Figure 65, as function of tailrace level, with different discharge combinations. Headrace level = 95.00 m; discharge over dam Q_w = = 438 m^3/sec.

1—bottom conduit closed; 2—bottom conduit closed, free access of air underneath nappe; 3—turbine operating, discharge over dam and through bottom conduit.

Another example of a negative ejection effect is the combined HPP with ejection in the diffuser of the draft tube (Figure 67). Laboratory investigations by the author showed that ejection in the diffuser of the draft tube

greatly reduces the power of the installation. At an excess discharge about equal to the turbine discharge, this reduction is 20 to 25 % of the power delivered in the absence of ejection.

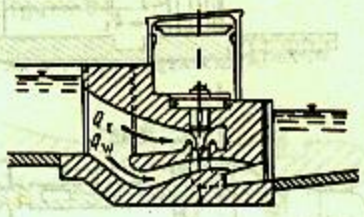

FIGURE 67. HPP with ejection in diffuser of draft tube, yielding negative ejection effect.

Chapter VII

COMPUTATION PROCEDURE

27. SELECTION OF DISCHARGE

The final aim of the ejection analysis is to determine the power and output effect of ejection.

The calculation is in each case based on the results of hydropower analysis.

The discharges may first be determined tentatively from Table 8, which gives the average values obtained by Dr. P. P. Laupman from an analysis of L. M. Kovalev's processing of the runoff data for lowland rivers in the European part of the USSR.

TABLE 8. Discharges characteristic for combined HPPs (according to P. P. Laupman)

River*	Head fluctuations, m	Discharge at which ejection begins	Maximum discharge of flood water in 100-year period	Characteristic discharge for ejection
		ratio to average discharge		
1	2	3	4	5
Large	12—35	2.5—3.5	8	5
Medium	10—30	3—5	15	8
Small	7—25	4—8	30	12

* Large rivers have discharges of 3,000 m^3/sec and above, averaged over the years; small rivers have discharges of 75 to 400 m^3/sec.

As was pointed out by Laupman, the average discharge characteristic of a combined HPP (column 5), is "close to the maximum discharge during an average flood (over a two-year period) and corresponds to the discharge of seven days, averaged over a period of many years."

28. OVERFLOW EJECTION

a. Computation procedure

The dimensions of the HPP, the headrace level, and the discharge capacity of the dam are usually given. The tailrace level is a known

function of the total discharge, while the turbine discharge is a known function of the head on the turbine.

We may use one of the expressions for the tailrace depth h_2, i.e., (16), (17), or (18), or for the piezometric head h_0 at the draft-tube outlet ((16a to c), (17a to c), or (18a to c)).

The first procedure is more convenient for plotting the ejection characteristic, which is the family of curves relating, for different overflow discharges, the ejection effect to the level of the free tailrace surface, i.e.,

$$h_{ej} = f(\nabla TR) \quad \text{or} \quad \Delta H = f(\nabla TR),$$

where ∇TR is the level of the free tailrace surface; h_{ej} is the piezometric effect of ejection (cf. Figure 15); ΔH is the head effect of ejection, corrected for the regain of head ($\Delta H = h_{ej} - \Delta h$).

This procedure is also advisable for calculations supplementing laboratory investigations.

The second procedure is more convenient for ejection analysis when the levels (depth) of the tailrace are given; in this case the calculation may also be reduced to plotting the ejection characteristic.

We shall first compute the ejection effect by (16), (17), and (18), determining the tailrace depth h_2 far downstream of the HPP. This will be done for a given overflow discharge. The procedure adopted, also for other magnitudes, is as follows:

1. Using (32), we plot in ∇TR, h_{ej} coordinates the curve which determines the first critical regime and separates the characteristic into regions of surface and bottom flow:

$$\nabla TR = \nabla \text{ (toe)} + \Delta h_2, \text{ where } \Delta h_2 = K_T h_{ej}^2.$$

This empirical formula corresponds to a turbine discharge approximately equal to 0.6 of the overflow discharge. At larger relative turbine discharges the curve determining the first critical regime is displaced in the direction of lower tailrace levels. The opposite effect is observed when the relative turbine discharge decreases. When the latter amounts to 0.3 of the overflow discharge or less, (31) should be used.

The coefficient K_T is found from Figure 47.

When the HPP parameters lie outside the range for which the curves in Figure 47 are valid, we use A. A. Sabaneev's condition $h_0 - h_1 \geq 0$ (cf. p. 13) for determining the flow regime corresponding to the computed value of h_{ej}. In this case the computed [tailrace] level corresponding to the first critical regime will be higher than the true value.

2. We assume several values of h_0. Using (10), we can then determine for each value of h_0 the unknown nappe depth h_1 at the end sill, entering in (16), (17), and (18). We can also determine the head on the turbine, and from it the turbine discharge Q_t, which we require for the following calculations.

The value of h_1 is found from the nomogram in Appendix I or from (10),

$$h_1 = \frac{q_w \sqrt{2}}{\sqrt{g}} \cdot \frac{1}{\sqrt{T_0' - h_1} + 2\sqrt{T_0' - h_0}},$$

which should be used only when the initial data are not represented in the nomogram in Appendix I. Use of the nomogram is illustrated in Figure 68.

FIGURE 68. Use of nomogram for determining nappe depth at toe.

In the case of a broad-crested dam h_1 is the critical depth.

3. We then select a formula for the tailrace depth h_2 corresponding to certain values of h_0 and h_1. This may be (16), (17), or (18) depending on the location of the sloping part of the apron and the nappe length (cf. § 23).

When the apron is horizontal (18') is always used.

The term R is found from Table 2 or 3 in accordance with the expected tailrace regime.

4. Use of (16) to (18') requires the knowledge of the ratio k of the overflow discharge to the total discharge: $k=\frac{Q_w}{Q_w+Q_t}$. The turbine discharge is found from the turbine characteristic, the head being in a first approximation

$$H_t=\nabla HR-\nabla TR+h_{ej}$$

or

$$H_t=\nabla HR-\nabla h_0=T_0-h_0,$$

where T_0' is the height of the free headrace surface above the overflow edge of the end sill.

The head on the turbine is determined more accurately by allowing for the regain of head,* i.e., for the difference between ∇TR and ∇h_0 when the overflow discharge is zero. In most cases, however, the accuracy is not much affected if the regain of head is taken into account only during the final stage of calculation.

5. Having a number of values of h_0, and those of h_1 and $k=\frac{Q_w}{Q_w+Q_t}$ corresponding to them, we obtain from (16) to (18') the tailrace depth h_2.

Since h_2 enters in the expression A in (16) to (18'), we assume in a first approximation some value close to the expected depth (for instance, using the curve relating discharges to levels). Working by the method of successive approximations, we determine in each approximation the value of A from the value of h_2 found in the preceding approximation (two approximations are usually sufficient). The term M in A is determined from (14) or (14'), or from the nomogram in Appendix II.

During the calculation it is necessary to check whether the computed points on the ejection characteristic lie in the zone of surface or of bottom flow, i.e., whether the correct expression for R is being used.

6. Having plotted the curves $h_{ej}=f(\nabla TR)$ we introduce in them the correction for the regain of head. The latter is, in accordance with (5),

$$\Delta h=\eta\,\frac{V_1^2-V_2^2}{2g}.$$

Having determined the head effect $\Delta H=h_{ej}-\Delta h$ of ejection, we plot the curves $\Delta H=f(\nabla TR)$, using which we can find $H_{ap}=H+\Delta H$ from ΔH. We then determine the power and output effects of ejection from the turbine characteristics. The formulas on which the characteristic is based were

* The additional losses ΔH_w are neglected.

derived for the case when the bay considered is at the same flow regime as the adjacent bays; nevertheless, the ejection characteristic permits approximative calculations also for an arbitrary distribution of the discharges between the spillways and turbine passages, or only between the latter.

The design must ensure free access of air underneath the nappe, hence, when $h_0 < 0$ the expression for R must be that corresponding to free access of air.

As mentioned before, (16) to (18') give satisfactory results in the case of a submerged jump only when the height, above the end sill, of the free tailrace surface is less than

$$\Delta h_2 = 0.8 \sqrt[3]{q_w^2}.$$

When (16a) to (16c), (17a) to (17c), or (18a) to (18c) are used to determine the piezometric head h_0 at the draft-tube outlet, the procedure is as follows:

1. We assume a certain piezometric effect h_{ej} of ejection (for instance, 1.0 m), and find the level of the piezometric-head plane at the draft-tube outlet

$$\nabla h_0 = \nabla TR - h_{ej},$$

and the piezometric head. $h_0 = \nabla h_0 - \nabla$ (toe).

2. Using the nomogram in appendix I or (10), we determine the depth h_1 at the end sill.

3. We find the effective head on the turbine

$$H_t = \nabla HR - \nabla TR + h_{ej},$$

then the turbine discharge from the characteristic $Q_t = f(H_t)$, and finally

$$k = \frac{Q_w}{Q_w + Q_t}.$$

4. From the given value of h_2 and those found for h_1 and k, we compute A by (13), and then determine h_0 by (16a) to (16c), (17a) to (17c), or (18a) to (18c). When the apron has a sloping part, the formulas to be used are determined according to the nappe length (§ 23).

5. Having found h_0 and ∇h_0 in a first approximation, we determine the [piezometric] ejection effect $h_{ej} = \nabla TR - \nabla h_0$.

6. Using (32) (§ 19) or Sabaneev's condition (cf. point 1 at the beginning of this section), we check whether the flow regime behind the dam is in fact that for which the formula used is valid.

7. We repeat the procedure in a second approximation, introducing a correction for the regain of head Δh, and obtain the head effect ΔH of ejection.

b. Plotting the ejection characteristic for an overflow HPP. (Example)

(using relationships for the tailrace depth h_2)

Figure 69 shows one of ten overflow-and-turbine bays of an HPP. The initial data are as follows:

$B = 16.00$ m; $b = b_t = 12.35$ m; $a = 12.45$ m; $a' = 9.68$ m; $d = 2.77$ m; $h_t = 6.40$ m; $p = 15.78$ m; $e = 1.07$ m; $l = 25.00$ m; $\nabla HR = 100.10$ m; $H_0 = 11.10$ m; $T_0' = 100.10 - 82.90 = 17.20$ m; $\varphi = 0.90$; $m = 0.40$.

Level of crest = 89.00 m: end-sill level = 82.90 m; level of raised part of apron = 73.22 m; level of downstream spillway apron = 72.15 m.

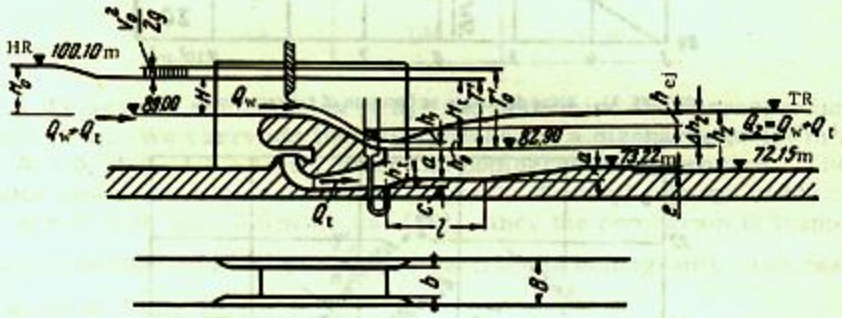

FIGURE 69. Overflow-and-turbine bay.

Curves of turbine discharge vs. head ($Q_t = f(H_t)$) (Figure 70), and of river discharge vs. tailrace level ($\Sigma Q = f(\nabla TR)$) (Figure 71) are also given.

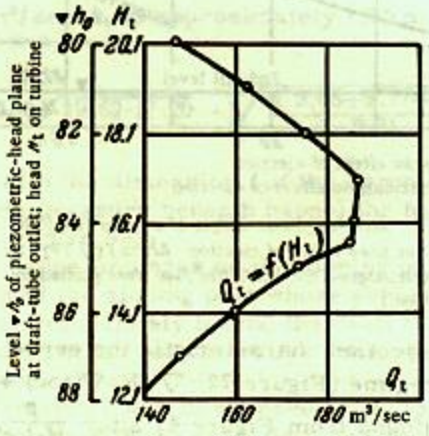

FIGURE 70. Turbine discharge as function of head. Headrace level: $\nabla = 100.10$ m.

The overflow discharges assumed (per bay) are $Q_w = 400, 600, 800\ m^3/sec$: the first two are discharges under the sluice gate, while the discharge of $800\ m^3/sec$ takes place at fully opened gate (for simplicity only the discharge of $400\ m^3/sec$ is considered; for the discharge of $800\ m^3/sec$ we shall only determine the nappe depth h_1 at the end sill). *

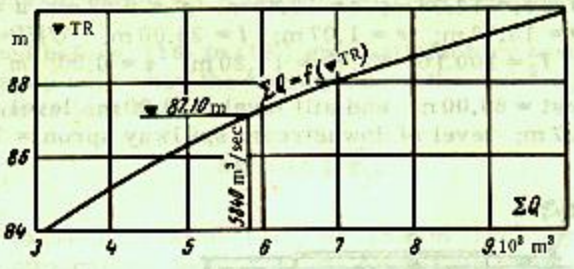

FIGURE 71. River discharge as function of tailrace level.

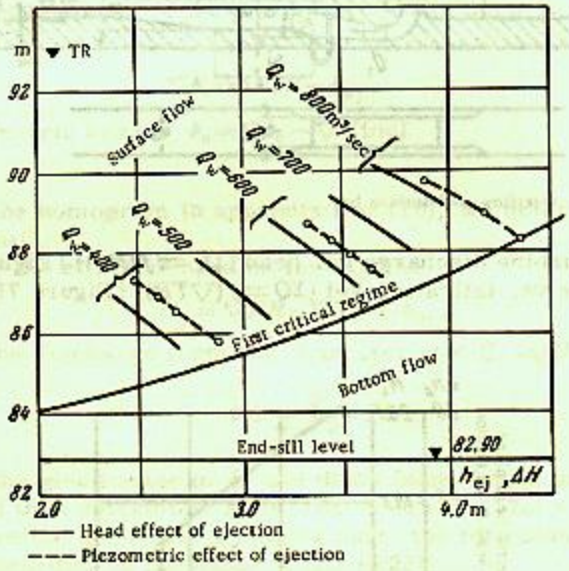

FIGURE 72. Ejection characteristic of an overflow HPP. (The curves of the head effect of ejection $\Delta H = f(\nabla TR)$ for overflow discharges of 500 and $700\ m^3/sec$ were plotted by interpolation.).

1. We plot on the ejection characteristic the curve $\Delta h_2 = K_T h_{ej}^2$ determining the first critical regime (Figure 72); $\nabla TR = \nabla(\text{toe}) + \Delta h_2$.

The value of K_T is found from Figure 47 after $\frac{p}{H+a'}$ and q_w have been determined. We assume $H \approx H_0$; in practice this does not affect the results:

* The headrace level is that of the reservoir. In HPPs the headrace level is reduced by the velocity head and the (in practice negligible) losses inside the reservoir.

$$\frac{p}{H+a'}=\frac{15.78}{11.10+9.68}=0.76,$$

$q_w = m\sqrt{2g}H^{3/2} = 0.40 \cdot 4.43 \cdot 11.10^{3/2} = 65.6$ m³/sec per running meter of the dam; from Figure 47 we find $K_T \approx 0.30$.

For some values of h_{cj} we find by (32) Δh_2 and then ∇TR corresponding to the first critical regime:

h_{cj}, m	$\Delta h_2 = 0.30\, h_{cj}^2$, m	$\nabla TR = 82.90 + \Delta h_2$, m
1.0	0.30	83.20
2.0	1.20	84.10
3.0	2.70	85.60
4.0	4.80	87.70
5.0	7.50	90.40

2. We assume some values of h_0* and determine the corresponding values of h_1. We carry out the calculations for a discharge of 400 m³/sec and $h_0 = 0$, 1.0, 1.5, 2.0 m, using the nomogram in Appendix I. The results appear in columns 2 to 7 of Table 9. For a discharge of 800 m³/sec and $h_0 = 0$, 1.0, 2.0, 3.0 m we use (10), since the nomogram is inapplicable in this case (the value of $\theta = \frac{T_0}{h_k}$ lies outside the nomogram). The results are given in Table 10.

We now select the formula determining the depth h_1.

Assuming the pressure to be atmospheric beneath the nappe ($h_0 = 0$), the nappe length is determined from (37):

$$X_0 = \varphi\sqrt{2gT_0'}\sqrt{\frac{2a'+d+h_1}{g}}.$$

For $Q_w = 400$ m³/sec h_1 is approximately 1.95 m in accordance with column 7 of Table 9**:

$$X_0 = 0.90\sqrt{19.62 \cdot 17.20}\cdot\sqrt{\frac{2 \cdot 9.68 + 2.77 + 1.95}{9.81}} = 25.9 \text{ m}.$$

Comparing X_0 with the dimension l of the apron, we see that for $h_0 = 0$ (atmospheric pressure beneath nappe) the nappe impinges on the apron as shown in Figure 59,b.

When $h_0 > 0$ the nappe impinges on the sloping part. When $h_0 < 0$ it impinges upstream of the sloping part whose superelevation is d.

The sloping part immediately behind the draft tube, whose superelevation is c, is always located in the bottom-roller zone; its presence does not affect the calculation.

In the case considered ($h_0 = 0$) we have $l < X_0$, and must use (16). We now determine the term R in the formula. The free surface level of the tailrace is sufficiently high for surface flow to be expected. We find

* If the tailrace levels and depths are such that surface flow is to be expected, we must assume $h_0 > 0$; if bottom flow is to be expected, we should first assume $h_0 = 1$; 0; −1; −2 m.

** Average of the four values given in column seven.

TABLE 9. Computation of piezometric effect of overflow ejection

Q_w, q_w, T'_0, β	$h_{cr}=\sqrt[3]{\frac{q_w^2}{g}}$, m	$\theta=\frac{T'_0}{h_{cr}}$	h_0, m	$\xi_0=\frac{h_0}{h_{cr}}$	ξ_1 – from appendix I	$h_1=\xi_1 h_{cr}$, m	$H_t=T'_0-h_0$	Q_t, m³/sec	$Q_s=Q_w+Q_t$, m³/sec	$\Sigma Q=10Q_s$, m³/sec	∇ TR for Figure 71, m	$k=\frac{Q_w}{Q_w+Q_t}$	$h_2=\nabla TR-72.15$, m	$\frac{h_2}{\beta}$	M from nomogram in appendix II	βq_w^2	$A=k\beta q_w^2 M$	$0.23h_0^2$	$22.13h_0$	$0.77h_1h_0$	$122.1+(19)+(20)+(21)$	$(22)+A$	$\sqrt{(23)}$	$h_3=(24)-0.31$, m	$\nabla TR=72.15+h_3$, m	$h_{ej}=\nabla TR-\nabla h_0$, m
1	2	3	4	5	6	7	8	9	10	11	12	13	14	15	16	17	18	19	20	21	22	23	24	25	26	27
$Q_w=400$ m³/sec $q_w=32.4$ m³/sec $T'_0=17.20$ m $\beta=\frac{b}{B}=0.77$	4.75	3.62	0	0	0.403	1.915	17.20	184	584	5,840	87.10	0.684	14.95	19.40	0.092	808	74.4	0	0	0	122.1	196.5	14.02	13.71		
													13.71	17.80	0.089	808	72.0	0	0	0	122.1	194.1	13.93	13.62		
													13.62	17.70	0.089	808	72.0	0	0	0	122.1	194.1	13.93	13.62	85.77	2.87
			1.0	0.211	0.410	1.945	16.20	185	585	6,850	87.15	0.684	15.00	19.50	0.089	808	72.0	0.23	22.13	1.50	145.96	217.96	14.76	14.45		
													14.45	18.78	0.088	808	71.2	0.23	22.13	1.50	145.96	217.16	14.74	14.43	86.58	2.68
			1.5	0.316	0.413	1.962	15.70	185	585	5,850	87.15	0.684	15.00	19.50	0.089	808	72.0	0.52	33.20	2.27	158.09	230.09	15.17	14.86		
													14.86	19.28	0.088	808	71.2	0.52	33.20	2.27	158.09	229.29	15.14	14.83	86.98	2.58
			2.0	0.422	0.416	2.004	15.20	176	576	5,760	87.00	0.695	14.85	19.28	0.087	808	70.4	0.92	44.26	3.08	170.36	240.76	15.52	15.21		
													15.21	19.76	0.088	808	71.2	0.92	44.26	3.08	170.36	241.56	15.54	15.23	87.38	2.48

Notes: 1. The numbers between parentheses in the headings of columns 22, 23, 24, and 25 denote the numerical values in the respective columns. 2. The accuracy corresponds to that of a slide rule and of three-figure mathematical tables.

from Table 2: $R=(1-\beta)h_0^2+\beta h_1 h_0$. Substituting in (16) this expression and the numerical values of the magnitudes entering in it, and rearranging, we obtain

$$h_2=-\frac{d-2e}{2}+\sqrt{\left[\frac{d-2e}{2}\right]^2+a^2-e^2+(e-a)d+(2a-d)h_0+A+R}=$$
$$=-0.31+\sqrt{122.1+0.23h_0^2+22.13h_0+0.77h_1h_0+A}.$$

The correctness of selecting (16) will be checked at step 5; if the computed points lie below the curve determining the first critical regime, we must take the expression for R corresponding to bottom flow.

The calculation of successive approximations is represented in Table 9.

4. We determine the head on the turbine, column 8 of Table 9, and find the turbine discharge (column 9) from the turbine-discharge curve in Figure 70. The regain of head, which must be subtracted from the head on the turbine, is neglected at this stage. From the turbine discharge we determine (column 13) $k=\frac{Q_w}{Q_w+Q_t}$.

5. We now determine the tailrace depth h_2 for the values of h_0 assumed initially and the corresponding values of h_1.

TABLE 10. Computation of nappe depth at toe, $Q_w = 800\ m^3/sec$

$$h_1=\frac{q_w\sqrt{2}}{\sqrt{g}}\cdot\frac{1}{\sqrt{T_0'-h_1}+\varphi\sqrt{T_0'-h_0}}. \qquad (10)$$

Q_w; q_w; T_0'	First approximation: $h_1=0$						Second and third approximations		
	$\sqrt{T_0'}$	h_0, m	$\varphi\sqrt{T_0'-h_0}$	(3)+(4)	$\frac{1}{(5)}$	$h_1=\frac{q_w}{2.21}\times(6)$, m	$\sqrt{T_0'-h_1}$	$\frac{1}{(8)+(4)}$	$h_1=\frac{q_w}{2.21}\times(9)$, m
1	2	3	4	5	6	7	8	9	10
$Q_w=800\ m^3/sec$	4.147	0	3.73	7.88	0.127	3.72 3.96*	3.67 3.64	0.135 0.136	3.96 3.98
$q_w=64.7\ m^3/sec$ $T_0'=17.20$ m		1.00	3.62	7.77	0.129	3.78	3.66	0.137	4.02
		2.00	3.51	7.66	0.131	3.84	3.65	0.140	4.11
		3.00	3.39	7.54	0.133	3.90	3.64	0.142	4.16
		4.00	3.26	7.41	0.135	3.95	3.64	0.145	4.25

Note: The numbers between parentheses in the headings of the columns denote the numerical values in the respective columns.

In computing A the initial value of h_2 in column 14 is determined from the tailrace level, using the curve $\Sigma Q=f(\nabla TR)$ (Figure 71).

Thus, for $Q_w = 400\ m^3/sec$ and $h_0 = 0$, we have:

$$Q_t = 184\ m^3/sec,\quad \Sigma Q=(400+184)\cdot 10 = 5{,}840\ m^3/sec;$$
$$\nabla TR = 87.10\ m,\quad h_2 = 87.10-72.15 = 14.95\ m.$$

Carrying out the operations in columns 10 to 25, we obtain h_2 and then (column 26) the tailrace level:

$$\nabla TR = \nabla(\text{apron}) + h_2.$$

* From column 10.

From the values in column 27, we plot curves of the piezometric effect of ejection as function of tailrace level and overflow discharge: $h_{ej}=f(\nabla TR)$.

The curves $h_{ej}=f(\nabla TR)$ corresponding to Q_w= 500 and 700 m³/sec are obtained by interpolation.

6. We must now replot these curves to represent the head effect of ejection. This is done by subtracting from the piezometric effect of ejection the regain of head: $\Delta H = h_{ej} - \Delta h$.

The magnitude Δh, which represents the influence of the turbine discharge on the piezometric head at the draft-tube outlet, is determined (Table 11) for tailrace levels corresponding to overflow discharges per bay of 400, 600, and 800 m³/sec, with Δh assumed as constant for each value of Q_w.

TABLE 11. Computation of regain of head

Overflow discharge Q_w, m/sec	∇TR, m	Piezometric effect of ejection h_{ej}, m	Tentative value of head on turbine H_t = 100.10 − ∇TR + h_{ej}, m	Turbine discharge Q_t, m³/sec	Tailrace depth h_2 = ∇TR − 72.15 m	$V_2=\frac{Q_t}{Bh_2}=\frac{Q_t}{16\cdot h_2}$, m/sec	$\frac{V_2^2}{2g}$, m	$V_t=\frac{Q_t}{Bh_t}=\frac{Q_t}{12\cdot 4,00}$, m/sec	$\frac{V_t^2}{2g}$, m	Regain of head $\Delta h=0.7\left(\frac{V_t^2}{2g}-\frac{V_2^2}{2g}\right)$, m
1	2	3	4	5	6	7	8	9	10	11
400	86.70	2.64	16.04	185	14.95	0.77	0.027	2.41	0.296	0.19
600	88.30	3.43	15.23	178	16.15	0.69	0.025	2.32	0.275	0.17
800	89.75	3.90	14.25	163	17.60	0.58	0.017	2.12	0.229	0.15

The regain of head is allowed for at the last stage of the calculation by a correction in the curves $h_{ej}=f(\nabla TR)$ of the ejection characteristic. The regain of head may also be allowed for in the beginning; this would yield at once a more accurate value of ΔH and then Q_t, and therefore a more exact final result. In the case considered this is, however, unnecessary since the increase in the accuracy of ΔH is measured in cm.

c. Computing the ejection effect for a given tailrace level. (Example)

(using relationships for the piezometric head h_0 beneath the nappe)

We shall determine for the HPP considered above the ejection effect at a discharge of 400 m³/sec over the dam and a tailrace level of 87.00 m (tailrace depth h_2 = 87.00 − 72.15 = 14.85 m; cf. Figure 69).

1. We assume arbitrarily that the piezometric effect of ejection is 1.00 m. The level of the piezometric plane at the draft tube-outlet is then

$$\nabla h_0 = \nabla TR - h_{ej} = 87.00 - 1.00 = 86.00 \text{ m},$$

and the piezometric head is

$$h_0 = \nabla h_0 - \nabla \text{ (toe)} = 86.00 - 82.90 = 3.10 \text{ m.}$$

2. We find the depth h_1 from the nomogram in Appendix I. As in the preceding example (cf. Table 9, columns 2 and 3), $\theta = \frac{T_0}{h_{cr}} = 3.62$ and $\xi_0 = \frac{h_0}{h_{cr}} = \frac{3.10}{4.75} = 0.653$. The nomogram yields $\xi_1 = 0.425$, and therefore, $h_1 = \xi_1 \cdot h_{cr} = 0.425 \cdot 4.75 = 2.02$ m.

3. The head on the turbine is

$$H_t = \nabla HR - \nabla TR + h_{cj} = 100.10 - 87.00 + 1.00 = 14.10 \text{ m.}$$

From the turbine characteristic on Figure 70 we obtain for $H = 14.10$ m, i.e., for a level of the piezometric plane at the draft-tube outlet

$$\nabla h_0 = \nabla TR - h_{cj} = 87.00 - 1.00 = 86.00 \text{ m,}$$

a turbine discharge $Q_t = 159$ m^3/sec.

Hence,

$$k = \frac{Q_w}{Q_w + Q_t} = \frac{400}{400 + 159} = 0.716.$$

4. We now obtain

$$A = \beta q_w^2 \frac{2}{g}\left[\frac{(1-k)^2}{k^2 h_t} - \frac{\beta}{k^2 h_2} + \frac{1}{h_1}\right] =$$

$$= 0.77 \cdot 32.4^2 \cdot \frac{2}{9.81}\left[\frac{(1-0.716)^2}{0.716^2 \cdot 6.40} - \frac{0.77}{0.716^2 \cdot 14.85} + \frac{1}{2.02}\right] = 69.0.$$

We can also find A from the nomogram in Appendix II: $\frac{h_2}{\beta} = \frac{14.85}{0.77} = 19.3$; for $k = 0.716$ and $h_t = 6.40$ m we obtain $M = 0.084$, hence $A = \beta q_w^2 M = 0.77 \cdot 32.4^2 \cdot 0.084 = 69$.

Having satisfied ourselves, as explained in step 3 of the preceding example, that the nappe impinges on the sloping part of the apron, and assuming surface flow, we obtain from (16a):

$$h_0 = \frac{(a-e)d - a^2 + dh_2 + (h_2 - e)^2 - A}{2a - d + h_1} =$$

$$= \frac{(12.45 - 1.07) \cdot 2.77 - 12.45^2 + 2.77 \cdot 14.85 + (14.85 - 1.07)^2 - 69.0}{2 \cdot 12.45 - 2.77 + 2.02} = 1.60 \text{ m.}$$

5. The level of the piezometric plane at the draft-tube outlet is in a first approximation:

$$\nabla h_0 = \nabla \text{ (toe)} + h_0 = 82.90 + 1.60 = 84.50 \text{ m.}$$

The piezometric effect of ejection is in a first approximation

$$h_{cj_1} = \nabla TR - \nabla h_0 = 87.00 - 84.50 = 2.50 \text{ m.}$$

6. Before determining the ejection effect in a second approximation, we must check whether the correct formula has been used.

The height, above the end sill, of the free tailrace surface is at the first critical regime

$$\Delta h_2 = K_T h_{cj}^2 = 0.30 \cdot 2.50^2 = 1.87 \text{ m}.$$

The value of K_T was determined in step 1 of the preceding example.

The level of the free tailrace surface, corresponding to the first critical regime is

$$\nabla TR = \nabla \text{ (toe)} + \Delta h_2 = 82.90 + 1.87 = 84.77 \text{ m}.$$

The given tailrace level is $\nabla TR = 87.00$ m; since 87.00>84.77 m, surface flow exists. The correct formula has been used.

7. We shall now obtain a more accurate value of h_0 by repeating the procedure.

We substitute in (16a) the values of h_1 and k corresponding to $h_0 = 1.60$ m. In this case $\xi_0 = \frac{h_0}{h_{cr}} = \frac{1.60}{4.75} = 0.337$. The nomogram in Appendix I yields $\xi_1 = 0.414$. Hence $h_1 = \xi_1 \cdot h_{cr} = 0.414 \cdot 4.75 = 1.96$ m.

To determine k we find H_t and then Q_t. The head on the turbine is in a second approximation, when no allowance is made for the regain of head,

$$H_t = \nabla HR - \nabla \text{ (toe)} + h_0 = 100.10 - 82.90 + 1.60 = 18.80 \text{ m}.$$

From the curve $Q_t = f(H_t)$ we find that the turbine discharge is 182 m³/sec. The regain of head is

$$\Delta h = \eta \frac{V_t^2 - V_2^2}{2g} = \eta \frac{Q^2}{2g} \left[\frac{1}{\omega_t^2} - \frac{1}{(Bh_2)^2} \right] =$$

$$= 0.7 \frac{182^2}{19.62} \left[\frac{1}{(12.00 \cdot 6.40)^2} - \frac{1}{(16.00 \cdot 14.85)^2} \right] = 0.18 \text{ m}.$$

Allowing for this, the head on the turbine is $H_t = 18.80 - 0.18 = 18.62$ m. The turbine discharge at this head is $Q_t = 170$ m³/sec, so that

$$k = \frac{400}{400 + 170} = 0.702.$$

From the nomogram in Appendix II we obtain for $\frac{h_2}{\beta} = 19.3$:

$$M = 0.088 \qquad A = \beta q_w^2 M = 0.77 \cdot 32.4^2 \cdot 0.088 = 71.1.$$

The piezometric head beneath the nappe is in a second approximation

$$h_0 = \frac{(a - e)d - a^2 + dh_2 + (h_2 - e)^2 - A}{2a - d + h_1} =$$

$$= \frac{(12.45 - 1.07) \cdot 2.77 - 12.45^2 + 2.77 \cdot 14.85 + (14.85 - 1.07)^2 - 71.1}{2 \cdot 12.45 - 2.77 + 1.96} = 1.52 \text{ m},$$

which differs only by 1.60 − 1.52 = 0.08 m from the value obtained in the first approximation.

The level of the piezometric plane at the draft-tube outlet is

$$\nabla h_0 = \nabla \text{(toe)} + h_0 = 82.90 + 1.52 = 84.42 \text{ m}.$$

The piezometric effect of ejection is

$$h_{ej} = \nabla TR - \nabla h_0 = 87.00 - 84.42 = 2.58 \text{ m}.$$

The head effect of ejection is

$$\Delta H = h_{ej} - \Delta h = 2.58 - 0.18 = 2.40 \text{ m}.$$

We shall now compare the results obtained by (16) and (16a).

The curve $h_{ej} = f(\nabla TR)$ (Figure 72), plotted from (16), yields for ∇TR= 87.00m: $h_{ej} \approx 2.58$ m; thus, (16) and (16a) give practically the same result.

When β is less than 0.6, the results obtained by (16a), (17a), (18a) will contain a considerable error (cf. p. 38).

29. EJECTION THROUGH CONDUITS

a. Calculation procedure

The HPP dimensions, headrace and tailrace levels, and turbine discharge capacity are usually given. It is not always possible to determine the discharge through the conduits from their carrying capacity, since it depends on the tailrace level near the conduit outlets when these are flooded. The tailrace level has, however, first to be determined.

The nappe depth h_1 depends on the height of the outlets or, in the case of discharge under a sluice gate, on the opening of the latter. It is therefore not necessary to determine h_1 as a function of h_0, and we use only the formula relating the tailrace depth to the pressure at the draft-tube outlet. For the final selection of the formula we must know the nappe length (when the apron has a sloping part), and whether the conduit outlets are flooded.

The procedure is as follows:

1. We determine the discharge through the conduits. The effective head is in a first approximation taken as the static head:

$$H_{st} = \nabla HR - \nabla TR.$$

At fully opened sluice gates the discharge through the conduits is

$$Q_w = \mu\omega\sqrt{2gH}.$$

The height h_1 of the opening in the case of discharge under a sluice gate, required for plotting the ejection characteristic $h_{ej} = f(\nabla TR)$ is approximately

$$h_1 = \frac{Q_w}{\mu b_w \sqrt{2gH}},$$

where μ is the discharge coefficient of the conduit for flow under the sluice gate; its value may be taken as that corresponding to a fully opened sluice gate; b_w is the total width of the outlets; H is the effective head; when there is a platform at the outlets it is determined as follows: when the outlets are flooded, from the difference $\nabla HR - \nabla h_t$ (where h_t is the surface level in the plane of the outlets); when the upper edges of the outlets are not flooded, irrespective of the tailrace level, from the difference $\nabla HR - \nabla(a+h_1)$, where $\nabla(a+h_1)$ is the level of the upper edges of the outlets.

The difference between the headrace and tailrace levels is to be taken as effective head when the discharge coefficient is referred to the

difference $\nabla HR - \nabla TR$ (far downstream of the HPP in section II-II), and the conduit outlets are flooded.

2. We must now decide which formula to use, according to whether the conduit outlets are flooded, and where the sloping part of the apron is located. Formulas (23), (24), (25) are used when the outlets are not flooded, and formulas (28), (29), (30), when they are. When there is free access of air underneath the nappe, the term $(1-\beta)$ in (23) to (25) is taken as equal to unity.

We determine the nappe length (when the apron has a sloping part) by the method described in § 23. When the outlets are flooded we make use of the criterion $h_2 \leq 1.18\sqrt[3]{q_w^2}$ (Chapter III).

3. We determine the discharge Q_t from the turbine characteristic. The head H_t is again taken in a first approximation as the static head (cf. step 1). From the turbine discharge we obtain $k=\frac{Q_w}{Q_w+Q_t}$, whence, by (10) or from the nomogram in Appendix II, we determine M and $A=\beta q_w^2 M$. The value of A can also be determined from (21).

4. Having determined h_0 and then $\nabla h_0 = \nabla$ (platforms at outlets) $+h_0$, or h_t and then $\nabla h_t = \nabla$ (apron below end sill) $+h_t$, we check whether the correct formulas have been used. Equations (23) to (25) are applicable when ∇h_0 is less than the level of the upper outlet edges, while (28) to (30) are applicable when ∇h_t is larger than the level of the upper edges. When $\nabla h_0 = \nabla h_t$, (23) to (25) and (28) to (30) are equivalent.

There is always a submerged jump in the tailrace when the conduit outlets are flooded. Surface or bottom flow may exist when the outlets are not flooded. In the latter case the mathematical models are the same, and there is no need to plot the curve determining the first critical regime on the ejection characteristic in order to check whether the correct formula has been used.

5. Having determined the piezometric effect of ejection for different excess discharges and tailrace levels:

$$h_{ej} = \nabla TR - \nabla h_0 \quad \text{or} \quad h_{ej} = \nabla TR - \nabla h_t,$$

we plot curves

$$h_{ej} = f(\nabla TR)$$

for different discharges Q_w and obtain the ejection characteristic.

We then deduct from the piezometric effect of ejection the regain of head, and obtain the head effect of ejection:

$$\Delta H = h_{ej} - \Delta h,$$

where, according to (5),

$$\Delta h = \eta\left(\frac{V_t^2 - V_2^2}{2g}\right).$$

6. We repeat the calculation, determining Q_w and Q_t from the effective instead of the static head.

We then plot the head effect of ejection as function of the tailrace level on the ejection characteristic.

If the data in § 7 can be used for estimating the additional losses ΔH_w, the head effect of ejection may be represented in the form

$$\Delta H = h_{ej} - \Delta h - \Delta H_w.$$

In a correctly designed HPP the additional losses should be minimum, so that $\Delta H_w \approx 0$.

It is convenient to compute the ejection characteristic in tabular form simultaneously for several tailrace levels.

As in the case of overflow ejection we must for $h_0 < 0$ use (23), (24) or (25), in which the free access of air underneath the nappe is taken into account, $(1-\beta)$ being taken as unity.

The flow regime behind the dam can be determined more accurately by plotting the curve determining the first critical regime on the ejection characteristic; in order to be able to use (31) and (32), the conduits must be replaced by the equivalent dam (cf. § 19). If the parameters of the equivalent dam lie outside the limits for which the empirical relationships (31) and (32) are valid, the tailrace regime has to be determined from the condition $h_0 - h_1 \leq 0$, considered in §§ 5 and 28.

b. Ejection in a combined HPP with conduits. (Example)

We shall analyze the ejection through conduits for the design shown in Figure 73: $B = 25.00\,\text{m}$; $b = b_t = 18.00\,\text{m}$; $\beta = \frac{b}{B} = \frac{18}{25} = 0.72$; $d = 11.75\,\text{m}$; $h_1 = 2.50\,\text{m}$; $h_t = 8.0\,\text{m}$.

Area of conduit outlets $\omega = 18.0 \cdot 2.5 = 45.0\,\text{m}^2$.

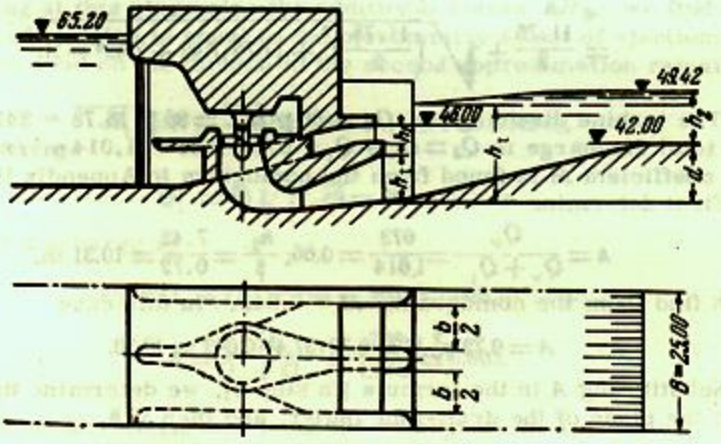

FIGURE 73. Combined HPP with conduit.

The discharge coefficient of the conduits, referred to the tailrace level in the plane of the outlets, is $\mu = 0.85$.

The turbine-discharge curve is defined by the equation $Q_t = 86\sqrt{H_t}$.

It is required to determine the ejection effect when $\nabla HR = 65.20$ m and $\nabla TR = 49.42$ m, i.e., for a static head $H_{st} = 65.20 - 49.42 = 15.78$ m and a tailrace depth $h_2 = \nabla TR - \nabla$(apron) $= 49.42 - 42.00 = 7.42$ m.

1. We first determine the excess discharge. The height of the free tailrace surface (far downstream of the HPP) above the upper edge of the outlet is $49.42 - 46.00 = 3.42$ m. The outlets will apparently be flooded. Assuming in a first approximation that the effective head is equal to the static head,* we have:

$$Q_w = \mu\omega\sqrt{2gH_{st}} = 0.85 \cdot 45.0 \cdot 4.43\sqrt{15.78} = 169.4\sqrt{15.78} = 673 \text{ m}^3/\text{sec};$$

$$q_w = \frac{Q_e}{b} = \frac{673}{18.0} = 37.4 \text{ m}^2/\text{sec}.$$

2. We must now select the formula to be used. Since it has been assumed that the outlets will be flooded, we must apply (28), (29), or (30). (Formula (30) is obviously inapplicable because the sloping part of the apron is very long).

For a final selection of the formula we make use of the criterion $h_2 \lesssim 1.18\sqrt[3]{q_w^2}$ (cf. § 13).

In our case

$$1.18\sqrt[3]{q_w^2} = 1.18\sqrt[3]{37.4^2} = 13.2 \text{ m}, \quad h_2 = 7.42 < 13.2,$$

i.e., we must use (28).

The apron has no step (Figure 37). We therefore take $e = 0$ in (28). Hence,

$$h_t = \frac{d}{2} + \sqrt{\left(\frac{d}{2}\right)^2 + dh_2 + h_2^2 - A} =$$

$$= \frac{11.75}{2} + \sqrt{\left(\frac{11.75}{2}\right)^2 + 11.75 \cdot 7.42 + 7.42^2 - A}.$$

3. The turbine discharge is $Q_t = 86\sqrt{H_{st}} = 86\sqrt{15.78} = 341.4 \text{ m}^3/\text{sec}$.
The total discharge is $Q_2 = Q_w + Q_t = 673 + 341 = 1{,}014 \text{ m}^3/\text{sec}$.
The coefficient M is found from the nomogram in Appendix II.
We first determine

$$k = \frac{Q_w}{Q_w + Q_t} = \frac{673}{1{,}014} = 0.66; \quad \frac{h_2}{\beta} = \frac{7.42}{0.72} = 10.31 \text{ m}.$$

We then find from the nomogram: $M = 0.042$. In this case

$$A = 0.72\, q_w^2 M = 0.72 \cdot 37.4^2 \cdot 0.042 = 42.30.$$

4. Substituting A in the formula [in step 2], we determine the tailrace depth in the plane of the draft-tube outlet, and then ∇h_t:

$$h_t = \frac{11.75}{2} + \sqrt{\left(\frac{11.75}{2}\right)^2 + 11.75 \cdot 7.42 + 7.42^2 - 42.30} = 5.87 +$$

$$+ \sqrt{176.77 - 42.30} = 17.46 \text{ m},$$

$$\nabla h_t = (42.00 - d) + h_t = 30.25 + 17.46 = 47.71 \text{ m}.$$

* When the outlets are not flooded the head on the conduits is $\nabla HR - \nabla$ (upper outlet edge).

The level ∇h_t of the tailrace surface in the plane of the outlets is thus higher than the level of their upper edges: 47.71 > 46.00. The outlets are therefore in fact flooded, and the correct formula has been selected.

5. We now determine the piezometric effect of ejection:

$$h_{ej} = \nabla TR - \nabla h_t = 49.42 - 47.71 = 1.71 \text{ m}.$$

The regain of head is neglected in a first approximation, and we take $\Delta H = h_{ej}$.

6. We proceed to the second approximation.

Allowing for the ejection, the effective head on the conduits is

$$H = H_{st} + h_{ej} = 15.78 + 1.71 = 17.49 \text{ m};$$

$$Q_w = 169.4\sqrt{17.49} = 708 \text{ m}^3/\text{sec},$$

hence,

$$q_w = \frac{708}{18.0} = 39.34 \text{ m}^2/\text{sec}.$$

When Q_t is determined in a second approximation the head on the turbine must be reduced by the regain of head Δh and the additional losses ΔH_w. We have

$$\Delta h = \eta \frac{V_t^2 - V_2^2}{2g} = \eta \frac{Q_t^2}{2g}\left[\frac{1}{\omega_t^2} - \frac{1}{(Bh_2)^2}\right] =$$

$$= 0.7 \frac{341.4^2}{19.6}\left[\frac{1}{(18.0 \cdot 8.0)^2} - \frac{1}{(25.0 \cdot 7.42)^2}\right] = 0.008 \text{ m},$$

i.e., the regain of head is less than 1 cm, and can therefore be neglected.

Neglecting at this stage also the additional losses ΔH_w, we find that the head effect of ejection is equal to the piezometric effect of ejection: $\Delta H = h_{ej}$.

Thus, the head on the turbine in the second approximation remains

$$H_t = H_{st} + \Delta H = 15.78 + 1.71 = 17.49 \text{ m},$$

and the discharge

$$Q_t = 86\sqrt{17.49} = 360 \text{ m}^3/\text{sec}.$$

The total discharge is

$$Q_2 = Q_w + Q_t = 708 + 360 = 1.068 \text{ m}^3/\text{sec},$$

$$k = \frac{Q_w}{Q_w + Q_t} = \frac{708}{1.068} = 0.663.$$

The value of M determined from the nomogram in Appendix II, remains practically the same, namely 0.042. By (14), $M = 0.0431$. Hence,

$$A = 0.72\, q_w^2 M = 0.72 \cdot 39.34^2 \cdot 0.0431 = 48.03,$$

$$h_t = 5.87 + \sqrt{176.77 - 48.03} = 17.21 \text{ m},$$

$$\nabla h_t = 30.25 + 17.21 = 47.46 \text{ m},$$

$$h_{ej} = 49.42 - 47.46 = 1.96 \text{ m}.$$

A third approximation is unnecessary.

The regain of head remains negligible as before, and if the additional losses ΔH_w can also be neglected, the head effect of ejection will be equal to the piezometric effect: $\Delta H = h_{ej}$.

If (for the same initial data) the design in Figure 18,b is considered instead (still assuming the outlets to be flooded), the computed effect of ejection remains unchanged. In this case it is, however, possible to estimate the additional losses during ejection, in accordance with § 7.

The intake area of the scroll casing is $\omega_v = 12.0 \cdot 18.0 = 216\,m^2$.

The scale factor of a model with $(\omega_v)_M = 1\,m^2$ is thus $\lambda = \sqrt{\omega_v} = \sqrt{216} = 14.70$.

The excess and turbine discharges of the model are respectively:

$$(Q_w)_M = \frac{Q_w}{\lambda^{5/2}} = \frac{708}{3{,}180} = 0.22\ m^3/sec;\ (Q_t)_M = \frac{Q_t}{\lambda^{5/2}} = \frac{360}{3{,}180} = 0.11\ m^3/sec.$$

According to Figure 19,b, these discharges correspond to losses ∇H_w of the order of 0.001 m, i.e., $0.001 \cdot 14.7 = 0.015$ m in full scale, which is practically negligible.

Additional losses of about the same order may be expected in the HPP for which the ejection effect was determined.

30. SIMPLIFIED METHOD OF EJECTION ANALYSIS

Accurate results are not required in the initial design stage; involved relationships should in this case not be used. Tentative relationships for ejection above the draft tube (Figure 74) can be obtained in a form independent of the flow regime and the location of the sloping part of the apron on the basis of the following assumptions, each of which has separately been made by different authors (Chapter IV).

1. The nappe depth h_1 at the toe and in the plane of the outlets is independent of the piezometric head beneath the nappe. The pressure distribution in the nappe in section I-I and beneath the nappe is hydrostatic at any flow regime behind the dam.

2. The pressures and their distribution are the same at the sides of the piers and at the end sill between the piers.

3. The pressure on the sloping part of the apron depends on the tailrace depth in section II-II, irrespective of the position of the sloping part and of the flow regime.

The other assumptions are the same as made in §§ 9 and 13.

When the jump is not submerged (Figure 74,a,b) the momentum equation has the following form (by analogy with (15) and (22)):

$$-\frac{B}{2}A = \left(ah_0 + \frac{a^2}{2}\right)B + \frac{h_1^2}{2}B - \frac{(h_2+d)^2}{2}B,$$

whence

$$h_0 = \frac{(h_2+d)^2 - a^2 - h_1^2 - A}{2a} \qquad (41)$$

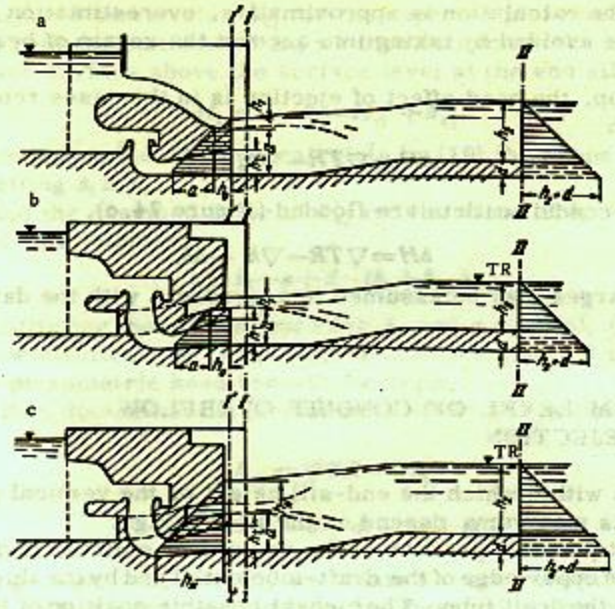

FIGURE 74. Simplified mathematical models for ejection into the tail-race.

a—overflow ejection; b—ejection through conduits with nonflooded outlets; c—ejection through conduits with flooded outlets.

When the conduit outlets are flooded we obtain, by analogy with (27):

$$-\frac{B}{2}A=\frac{h_1^2}{2}B-\frac{(h_2+d)^2}{2}B$$

and

$$h_1=\sqrt{(h_2+d)^2-A}, \qquad (42)$$

which is a particular case ($e = 0$) of (29).

The value of A is determined, as before, from (13) or (21). The nomogram in Appendix II may also be used.

The depth h_1 at the toe is determined from the formula for the nappe contraction:

$$T_0=h_1+\frac{q_w^2}{2\varphi^2 h_1^2},$$

for which nomograms are given in books on hydraulics. The nomogram in Appendix I (setting $\xi_0=\xi_1$) may also be used. In the case of conduits h_1 is the height of the outlets (or the opening of the sluice gate).

In the case of ejection through conduits (41) has to be replaced by (42) when $h_0 > h_1$, i.e., $\nabla h_0 > \nabla (a + h_1)$.

Although the calculation is approximative, overestimation of the ejection effect must be avoided by taking into account the regain of head Δh, using (5).

Summing up, the head effect of ejection is in the cases represented in Figure 74,a,b

$$\Delta H = \nabla TR - \nabla h_0 - \Delta h,$$

and when the conduit outlets are flooded (Figure 74,c),

$$\Delta H = \nabla TR - \nabla h_t - \Delta h.$$

The discharges may be assumed in accordance with the data given in § 27.

31. OPTIMUM LEVEL OF CONDUIT OVERFLOW EDGE FOR EJECTION

The limits within which the end-sill height or the vertical position of the conduit outlets may vary, depend on the HPP design.

The lowest possible position of the end sill or outlets* is determined by the level of the upper edge of the draft-tube outlet and by the thickness of the slab covering the draft tube. The highest possible position of the end sill is with overflow ejection determined by the location of the bridge crossing the structure. (In the case of ejection through conduits the position of the outlets depends on the location of the operators' room.)

Small variations of the end-sill height (or of the vertical position of the conduit outlets) influence negligibly the ejection effect. Determination of the end-sill level (or of the level of the lower outlet edge) is therefore necessary only when this level may vary within fairly wide limits.

Formulas for determining the optimum toe height have been proposed by I. I. Veits /3/, Kh. Sh. Mustafin /14/, and D. I. Kumin /8/ for dams with horizontal end sills longer than 1.5 to 2 times the nappe depth at the end sill, for broad-crested dams, and for conduits with horizontal ends. These formulas will not be discussed here, and we refer the interested reader to the sources. Unfortunately, these authors did not compare the results obtained by their formulas with those obtained in the laboratory.

A problem arising during the design stage is that of selecting the end-sill level for a HPP having an apron with sloping part. In addition, a variation of the end-sill height leads to a change in the ejection effect, which alters the turbine discharge; this cannot always be neglected, although in the formulas proposed by the above-mentioned authors the turbine discharge is considered as constant.

If the end-sill level is determined so as to obtain surface flow near the upper boundary of the first critical regime, the procedure proposed by Dr. P. P. Laupman** may be adopted.

Laupman assumes that when the nappe leaves the end sill horizontally, the piezometric effect of ejection is equal to the difference between the tailrace

* We consider ejection above the draft tube.

** Cf. the reference on p. 97

level and the free surface of the nappe at the end sill. His method becomes clear from the procedure proposed below.*

I. We assume some value h_{ej} for the expected piezometric effect of ejection. From the static head H_{st} we then determine the height of the free headrace surface above the surface level at the end sill:

$$H_1 = T' - h_1 = H_{st} + h_{ej}.$$

II. From this value of H_1 we calculate by (10) the nappe depth at the end sill, setting $h_0 = h_1$.

III. From the assumed value of h_{ej} and the value of h_1 found by (10) we find the end-sill height:

$$a = h_2 - e + d - (h_1 + h_{ej}).$$

IV. Substituting the values found for h_1 and a in (16a), (17a), or (18a) (for overflow ejection), or (23), (24), or (25) (for ejection through conduits), we find the piezometric head beneath the nappe.

V. We then determine the piezometric effect of ejection:

$$h_{ej} = \nabla TR - \nabla h_0$$

or

$$h_{ej} = (h_2 - e + d) - (a + h_0).$$

Repeating steps I, II, and III, we obtain a more accurate value of a. If the latter differs considerably from the first value obtained for a, we repeat steps IV, V, I, II, and III, which ends the calculation.

An accuracy of 0.5 m in the determination of a is sufficient, according to Laupman.

When this method is used to determine the vertical position of the conduit outlets, steps I and II are omitted, since the height h_1 of the outlets is known.

The best method to determine the level of the overflow edge is, however, to analyze several designs and plot the ejection effect as function of the level of the overflow edge.

When the tailrace depth h_2 is given, each design is analyzed as follows:

I. We assume a certain value h_0 for the piezometric head beneath the nappe, finding

$$\nabla h_0 = \nabla a + h_0$$

and

$$H_t = \nabla HR - \nabla h_0,$$

where ∇a is the level of the overflow edge.

We determine Q_t from the turbine characteristic and Q_w for the value assumed for h_0, and then obtain A from (13).

In the case of overflow ejection we find h_0 from (16a), (17a), or (18a), performing successive approximations until the value assumed for h_0 coincides with that obtained by these formulas.

In the case of ejection through conduits we use (23), (24), or (25).

* The method is discussed as applicable to the formulas in Chapters II and III.

II. Having determined h_0 (and therefore also ∇h_0), we calculate the piezometric effect of ejection:

$$h_{ej} = \nabla TR - \nabla h_0.$$

III. Plotting the value found for h_{ej} on the ejection characteristic, we check if the selected formula corresponds to the tailrace flow regime by establishing whether the computed point lies above or below the line determining the first critical regime (cf. § 28).

Repeating this procedure for each different level ∇a of the overflow edge, we plot the curve $h_{ej} = \varphi(\nabla a)$, whose extremum corresponds to the optimum level of the overflow edge.

An important problem in this connection is the selection of the computed excess discharge. Laupman's data may be used tentatively depending on the size of the river; the average characteristic discharge for a combined HPP can be taken from column 5 of Table 8.

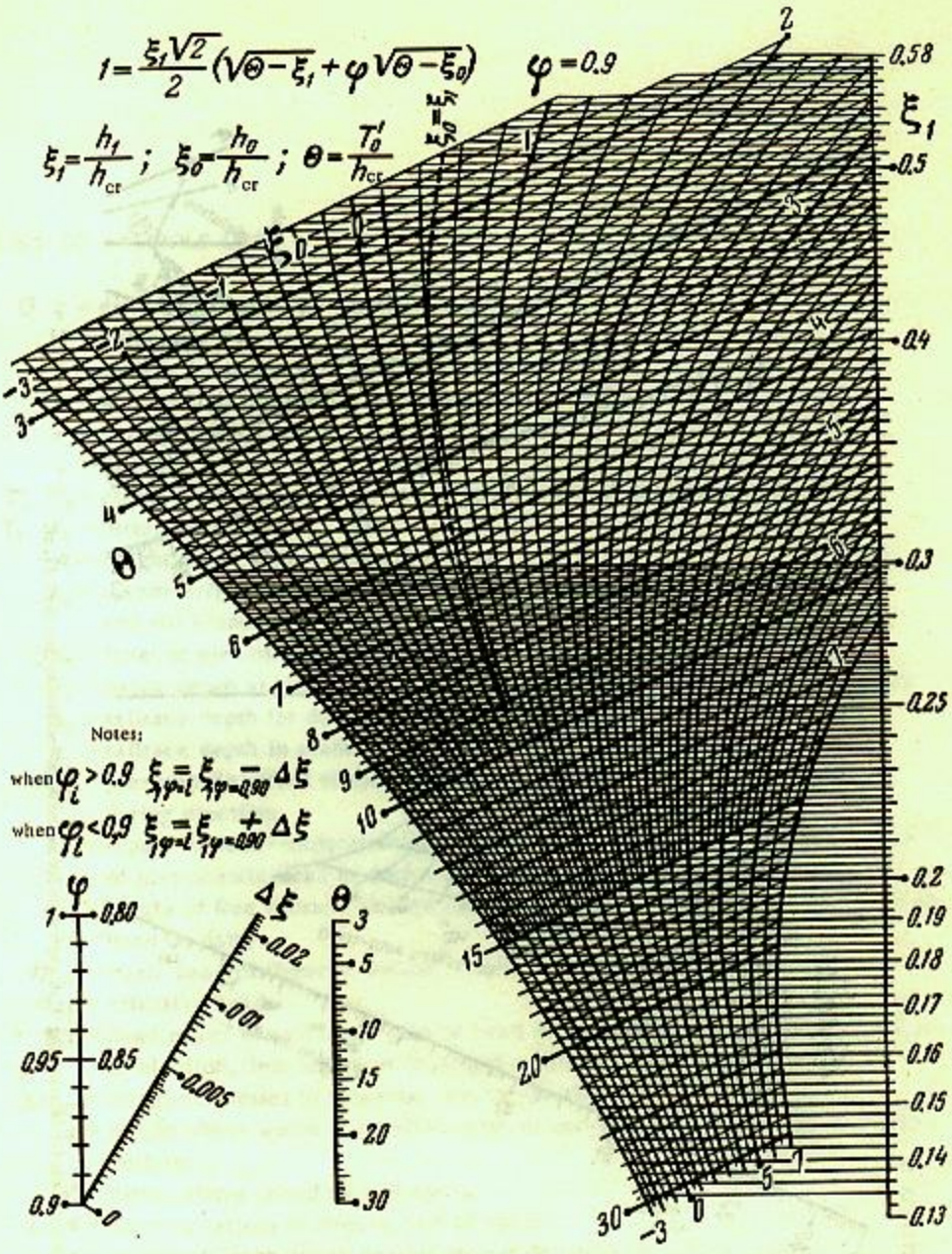

Nomogram for determining flow depth h_1 at toe when h_0 and T_0' are known. (See example on p.103) Notes show how connnection $\Delta\xi$ is to be introduced in value of ξ_1, when $\varphi\neq0.9$.

APPENDIX II

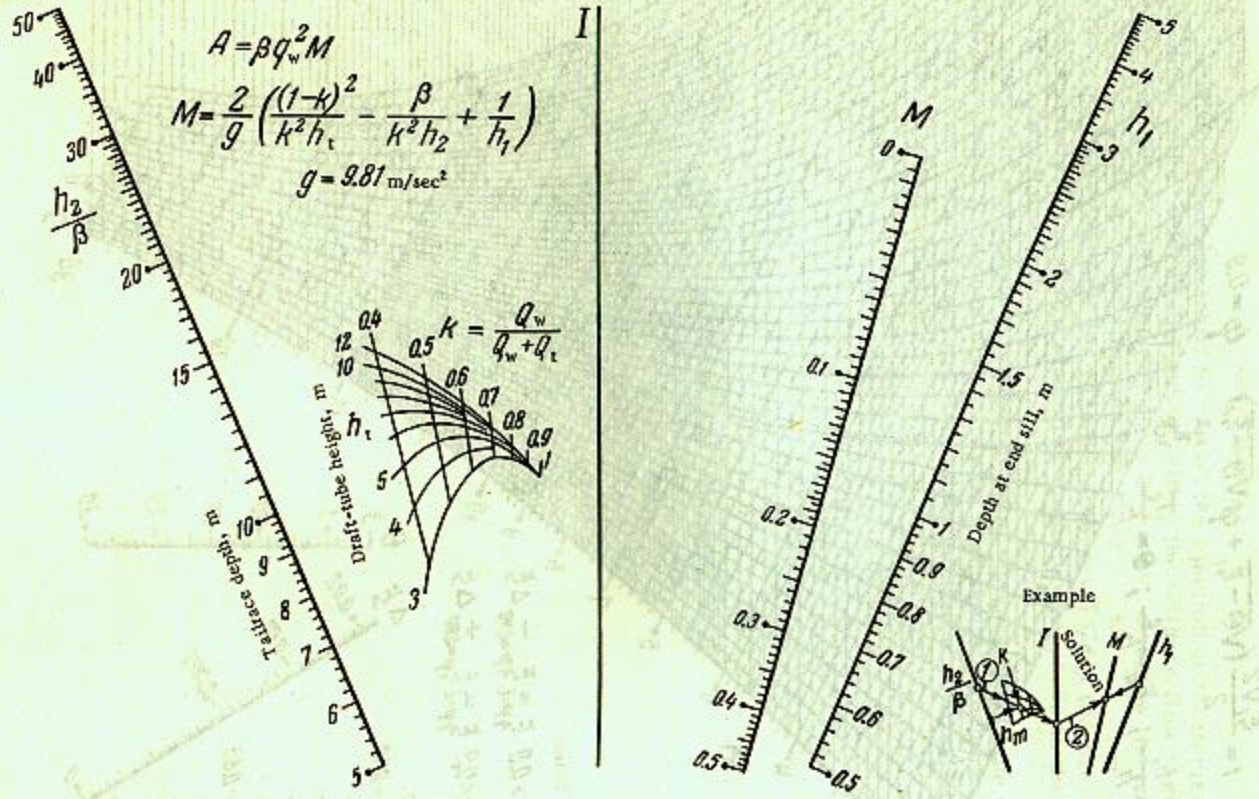

Nomogram for determining M in expression for momentum increment (see Sect. 11, a).

LIST OF SYMBOLS USED

Q, q = discharge, discharge per unit length;
V = velocity;
1 = section I-I in plane of end sill or conduit outlets;
2 = section II-II in tailrace far downstream of HPP;
w = dam (conduit);
t = turbine;
T', T'_0 = energy, per unit mass, above overflow edge of dam (conduit);
T, T_0 = ditto, above apron;
h = height of air pocket beneath nappe;
h_0 = piezometric head at draft-tube outlet, measured from overflow edge of end sill (conduit)
∇h_0 = level of piezometric-head plane at draft-tube outlet;
h_1 = nappe depth at end sill; height of conduit outlets; opening of sluice gate;
h_2 = tailrace depth far downstream of HPP;
h_t = tailrace depth in plane of conduit outlets;
h_{ej} = piezometric effect of ejection—pressure drop at draft-tube outlet during ejection;
Δh = regain of head—reduction (compared to tailrace depth far downstream of HPP) of piezometric head at draft-tube outlet, due to turbine discharge;
Δh_2 = height of free tailrace surface (far downstream of HPP) above end-sill level;
H = head on dam;
H_{st} = static head (difference betwen headrace and tailrace levels);
H_{ef} = effective head;
ΔH = head effect of ejection—gain in head due to ejection (= piezometric effect of ejection, less regain of head and additional losses in receiver);
ΔH_w = additional losses in receiver, due to ejection;
a = height above apron of overflow edge of end sill or of lower edge of conduit outlets;
a' = ditto, above raised part of apron;
c, d = superelevations of sloping part of apron;
e = height of apron above nearest part of downstream spillway apron;
p = height of crest above apron;
b = dam width at overflow edge; width of conduit outlets;
b_t = width of draft-tube outlet;
B = theoretical width of tailrace (between center lines of piers).

BIBLIOGRAPHY

1. Aleksandrov, B.K. Puti k uskoreniyu i udeshevleniyu stroitel'stva priplotinnykh gidroelektrostantsii (Ways for Accelerating and Reducing the Costs of Building HPPs on Dams).— Gidrotekhnicheskoe Stroitel'stvo, Nos.1—2. 1944.
2. Ananyan, A.K. O propusknoi sposobnosti dvukhyarusnykh vodosbrosov (On the Carrying Capacity of Two-level Spillways).— Izvestiya Akademii Nauk Armyanskoi SSR, Vol.3, No.3. 1950.
3. Veits, I.I. Osnovnye zadachi soedineniya dvukh potokov (Basic Problems of the Combining of Two Flows).— Izvestiya VNIIG, Vol.32. 1947.
4. Egorov, S.A. Ezhektsiya v nizhnii b'ef gidrostantsii (Ejection into the Tailrace of HPPs), Moskva-Leningrad. 1948.
5. Egorov, S.A. Ezhektsiya v nizhnii b'ef na malykh gidrostantsiyakh (Ejection into the Tailraces of Small HPPs).— Gidrotekhnicheskoe Stroitel'stvo, No.8. 1949.
6. Egorov, S.A. O formulakh Sabaneeva i Levi dlya rascheta gus'ka plotiny (On the Formulas of Sabaneev and Levi for Analyzing a Series of Dams).— Volgostroi, Nos.5—6. 1936.
7. Kachanovskii, B.D. Opredelenie effekta ezhektsii pri propuske pavodkov cherez donnye otverstiya GES (Determination of the Ejection Effect during the Discharge of Flood Water through the Bottom Outlets of an HPP.— Izvestiya VNIIG, Vol.34. 1947.
8. Kumin, D.I. Maksimal'nyi ezhektsionnyi effekt v vodoslivnykh gidrostantsiyakh (Maximum Ejection Effect in Overflow HPPs).— Izvestiya VNIIG, Vol.44. 1951.
9. Kumin, D.I. Sopryazhenie b'efov pri poverkhnostnom rezhime (Tailrace Regimes with Surface Flow).— Gosenergoizdat. 1948.
10. Kumin, D.I. Opredelenie ezhektsionnogo effekta v gidrostantsiyakh s ezhektorami vo vsasyvayushchikh trubakh (Determination of the Ejection Effect in HPPs with Ejection in the Draft Tubes).— Izvestiya VNIIG, Vol.32. 1947.
11. Laupman, P.P. Vstroennaya sifonnaya gidrostantsiya (Built-in Siphon HPP).— Gidrotekhnicheskoe Stroitel'stvo, Nos.7—8. 1945.
12. Laupman, P.P. Vodoslivnaya GES dlya rek s razmyvaemym ruslom (Overflow HPPs for Rivers with Beds Subject to Scouring).— Gidrotekhnicheskoe Stroitel'stvo, No.7. 1940.

13. Levi, I.I. K voprosu o teorii poverkhnostnogo pryzhka i o raschete plotin pri poverkhnostnom rezhime (On the Theory of the Surface Jump and on the Computation of Dams with Surface Flow).— Izvestiya VNIIG, Vol. 7. 1932.
14. Mustafin, Kh. Sh. Gidravlicheskie laboratornye issledovaniya gidrostantsii, razmeshchennoi v tele vodoslivnoi plotiny (Hydraulic Laboratory Studies of an HPP Located Inside an Overflow Dam).— Ph. D. thesis, Leningrad. 1951.
15. Perfil'ev, V.V. Izuchenie mer bor'by s padeniem napora na gidroustanovkakh (Studies of Measures for Preventing Head Reduction in HPPs).— Izvestiya VNIIG, Vol. 4. 1932.
16. Sabaneev, A.A. O forme sopryazheniya vodoslivnoi poverkhnosti plotin s dnom nizhnego b'efa (On the Form of the Transition from the Streamlined Spillway Face of a Dam to the Tailrace Bottom).— Trudy MIIT, No. 11. 1929.
17. Chertousov, M.D. Raschet vysoty ustupa, sopryagayushchego vodoslivnuyu poverkhnost' s dnom nizhnego b'efa i obespechivayushchego nezatoplennyi poverknostnyi rezhim (Determination of the Height of the Step between the Streamlined Spillway Face and the Tailrace Bottom, Ensuring Surface Flow).— Izvestiya VNIIG, Vol. 32. 1947.
18. Die elektrischen Einrichtungen der neuen Draukraftwerke.— Elektrotechnik und Maschinenbau, No. 5. 1946.
19. Power Plant Engineering, Chicago. 1927.

EXPLANATORY LIST OF ABBREVIATED NAMES OF USSR INSTITUTIONS, ORGANIZATIONS, JOURNALS, ETC. APPEARING IN THIS TEXT

Abbreviation	Full name (transliterated)	Translation
MEI	Moskovskii Energeticheskii Institut (im. Molotova)	Moscow Institute of Energetics (im. Molotov)
MIIT	Moskovskii Institut Inzhenerov Zheleznodorozhnogo Transporta (im. I. V. Stalina)	Moscow Institute of Railroad Engineers (im. I. V. Stalin)
TsAGI	Tsentral'nyi Aero-Gidrodinamicheskii Institut (im. N. E. Zhukovskogo	Central Aero-Hydrodynamical Institute (im. N. E. Zhukovskii)
TsKTI	Tsentral'nyi Komitet Tyazheloi Industrii	Central Committee for Heavy Industry
TsKTI	Tsentral'nyi Nauchno-Issledovatel'skii Kotloturbinnyi Institut	Central Scientific Research Institute for Boilers and Turbines
VIGM	Vsesoyuznyi Institut Gidromashinostroeniya	All-Union Institute of Hydromachinery
VNIIG	Vsesoyuznyi Nauchno Issledovatel'skii Institut Gidrotekhniki	All-Union Scientific Research Institute of Hydro-Engineering

S. M. SLISSKII / EJECTION INTO TAILRACES OF HYDROPOWER PLANTS

Table of Contents

FOREWORD

Combined hydroelectric power plants (HPPs), i.e., those with dam and powerhouse forming a single structure, have the advantages of a shorter spillway front and a complete or partial regain of head during construction.

In designing combined HPPs the ejection effect has to be computed; this is most important for comparing different variants and for economy calculations.

A method for computing the effect of ejection into the tailrace, and the corresponding relationships, are proposed in this book. Other problems of the hydraulics of combined HPPs are also discussed, and some recommendations on design are made.

The relationships proposed for analyzing ejection were tested by comparing the results obtained by them with those of model tests performed by the author at the MEI imeni V. M. Molotov, and by other scientists at the VIGM and VNIIG imeni B. E. Vedeneev. The satisfactory agreement between computed and experimental results permits the method proposed to be used in practice. The ejection effect in some HPPs now being built or designed was computed by the formulas and methods described here.

In estimating the accuracy of the calculations it is necessary to distinguish between simple and difficult cases. In the simplest cases, such as overflow ejection from a straight dam with horizontal apron, the accuracy is so high that laboratory study of the ejection becomes unnecessary. In difficult cases the calculations may considerably reduce the amount of necessary laboratory work. In addition, the formulas proposed make it possible to apply the results of laboratory studies to the design finally adopted, since it happens frequently that the design investigated in the laboratory differs from the final one by, e.g., the discharge capacity.

The methods described may be used for energy calculations during the exploitation of combined HPPs, and also for the design of two-level conduits.

Involved relationships should not be used at the initial stages of design, since the calculations are usually based on approximate data. A simplified mathematical model is accordingly proposed in the book for the initial, tentative, calculations.

Some of the conclusions and relationships should be considered as tentative. This applies mainly to the empirical formulas, which the author has included in order to satisfy the immediate needs of design organizations, which possess hardly any data on this problem. These empirical formulas can, of course, be refined when new and more accurate experimental data become available. Further refinement requires mathematical models for

the pressure distribution on the sloping part of the apron and a means for determining the point at which the nappe impinges on the apron.

The author acknowledges the help given to him by Prof. Dr. S. B. Izbash, under whose guidance the basis of this work was prepared.

The author will be glad to receive readers' comments on the book. These should be addressed to Gosenergoizdat, Shlyuzovaya nab., 10, Moskva.

The author